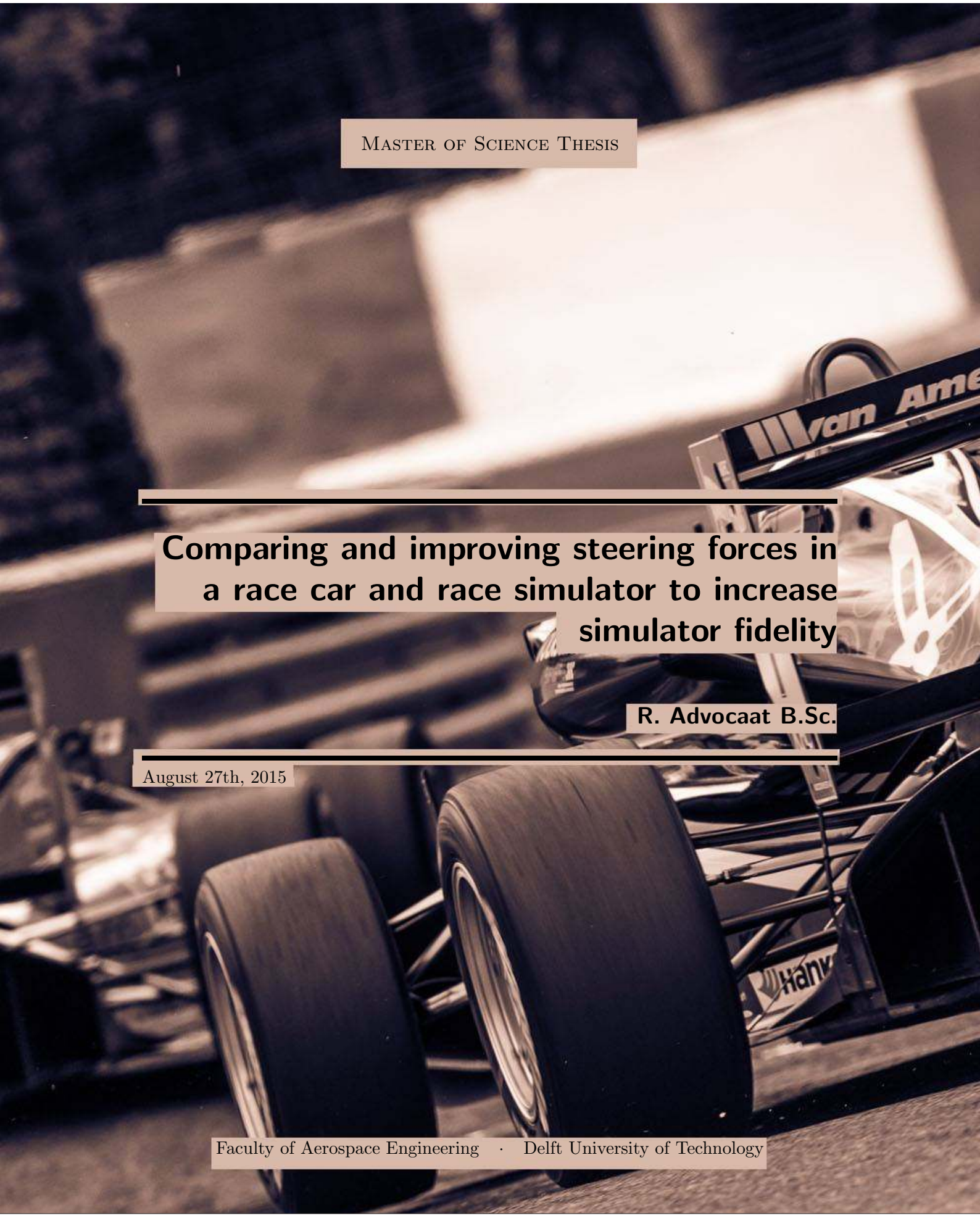

Master of Science Thesis

Comparing and improving steering forces in a race car and race simulator to increase simulator fidelity

R. Advocaat B.Sc.

August 27th, 2015

Faculty of Aerospace Engineering · Delft University of Technology

Comparing and improving steering forces in a race car and race simulator to increase simulator fidelity

Master of Science Thesis

For obtaining the degree of Master of Science in Aerospace Engineering at Delft University of Technology

259#15#MT#DAR-FPP

R. Advocaat B.Sc.

August 27th, 2015

Faculty of Aerospace Engineering · Delft University of Technology

Delft University Of Technology
Department Of
Flight Performance and Propulsion

Formerly known as
Design, Integration and Operations of Aircraft and Rotorcraft

The undersigned hereby certify that they have read and recommend to the Faculty of Aerospace Engineering for acceptance a thesis entitled **"Comparing and improving steering forces in a race car and race simulator to increase simulator fidelity"** by **R. Advocaat B.Sc.** in partial fulfillment of the requirements for the degree of **Master of Science**.

Dated: August 27th, 2015

Head of department: _____
prof.dr.ir. L.L.M. Veldhuis

Supervisor: _____
dr.ir. M. Voskuijl

Reader: _____
dr. ir. B. Shyrokau

Reader: _____
ir. Rik Vernooij

Abstract

As circuit testing days are expensive and limited by regulations, racing teams are more and more dependent on simulation tools. Van Amersfoort Racing built their own racing simulator to train drivers in an fully controlled environment. This environment is based on commercially available simulation software rFactor. However, no research on the accuracy of the physics of this software is available. Since level of fidelity of race simulators is important for the perception of racing drivers, force feedback steering forces are analyzed. Information of the real Formula 3 car is used to upgrade the vehicle model used in rFactor and to develop a Multibody Dynamic vehicle model of the same car.

Steering metrics are used to make qualitative comparisons between steering force measurement in the real car, the simulator and the Multibody Dynamic model. It is shown that the baseline simulator vehicle model is less sensitive to steering input compared to the real car. Furthermore the simulator driver theoretically senses higher steering torques for a given lateral acceleration discarding electric power limitations of the force feedback motor. As a desire to improve simulator fidelity, a Pacejka tyre model of the Hankook Formula 3 tyre is converted to an rFactor model together with an improved suspension model using the exact suspension geometry as provided by car manufacturer Dallara. Simultaneously, the Multibody Dynamic vehicle model is constructed from these submodels, which purely focusses on lateral dynamics.

In order to use the lateral based Multibody Dynamic model as a tool for simulation and assessment, its response is tested given the same input as the real Formula 3 car experienced during a particular test. Three cases are considered: weaving on a straight, a low speed corner and a high speed corner. Longitudinal load transfer is inherent in low speed corners, which, due to its limitation in the Multibody Dynamic model, leaves the model adjustments inconclusive. Furthermore, tyre relaxation plays an important role in low speed corners following each other up in a short period of time, which affect low speed steering metrics. The Multibody Dynamic model showed close correlation of steering metrics with real car measurements for the high speed corner. The updated rFactor model improved steering torque feedback despite higher required steering angles.

Acknowledgements

After my internship at Van Amersfoort Racing during the final part of the 2012 season, I was asked to design and build a racing simulator for their team. This allowed me to gain practical knowledge and have a graduation subject for my Master Thesis in Aerospace Engineering. Now, almost two and a half year later, my thesis is finished. During this time I have not only worked on my thesis, but learned a lot about race cars which has always been my childhood passion.

I would like to thank Van Amersfoort Racing and all its staff for the opportunity they offered me to perform this interesting and relevant research and gave me the freedom to finish my thesis throughout the hectic moments of a racing season. The critical opinions of race engineers Rik and Peter are appreciated as their feedback allowed more than once to have a fresh look into the subject. Furthermore, I would like to thank my test drivers Atze Kerkhof and Arjun Maini for their time to test the rFactor models and their sharp feedback.

Needless to say, I would like to thank all members of my graduation committee for reading my thesis and attending and grading my presentation and defence. Mark Voskuijl has provided me with perfect guidance and feedback throughout the project, while Barys Shyrokau helped me out with the implementation of SimMechanics.

Lastly, thanks to my family, my girlfiend and friends for the support and confidence during the complete length of my studies.

Remco Advocaat
August 14th, 2015

Contents

List of Figures

List of Tables

Glossary

List of acronyms

FL	Final load
FM	Final grip multiplier
IS	Initial slop of grip mulitplier
MD	Multibody dynamic
TLS	Tyre load sensitivite grip mulitplier
VAR	Van Amersfoort Racing

List of symbols

α	Slip angle
δ	Rocker pivot rotation angle
δ_{steer}	Steering wheel angle
γ_x	Negative camber angle
λ_{Hx}	Scale factor of horizontal shift in Pacejka tyre model
$\lambda_{\mu x}$	Scale factor of longitudinal peak friction coefficient in Pacejka tyre model
$\lambda_{F_{z0}}$	Scale factor of nominal (rated) load in Pacejka tyre model
μ_y	Lateral friction coefficient
μ_x	Longitudinal friction coefficient
ω	Wheel rotational velocity
a_{lat}	Lateral acceleration
c_{ground}	Damping coefficient of ground model

d_{fz}	Normalized change in vertical wheel load
F_x	Longitudinal tyre force
F_y	Lateral tyre force
F_z	Normal/vertical wheel load
F_{z0}	Nominal normal/vertical wheel load
G_{real}	Gradient of steering torque gradient regression line of real measurements
G_{sim}	Gradient of steering torque gradient regression line of simulator measurements
h_0	Wheel reference height
$h_{measured}$	Measured wheel height
I_{xx}	Moment of inertia about x-axis
I_{yy}	Moment of inertia about y-axis
I_{zz}	Moment of inertia about z-axis
k_{front}	Selected spring stiffness coefficient at front axle
k_{ground}	Stiffness coefficient of ground model
k_{rear}	Selected spring stiffness coefficient at rear axle
$k_{rotation}$	Equivalent rotational spring stiffness coefficient
$k_{translation}$	Equivalent translational spring stiffness coefficient
l	Length
L_{rocker}	Rocker pivot arm length
m	Mass
p_{Dx1}	Scale factor of longitudinal friction coefficient at nominal wheel load
p_{Dx2}	Scale factor of variation of longitudinal friction coefficient with load
p_{Dx3}	Scale factor of variation of longitudinal friction coefficient with camber angle
p_{Hx1}	Scale factor of horizontal shift at nominal load in Pacejka tyre model
p_{Hx2}	Scale factor of variation of horizontal shift with load in Pacejka tyre model
R	Corner radius
r	Radius
Re	Effective tyre radius
S	Slip ratio
S_h	Horizontal shift in Pacejka tyre model
S_{hx}	Horizontal shift in longitudinal direction in Pacejka tyre model
S_{real}	Gradient of steering sensitivity regression line of real measurements
S_{sim}	Gradient of steering sensitivity regression line of simulator measurements
S_v	Vertical shift in Pacejka tyre model
t	Time
T_{steer}	Steering column torque
V_x	Wheel velocity in x-direction
V_y	Wheel velocity in y-direction

Chapter 1

Introduction

Van Amersfoort Racing is a racing team based in Huizen, The Netherlands. The team will celebrate its 40th anniversary this year, as the team was founded in 1975 by team owner Frits van Amersfoort [1]. In the 2015 season, Van Amersfoort Racing participates in two race classes: the FIA Formula 3 European Championship and the ADAC Formula 4. It is important in both series to drive the cars as much as possible, since driver experience is really valuable for young drivers. However, there are several reasons why the team is not able to drive the cars as much as they would prefer. The testing ban in the FIA Formula 3 European Championship limits the amount of testing days the team would like to make with the Formula 3 cars [2]. As the ADAC Formula 4 Championship is founded to give young drivers race experience in a racing car, testing days are unlimited. According to De Groot (2011), race teams have limited possibilities to train throughout the year due to financial budgets, personnel, maintenance and preparation time prior to each day of testing [3]. The purpose of the Formula 4 championship is to let drivers race with a limited budget [4], which has its effect on the amount of testing days available.

To cope with limited testing facilities, race teams rely more and more on computer based simulation tools to improve performance on track. Because simulations with automatic controllers do not accurately evaluate the human-machine interaction, drivers should be adopted into the simulation tools by means of the human-in-the-loop principle [3]. According to De Groot (2011) [3], human-in-the-loop driving simulators are developed and used as both an engineering tool and a driving training tool for the Formula Student competition. The advantages of driving simulators are summed up by De Groot (2011) as being inexpensive training and testing time, experimental control of the environment, accurate possibilities of the measurements on vehicle state and a safe environment for the driver [5]. Especially the repeatability as explained by Koskela (2012), the ability to repeat a condition numerous times without any changes in weather or tyre condition [6], is for Van Amersfoort Racing of importance. This repeatability gives the team a powerful tool to assess the capabilities of drivers, since they are all faced with the same track and vehicle conditions.

Besides training facilities, racing simulators are a valuable extra for teams in determining setup development. SimHQ Motorsports features an article in which they describe the added value in setup development in racing simulators. According to Scott Raymond, Professor of Motorsports Engineering at Indiana University, it is beneficial being able to sit next to a driver and make setup changes in matters of seconds before heading back to the virtual track [7]. Furthermore, simulators offer possibilities to accurately measure the effect of design choices [8]. According to Hoeberichts (2013), Dallara has reduced its design and development times for complete models and car parts and bodies by making use of racing simulators. Dallara says that a racing simulator verifies certain driving aspects of a car design in the same fashion as a wind tunnel verifies aerodynamic design changes. Their racing simulator is able to be used for assessing new aerodynamic parts, spring and damper adjustments and influences of fuel load on tyre behavior and tyre degradation. It is demonstrated that racing simulators not only aid the development of driving skills, but also helps engineers in their task to generate the best possible setup for a specific track.

The necessity of having a driving simulator is proven by the amount of companies possessing simulators. The well known car manufacturers as Volkswagen, Daimler-Benz, Mazda, Ford, BMW, Nissan and Renault posses simulators according to Slob (2008) [9]. The main purpose of these type of driving simulators is however different than for racing teams. Slob (2008) mentions the actual purpose of these simulators: operation of simulators is mainly for the sake of designing car interior or test new systems which are called Advanced Driver Assistance Systems [9]. The safety of the implementation of satellite navigation systems, cell phones and e-mail systems in vehicle is assessed in their simulators. Obviously, this is not the only field of research where simulators come into play. Ciáurriz (2013) describes how drive-by-wire systems will be incorporated in future car designs, reducing the number of moving parts in vehicles and thus simplifying vehicle design [10]. In order to test these novel drive-by-wire systems with haptic feedback, they built a simulation platform equipped with the developed drive-by-wire haptic system. Apart from design purposes, driving simulators are used for medical research as well. T. Akerstedt (2004) describes a research in which the effect of tiredness of drivers driving home from night shifts is analyzed. The results show that tiredness has a negative influence on driver performance and driving home from night shifts increase crash rates for drivers [11]. Contrary to short term effects as tiredness, research shows that simulator driving can be used to determine the amount of driving errors combat veterans make due to posttraumtic stress disorders. Classen (2014) describes a driving simulator test in which combat veterans conduct a driving test of approximately 15 minutes in which the driver errors made are compared to driving errors of healthy control participants [12].

A known problem of driving simulators is the level of fidelity experienced by drivers [13]. De Winter (2012) explains that unrealistic driver behavior might be evoked by low level of fidelity in driving simulators. Test drivers might become demotivated because of the limited-fidelity level of a simulator. Furthermore, the fact that safety is not any issue in driving simulators, drivers might be prone to a false sense of safety, responsibility or competence [13]. Especially these arguments give rise to the need for high fidelity in a simulator for a racing team. Information about the instantaneous dynamics of the vehicle is carried by steering wheel force feedback according to Toffin (2003). This information

reinforces the visual information in order to perform the driving task [14]. Liu (1995) confirms this statement: "Although drivers obtain a substantial amount of information for driving from vision, information from other sensory modalities may also provide relevant information about the state of the car or even the surrounding environment" [15]. Examples of these other sensory modalities are steering wheel feel and transverse acceleration. The same article states that drivers asked to perform a driving task relied on steering feel to help steer. Another important finding is that the same drivers were sensitive to changes in vehicle handling characteristics. Lui (1995) emphasizes that feel in the steer is critical for automobile racing. To avoid losing speed or crashing, racing drivers must monitor and modulate the state of the car through steering movement.

Software used on current state of the art simulators can be developed in house to meet the end user's demand or can be a commercial alternative [16]. Weinberg (2009) performed research on available open-source and commercial simulator software. They chose rFactor as their base platform due to its convincing, realistic driving experience which followed from the available graphics, accurate vehicle physics and full steering wheel force feedback support [16]. Another advantage of rFactor is the possibility to capture vehicle telemetry at rates up to 90 Hz [16]. The downside of using rFactor is described by Koskela (2012). Although they found the subjective feeling for the driving quite realistic, no research data on the accuracy of game physics could be found [6]. Moreover, experienced and professional users of the software admit that they are not always aware of the assumptions made by the source code, as the rFactor physics are hidden from the end-user. This black-box nature of the software forces them into tricking the vehicle models until the output is as desired [17]. This leaves a research area open for the current thesis. rFactor has proven its ability to deliver a good basis for race simulators, as even half of the field of Formula One teams utilizes rFactor on their racing simulators [18].

The high level of nowadays racing simulators and their relevant applications as mentioned before, led to the need for a high fidelity racing simulator for the Van Amersfoort Racing team. Up until now, the team strongly relied on submodels of their vehicles to determine gear ratios and general setups. However, the first verifications of the results of these simulations were performed on track, whereas racing simulators can verify the setup even before the team heads out to the track. This aspect, together with a platform for training and assessing driving skills is the starting point for the research of this thesis.

This thesis describes the designed and produced racing simulator for the Van Amersfoort Racing team. The software to be used on the simulator is rFactor given the fact that it has proved to be a reliable platform for real-time racing simulations. However, as discussed there is not much research performed on the accuracy of the game physics. Therefore, steering forces on the real Formula 3 car and in the simulator will be measured and compared. A Multibody Dynamic model of the actual Formula 3 car is developed in the SimMechanics environment [19], which will help assessing the physical capabilities of rFactor, by reproducing specific vehicle motions. This Multibody Dynamic model enables a straightforward update of the standard rFactor Formula 3 model with an accurate model based on the Multibody Dynamic model. Apart from suspension geometry, a complete Pacejka tyre model [20] is developed and linked to the Multibody Dynamic model and

converted to an rFactor model. Finally, with an equal suspension geometry and equal tyre model, the output of the updated rFactor model is compared to results of the Multibody Dynamic model and the measurements of the real car. This step enables the analysis whether the recommendations coming from the updated rFactor model will result in improved physics and a higher level of simulator fidelity. To summarize, the following vehicles and vehicle models are encountered during this research:

- Dallara F312 Formula 3 race car
- Baseline Formula 3 rFactor vehicle model
- Updated Formula 3 rFactor vehicle model
- Multibody Dynamic Formula 3 vehicle model

Ultimately, the successful development of a Multibody Dynamic model of the actual Formula 3 could lead to a basis to replace the commercial simulation software rFactor. The advantage for the team of such a replacement is the adjustability of the Multibody Dynamic model. New design features are straightforwardly added to the Formula 3 vehicle model. Moreover, the generation of a Multibody Dynamic model allows for system identification, both for the real Formula 3 car as for the rFactor model. Given the hidden source code of physics of the game, system identification provides a technique in the identification of non-linear structures given the known input and output to find a dynamical model [21] [22].

To conduct this research, profound knowledge of developing and utilizing Multibody Dynamic models is required. Furthermore, the implementation of a Pacejka tyre model into a generic suspension and vehicle design provides a powerful tool for many racing teams in assessing vehicle and setup capabilities. The comparison of real track data with simulation results of the Multibody Dynamic model also emphasizes the fact that verification of simulation results is an important step in working with simulations and race simulators.

Chapter 2

Racing simulator properties and operation

This chapter is intended to give an overview of the properties and capabilities of the race simulator, both software as hardware related. First, the software used for the simulation is discussed, followed by the description of the current Formula 3 car. This gives an insight in the hardware requirements for the simulator. Given these requirements, all relevant aspects of the simulator are discussed why and how they are designed. Lastly, the way measurements are performed in the simulator is explained.

2.1 Simulation software

The simulation software on which the simulator will operate is chosen to be rFactor. This game has proven to be one of the most realistic, open-endedness, fully modability [23] and easily available race simulation software in the current segment of racing simulators. Moreover, even Formula One teams base their simulators on rFactor [24] due to its open source character. Although the game has been developed and released in 2005, daily modifications are released by the game developer (Image Space Incorporated, ISI) or the immense community supporting the game. These facts made the decision to work with rFactor the logical step in the development of a high end race simulator for Van Amersfoort Racing.

As mentioned earlier, rFactor has full ability of customization of vehicle and track models. The files of rFactor are designed and organized as such, that so called modders (community members which develop extra content for the game in terms of cars or tracks) are allowed to have full access to car and track models. The real physics of the game however, are hidden to all people, as this is the intellectual right of the game developer (ISI). Appendix A explains the file structure of rFactor and the way the software copes with track and vehicle models.

2.2 Simulator hardware

Before the start of this research, there was no racing simulator available for the Van Amersfoort Racing team. This section highlights the hardware properties and abilities of the built simulator. The simulator can be divided into two main parts, being the monocoque and its components and the simulator room in which the monocoque is placed.

2.2.1 Driver situation

The Formula 3 cars used in the FIA European Formula 3 Championship are manufactured by Dallara, an Italian race car manufacturer involved in many current race categories. The current version of the Formula 3 design is designated as the F312 car, which is homologated by the FIA up to 2015 [25]. The cars are powered by a four-cylinder engine having a maximum capacity of 2000 cc. The power is however limited by an air intake restrictor with a diameter of 28 mm. In the European Formula 3 Championship, use is made of Hankook tyres on 13 inch rims. The suspension is a double wishbone structure with adjustable pushrods. The gearbox is a sequential six gear box. All electronics are provided by Bosch [27].

The dimensions of the car are restricted by regulations. The car width including tyres may not exceed 1850 mm, while the wheelbase minimum value is 2000 mm. The car is shown in figure 2.1 in top view. The weight of the vehicle is measured with all fluids present in the vehicle, fuel excluded. Furthermore, the driver's weight is added to the total, including helmet and other racing gear. The total weight may never be lower than 565 kg during officials tests or race weekends [25].

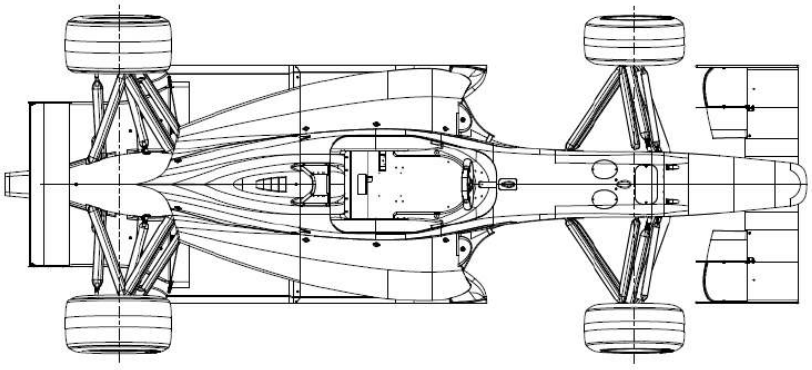

Figure 2.1: Top view of the F312 Formula 3 car developed by Dallara. Source [29].

Introduced in the 2014 season are new engines equipped with alternators to be self-sufficient in terms of electrical power. Both Volkswagen, Mercedes and Neill Brown designed new engines with the same capacity, but direct injection may be used from now on [26]. Apart from that, Bosch renewed all electronics on the car which also allowed for pneumatic shifting activated by paddles on the new steering wheel.

The monocoque

The driver is positioned in a monocoque to replicate the position of the driver as he would have in the real car. The monocoque chosen is a Formula Renault 2.0 liter monocoque. The choice for this monocoque is based on table 2.1, where the general dimensions of both cars are given. As can be read from this table, the simularity of both cars justifies the choice for this monocoque, as the cars are in the same class of size. Furthermore, due to the introduction of new monocoques in the Formula Renault 2.0 championships since 2013 [31], the former version monocoques are widely available.

Table 2.1: Dimensions of Formula 3 and Formula Renault 2.0 cars. Source: [28] & [29]

Dimension	Formula 3	Formula Renault 2.0
Wheelbase	2800 mm	2730 mm
Front track	1595 mm	1502 mm
Rear track	1540 mm	1440 mm
Overall length	4351 mm	4363 mm
Overall width	1845 mm (including tires)	1733 mm
Overall height	945 mm	963 mm
Weight	550 kg incl. driver and ballast	505 kg

2.2.2 Pedal box

The pedal box of the simulator consists out of a brake pedal and a throttle pedal. No clutch pedal will be adopted in the system, since no practice starts will be simulated. That means that the clutch usage of the model of the car in the simulation software should be set to semi automatic, to automatically operate the clutch pedal [30].

The simulator is used by a large number of drivers. The requirement of easily adjustable pedals is obvious from different driver lengths. To solve this problem, the bottom side of the front monocoque is cut out and replaced by an aluminium plate in which 8 slots have been machined to slide the individual pedals backwards and forwards. As can be seen in figure 2.2, there are two different slots in the plate. The one machined completely through the plate having a width of 4 mm is for mounting the pedals to the plate, whereas the 5 mm wide slot is for maintaining the orientation of the pedal correctly. In figure 2.3, two bushings for the wider slots can be seen at the bottom of the bracket.

Throttle pedal

The input signal for the throttle pedal for the simulation software is a signal between 0 and 5 Volts [32]. This fact gives rise to the need for a sensor which is able to convert throttle pedal movement into a 0 - 5 Volts signal. The Formula Renault cars are equipped with a drive-by-wire system [33], which exactly fulfills the need mentioned here. Therefore, the sensor used in the Formula Renault racing classes is used as throttle sensor for the simulator.

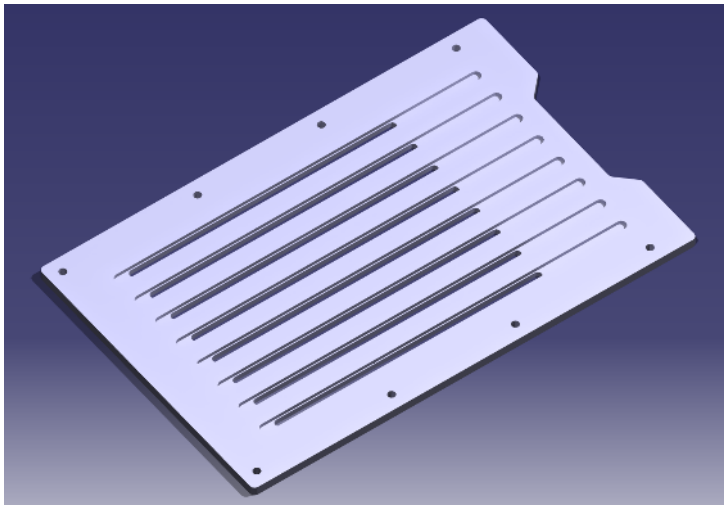

Figure 2.2: Aluminium plate mounted on the lower side of the monocoque with machines slots for individual pedal movement.

The sensor is a rotary sensor, which is able to rotate 120°. There is a spring mounted in the sensor unit such that the throttle pedal will be forced to the neutral position if no throttle is applied by the driver. Since the sensor is fragile in its end stops, a pedal stop is designed on the pedal bracket in order to protect the sensor from overloading.

Brake pedal

The braking system is one of the main systems of a vehicle and important for the performance of competition cars [34]. It is therefore important to have the right feeling in the brake pedal. Especially given the fact that during intense braking situations, the pressure in the braking system may rise up to 110 bar [35]. To simulate the brake pedal properties in the simulator as much as possible to the brake pedal in the real car, it was decided that the braking system in the simulator had to be a hydraulic system.

Drivers use a braking force with a maximum of 800 Newtons on the brake pedal [36]. This force is guided through the pedal into the master cylinders, which are coupled to a hydraulic cylinder which mimic the function of the brake calipers in the real car. In figure 2.3, the pedal and master cylinders are shown mounted on the brake pedal bracket.

To replicate the squeezing effect of the brake calipers, the high pressure braking fluid is guided into a hydraulic cylinder having a suction working principle. The main shaft will therefore not be pushed outside, but will retract under the influence of a high pressure fluid. The retracting motion is then counteracted by a spring being loaded in compression.

The hydraulic cylinder chosen for the given operation is the Specken/Drumag hydraulic cylinder type "ZU-Gz 16/100 NHR16-EZ-H00-E11-ES-As1". This cylinder has a bore area for pulling of 150 mm^2 [38]. The shaft of the hydraulic cylinder is equiped with a

Figure 2.3: Master cylinder inclination.

compression spring having a stiffness as such, that the brake pedal stiffness of the simulator equals the stiffness of the real car brake pedal.

The braking signal is generated by a pressure sensor in the hydraulic line. This sensor measured the pressure in the line and converts it to an electrical signal as an input for rFactor. In figure 2.4 the total construction of the braking system is visible, including the single brake pressure sensor.

The electronic signals generated by the throttle position sensor and the brake pressure sensor have to guided to the computer on which the simulator software is running. To do so, use is made of a 12-bit joystick controller designed and produced by Leo Bodnar [40]. It converts the analog inputs to USB standards, usable for standard computers.

2.2.3 Steering column

The design of the steering column is for the current research most interesting. At one side of the steering column is the racing driver which has to feel steering forces as he would feel in the real car and give his steering input to steer the car. At the other side a device is required which has to generate the steering forces coming from the real racing car and has to process the inputs of the driver. The "SimSteering Force Feedback System" from Leo Bodnar generates the steering forces. It is able to generate torques up to 16 Nm with a 10,000 pulses per revolution sensor [41].

The system consists out of an electic motor manufactured by Kollmorgen, two motor cables, an electric converter and a steering column clamp. The electric motor is mounted to the front bulkhead in such a way that the steering column ends up at the driver in a straight line to reduce play in the system. The assembly is shown in figure 2.5.

Figure 2.4: Complete brake pedal assembly.

2.2.4 The beamerroom

The monocoque is placed in a separate room, to reduce other influences than the simulator itself. In this room, a screen is placed at which the simulator visuals are projected. This section describes the layout of this room and the screen dimensions.

Beamers

The primairy selection property of the beamers is the delay time between the generation of an image on the computer to the actual projection on the screen called input lag [42]. If the time delay in generating images on a screen becomes too large, the state of the vehicle may not be actual anymore when the image is projected and seen by the driver. Therefore, the smallest input lag possible is required to have direct control of the vehicle. The most suitable beamer for this task is the Optoma GT 750 XL.

Screen design

To have the highest possible horizontal field of view, three beamers are used to project images on the screen. In order to warp these images without discontinuities in the screen, use is made of Immersive Display software by Fly Elise-NG. Using this software, the image of three beamers is warped on a wide, curved screen.

Using CATIA, the best possible set up for the beamers was computed as shown in figure 2.6. The result is a screen height of 80 cm with a horizontal field of view from the driver's

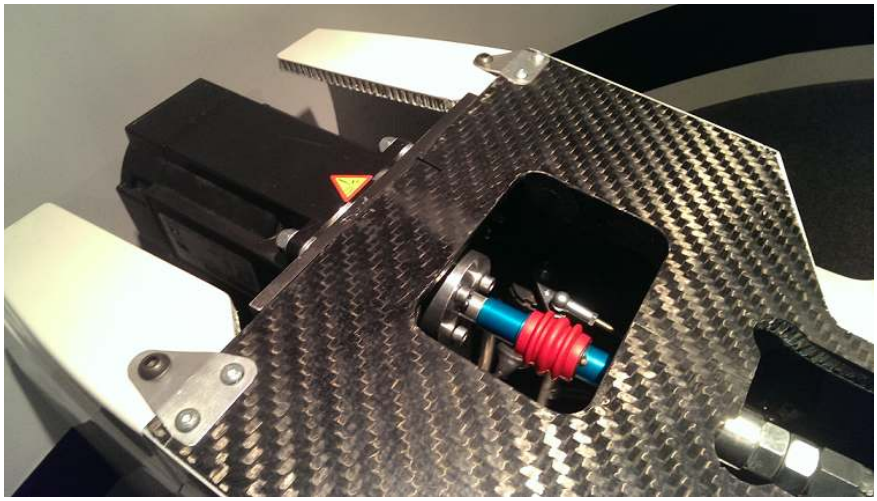

Figure 2.5: Electric motor for force feedback system mounted on the monocoque front bulkhead.

point of view of 117°. The radius of the screen is 160 cm which allows the driver to always have a perpendicular view on the screen for the best possible view.

2.2.5 Simulator room

In section 2.2.4, the horizontal position of the beamers have been discussed, together with the dimensions of the curved screen. Due to the current design, the height of the image is 80 cm. The height of the screen is chosen such that the driver sitting in the monocoque is just able to see the lower edge of the screen. The height of the lower edge of the screen is determined visualy by putting a driver in the seat. Then the optimal height of the lower edge turns out to be 28 cm above the floor.

The Optoma GT750XL is a so called short throw beamer, which means it can generate images from a short distance. This property of the beamers is especially favorable for the vertical projection of the image. Using the table provided in the user manual of the beamer [45] and the beamer dimensions, the beamers are suspended at a height of 124 cm upside down in order to have the correct image on the screen given the height as discussed above. The completely installed simulator room is designed to look as shown in figure 2.7.

2.3 Simulator operation

Important during the operation of the simulator is the continuous processing of gathered data. This section shows how the data is acquainted and the measurements are processed focussing on steering forces. In figure 2.8, the simulator is shown in operation.

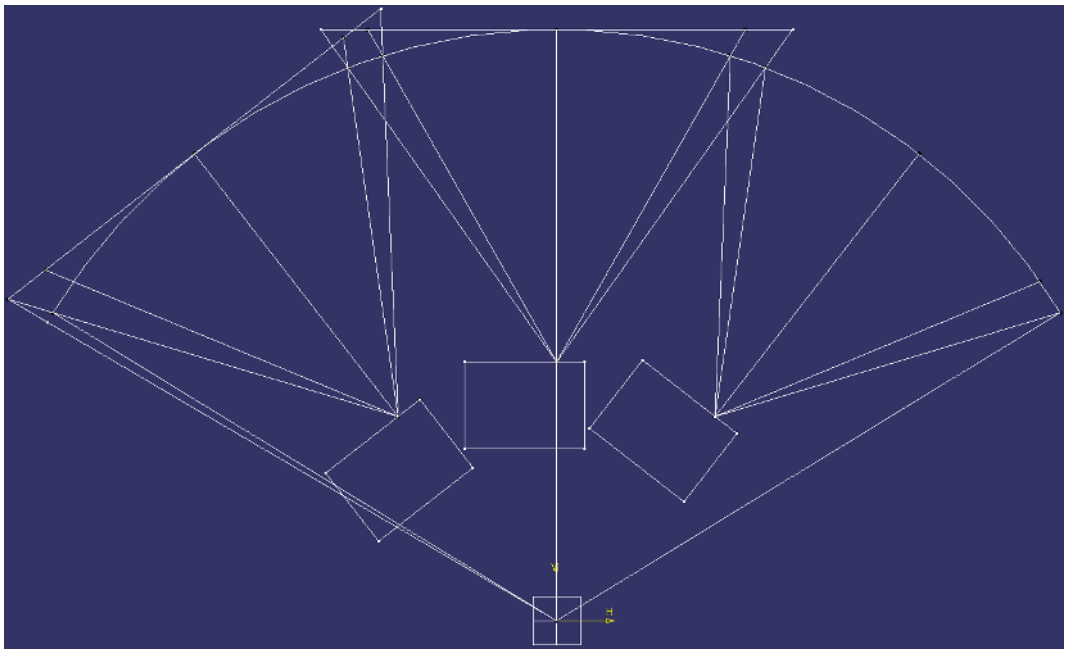

Figure 2.6: Individual orientation of the three beamers including 10% overlap. Top view.

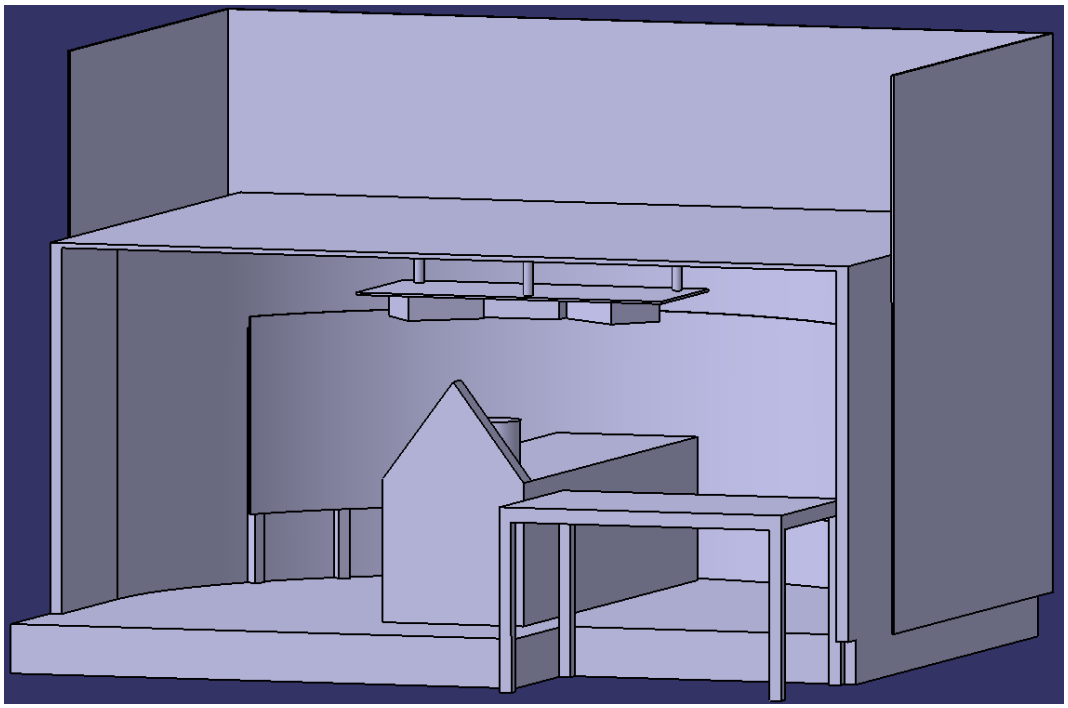

Figure 2.7: The complete simulator room as constructed at Van Amersfoort Racing.

Figure 2.8: Race simulator in operation with Max Verstappen behind the wheel.

2.3.1 Car steering force measurements

The amount of sensors on a Formula 3 car is limited by regulations [47]. Additional sensors are not allowed during official racing weekends or official test days. Therefore the only time span in which measurements during car operation can be performed are during the (private) winter test days. However the time span in which these test days take place is limited due to the testing restriction. The only (private) testing is allowed after the last event of the championship and December 21st 2013 [47].

Since the steering forces in the car are measured by an additional sensor, the measurements have to take place during the test days as described above. The steering forces are measured by a strain gauge attached to the steering column. This strain gauge is then connected to the data acquisition system and its measurements are recorded in the same fashion as all other sensors. The actual parameter the strain gauge measures is the torque in the steering column by detecting strain in the material of the column. If calibrated correctly, the strain is coupled to a corresponding quantity of steering torque.

2.3.2 Simulator steering force measurements

Since the amount of testing time and the variety of sensors in the simulator is unlimited, steering forces can be measured in different manners. To elaborate on the methods, a brief discussion about how the steering torque is generated is required.

Generation of force feedback

As discussed in section 2.2.3, the simulator has a steering wheel connected to an electric motor to generate steering forces. This electric motor is driven by the simulation software, being rFactor for the VAR simulator. The two main aspects by which the simulation software determines the output torque is current vehicle state. The software computes the combination of all forces in the steering rack based on the front tire vertical load, wheel rotation speed and the position angle of the front wheels, whereas the orientation of the front wheel directly follows from the steering wheel angle [48].

Now that the software has determined the force in the steering axis, it has its own algorithm to compute the exact output for the electrical motor. However, there are additional software packages which enhance the output of the the software. Two of these so called plugins are the RealFeel plugin and LeoFFB plugin. In the VAR simulator, both plugins are used. LeoFFB mainly adjusts force feedback while stationary or moving at low velocities where the RealFeel plugin adjusts force feedback in the high speed domain.

Simulator data acquisition

As described above, the steering forces in the simulator are determined by the simulation software before being sent to the electric motor connected to the steering column and steering wheel. A data acquisition plugin is available for rFactor which logs most of the parameters of the simulation vehicle real time. Moreover, more parameters are logged compared to the real Formula 3 car since there are no restrictions on the amount of sensors and no physical sensors are needed to log parameters because all parameters are known from the vehicle model for the sake of simulation. Therefore steering rack forces are measured in the simulator by this data acquisition tool which directly follow from the vehicle model simulation. The data can be accessed by using the data analysis program MoTeC.

Apart from measurements in the simulation software, the steering wheel with electric motor offers a way of measuring the force generated by the electric motor. According to its builder, inputs and outputs on the simulator steering system are visible in DIView, a separate software tool to show parameters in auxiliary connected hardware [49].

Not only DIView can be used to log the feedback in the steering system, MATLAB is able to access the same channels of the system. The Joystick Input block in Simulink reads out the output values of any joystick or controller [50]. In order to store the readout values of the Joystick Input block, a To File Simulink block is attached to the Joystick Input block.

Test cases showed however that the simulation time in Simulink is not in correspondence with the actual time. To overcome this obstacle, use is made of the Real-Time Pacer [51]. The Real-Time Pacer slows down the simulation time such that it synchronizes with the real elapsed time.

Due to the limited time span in which DIView is able to log the measurements, this option is neglected for further usage. The software data acquisition plugin is compared to the Simulink Real-Time Pacer tool as the two remaining options. The result of a testlap is shown in figure 2.9. As can be seen in this figure, both parameters are plot simultaneously. The Simulink tool is able to only log amplitudes up to 1 and -1. The data acquisition plugin for rFactor shows the steering rack force in Newtons. If the Simulink logged data is multiplied by a factor of 1000, the plots look like figure 2.9. Up to the imaginary values of -1000 and 1000, both measurements correspond accurate. Beyond these tresholds, the Simulink tool is not able to show any more data, where the simulation software still computes values above this point. This phenomenon in sim racing is known as clipping.

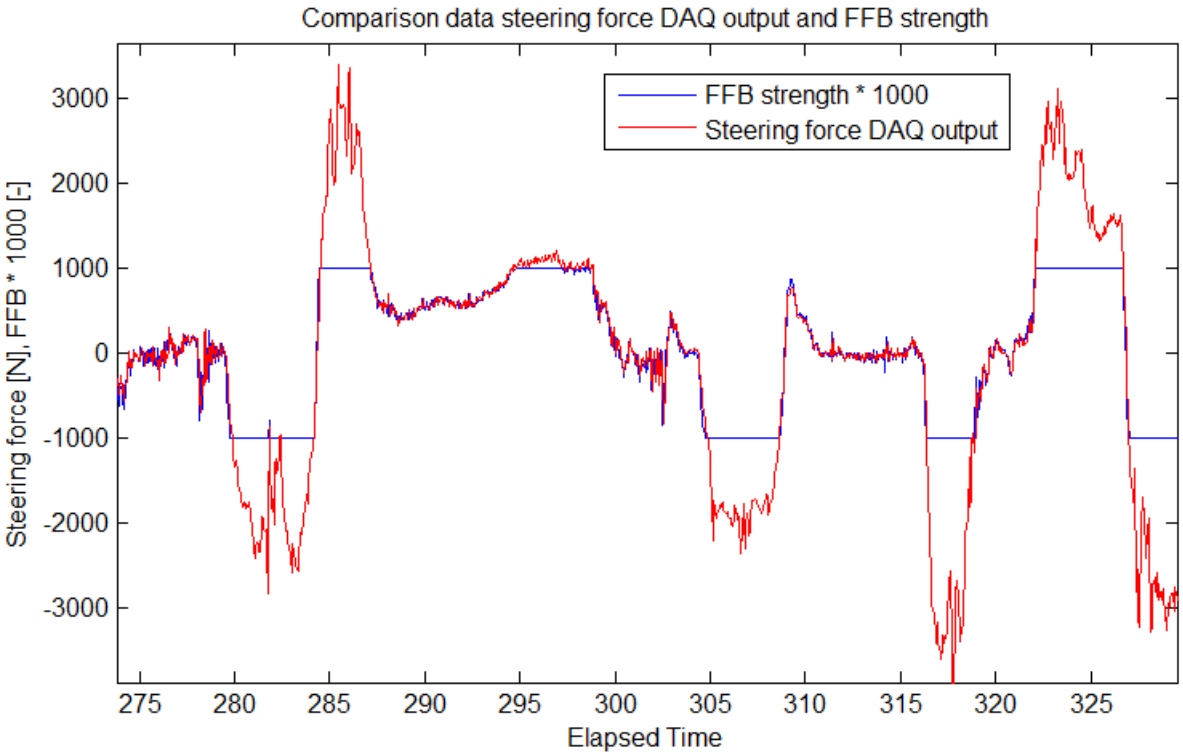

Figure 2.9: Comparison between rFactor DAQ plugin data and Simulink data for steering forces.

Clipping

Simulator steering systems have a limited amount of torque which the electric motor is able to generate. For the VAR simulator, the maximum torque which can be generated is not limited by the electric motor, but by the power supply. However, the simulation

software is not aware of the maximum capacity of the system. The simulation software calculates a steering rack force or steering torque dependent on the current state of the car. In the simulation software, a setting is present which defines the magnitude of the steering forces, varying from -100% to 100% (the negative value is for reversal of forces in the steering wheel).

Assuming a variation of computed rack forces of -5000 N to 5000 N, ideally the maximum capable force in the steering wheel should be aligned with the -5000 N or 5000 N peak value. The rest of the steering forces should then be spread evenly over the range of the steering wheel capability [52]. If the force are scaled too much down, the force feedback is too weak. Underscaling results in torque request of the simulator software which are higher than the physical limit of the system. In figure 2.10, an assumed calculated force feedback response as a function of steering wheel angle is plotted. Selecting a force feedback setting of 20%, it can be seen that the complete response curve fits exactly within the boundary of the steering system. By setting the absolute force feedback strength too high (100%), the reponse curve is cut. The steering system is not able to output the curve as drawn in the figure. Although the figure's horizontal axis is named steering wheel angle, slip angle would be a better fit. It is not possible to link a force feedback force directly to steering wheel angle. It is dependent on the state of the vehicle. Therefore, slip angle would be a better alternative.

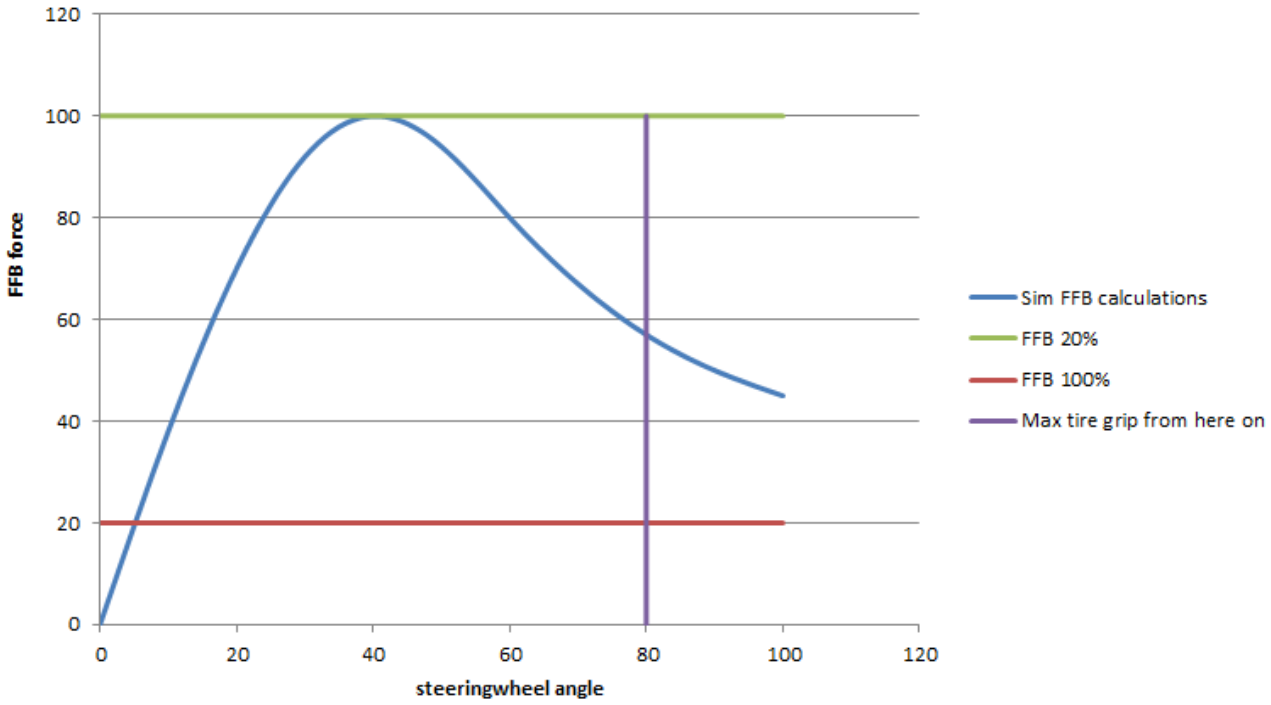

Figure 2.10: Given force feedback response as a function of steering wheel angle. Simulator force feedback levels are indicated. FFB force and steering wheel angle indicated in percentage. Source [52]

The result of improper scaling is shown in figure 2.11. As can be seen, the original curve

of figure 2.10 is still present as the dashed, red line. Since the maximum performance of the steering system is at the 20% line, no more force can be generated than that maximum value. The red line shows the output of the steering system is the force feedback setting is 100%. The simulation software wants the steering system to generate the forces as indicated by the dashed line, however due to the system limitations, the actual output is the red, flat line. If the force feedback setting is scaled down to 20%, as indicated by the green line, the top of the curve is exactly touching the maximum output line of the steering system. This implies proper force feedback scaling.

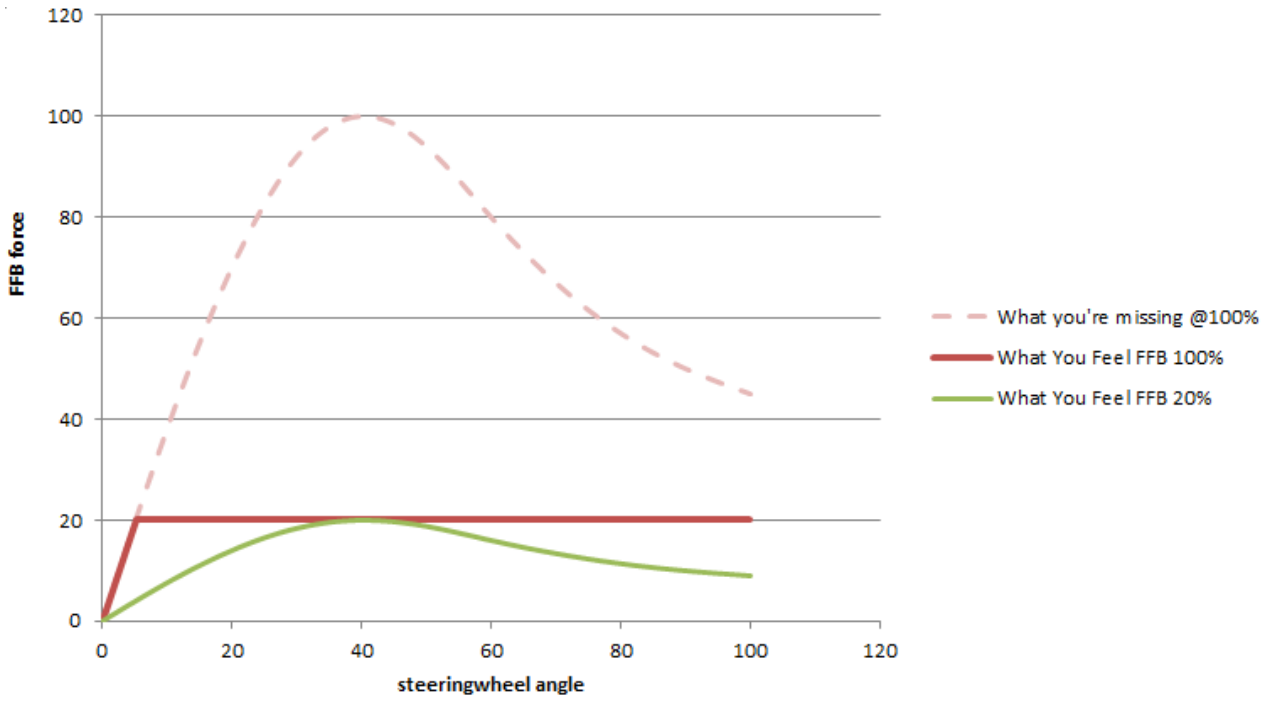

Figure 2.11: Proper and improper scaling of force feedback settings and its consequence. FFB force and steering wheel angle indicated in percentage. Source [52]

The effect of improper force feedback scaling as shown in figure 2.11, is that the driver will not notice any force variation from the moment that the maximum value is reached, i.e. only 20% of the the characteristic force feedback curve is felt by the driver [52]. The consequence of this is that the complete car characteristic is removed from the feeling from the driver. For example, the driver is not able to feel the optimum steering angle for maximum grip, since the force does not vary over the steering angle span. It can be concluded that most of the details of the force feedback is lost due to improper setup [52].

Apart from the loss in detail, there are other negative side effects of clipping. Imagine the car driving on a straight with no significant steering movements present. Every slight bump in the track surface will yield a certain force in the steering wheel. If this bump causes a steering force equivalent to 22% of the maximum computed steering force, the clipped setup will directly yield a steering force of 100% of the steering wheel systems capacity. Corrections of the driver due to grasping the steering wheel and counteracting

this bump force results in a counteracting force on the wheel, which is compensated by the simulator. This iteration continues until the motion is damped out. Therefore, large oscillations can be present in such setups [47].

2.3.3 Steering force measurements

As discussed in the previous sections, the power supply of the steering system is not sufficient to output the requested steering torque as computed by the simulation software. Therefore logging the force feedback output of the steering system will not yield usable results, because the force in the non-linear area of the vehicle are filtered by the maximum performance of the system.

By taking a closer look at figure 2.9, one can see that the output signal of the simulation software corresponds with the output forces of the steering system. For the sake of logging steering forces in the simulator, use is made of the output signal of the simulation software. This force however, is a steering rack force. To convert it to steering column torque, the transversal force needs to be recalculated to a torque by using the steering gears. By consulting the manual for the F312 Formula 3 car, the pinion primitive diameter is 15.60 mm [29]. Given this value, either the rack force of the simulator can be converted to a steering torque or the steering torque of the car can be converted to a rack force.

Chapter 3

Analysis of test and simulation data

Whereas measurements in the simulator can be done without any limitations, measurements on the car are limited to private testing days as discussed in chapter 2. This chapter will elaborate on measurements performed in the real car and in the simulator with the baseline rFactor vehicle model. Differences and similarities will be discussed in order to know where the current model of the rFactor Formula 3 car lacks reality.

3.1 Circuito de Barcelona - Catalunya

During the winter test season preparing for the 2014 season, Van Amersfoort Racing performed a two-day test session at Circuit de Barcelona - Catalunya, Spain. This track is ideal due to its technical nature. The track contains both high speed and low speed section and makes it therefore ideal for performing steering torque measurements. The track layout is shown in figure 3.1.

In order to perform proper measurements, the same track has to be driven in the simulator. Given the open source character of rFactor, there are a wide variety of track maps available. The best track map is chosen by driving a few laps and compare the resulting data with real data retrieved from the cars. Trade-off criteria are corner radii, mid-corner speeds and grip levels. These aspects will be discussed in section 3.2. In the end, one track map remained, which forms the basis of measurements in the simulator.

It is common to give all corners on a track a specific number. This numbering is shown in figure 3.1 and used throughout this research. This track layout is generated by WinDARAB using lateral acceleration and speed information of one lap.

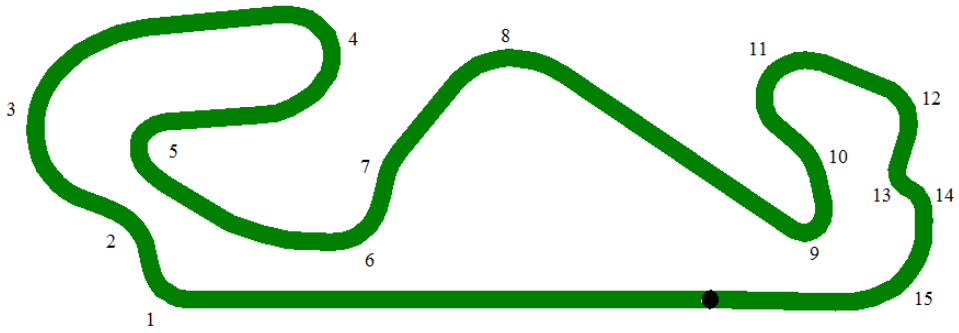

Figure 3.1: Circuit de Barcelona - Catalunya corner numbering.

3.2 Track map comparison

During the winter test sessions, one of the Formula 3 cars of Van Amersfoort Racing was equipped with a strain gauge on the steering column. Gustavo Menezes was the driver driving this strain gauged car. In the simulator, Atze Kerkhof drove the virtual rFactor Formula 3 car over the same track. The comparison between both laps are shown in figure 3.2, where speeds of both vehicles are shown. As can be seen, the highest difference in speed is on the straights where steering torque does not play a role, since there is no specific steering input by the drivers on normal straights. This difference is caused by an inadequate aerodynamic model of the rFactor Formula 3 car. The differences in speed start to grow from approximately 200 km/h, a region where aerodynamic effects are starting to become dominant. Taking a closer look at the corner speeds, the largest difference is present in turn 1, after the first braking zone. The difference in corner speed is 6.1 km/h. Since racing a Formula 3 car or a racing simulator is a human-in-the-loop interaction, every lap is different. Moreover, making use of two test drivers might cause difference in driving style. This however, is brought to a minimum by proper coaching.

In figure 3.3, two plots are shown. In the upper plot, lateral acceleration is shown as a function of distance. The lower figure shows the steering wheel angle as a function of distance. A general note which can be drawn from both figures, is that the drivers use the capabilities of the car to an equal extend. Peak lateral accelerations are similar. Steering wheel angles however, are harder to compare since they inhibit important balance information. Understeered cars require higher steering angles to perform a certain cornering maneuver compared to oversteered cars [54].

To compare each corner of the track, corner radii should be investigated. The corner radius of a corner is determined by the law of centripetal acceleration [55], given by equation 3.1. To be able to use this equation correctly, velocity and lateral accelerations should be measured at the center of gravity of the vehicle. In the Formula 3 car, the sensor is placed at the bottom of the monocoque underneath the safety seat. This is not the exact center of gravity of the vehicle as will be discussed in chapter 5, but the closest it can be placed given limitations and regulations. Apart from longitudinal and lateral accelerations, yaw rate is measured. These are the only sensors measuring the state of the vehicle. Velocity

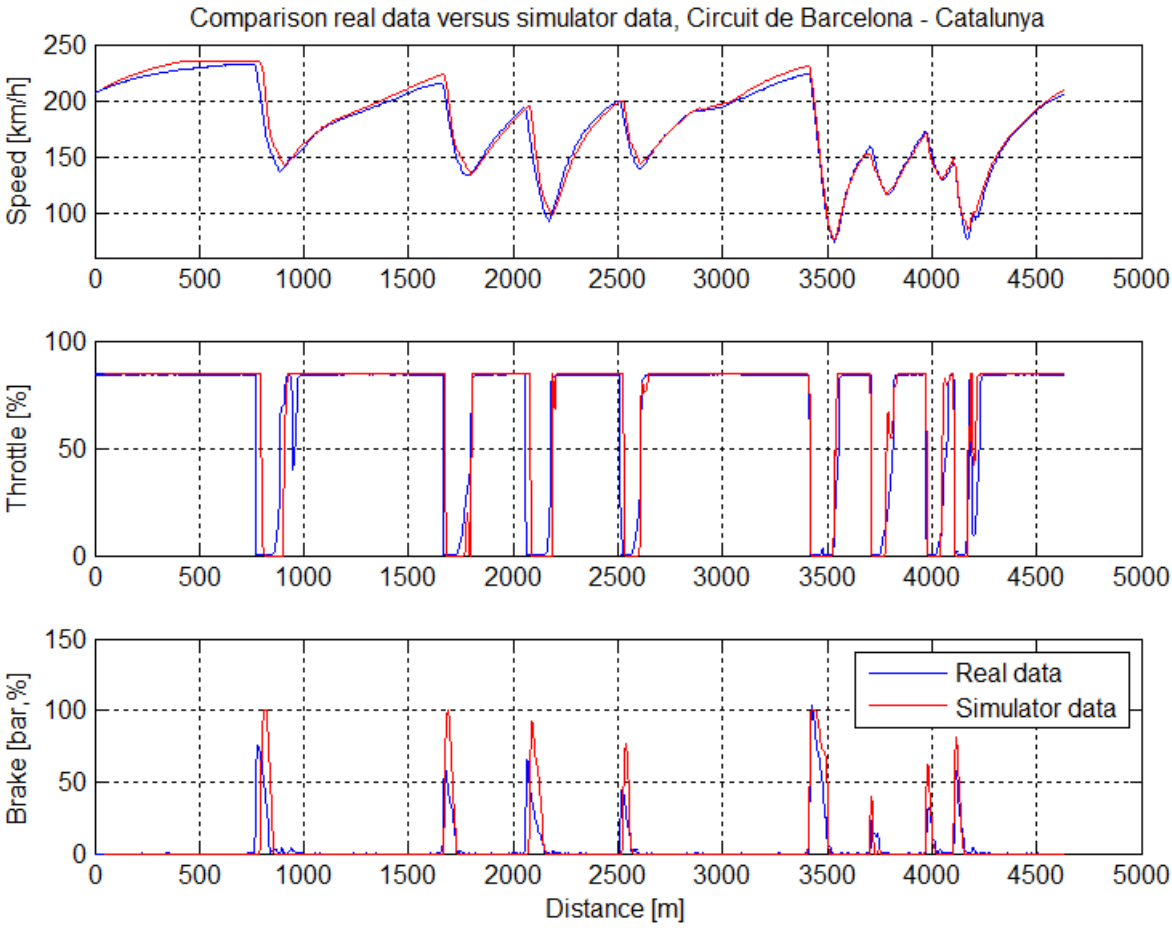

Figure 3.2: One lap compare. Speed, throttle and brake channels visible. Source [35] & [53]

is computed as the average of two wheel speed sensors. This is not always accurate as one of both wheels may lock during intensive braking. Suspension damper potentiometers read the lengthening and shortening of the dampers. This information can be used to determine the height of the vehicle or the roll angle in corners.

$$a_{lat} = \frac{V^2}{R} \tag{3.1}$$

Given this relation between lateral acceleration (in m/s^2), speed (in m/s) and radius (in m), the radius of the turn which the drivers tend to make while driving the track can be visualized, shown in figure 3.4. This figure shows the corner radii of all maneuvers having a lateral acceleration larger than 0.8 g. This filtering technique is required to filter out all noise in the acceleration channel. Without filtering, a small disturbance in lateral acceleration would lead to a large corner radius, according to equation 3.1.

Figure 3.4 can be used both to check racing lines of the drivers (the way they approach corners) and track layout of the real track and the rFactor track model. Turn 1 and 2

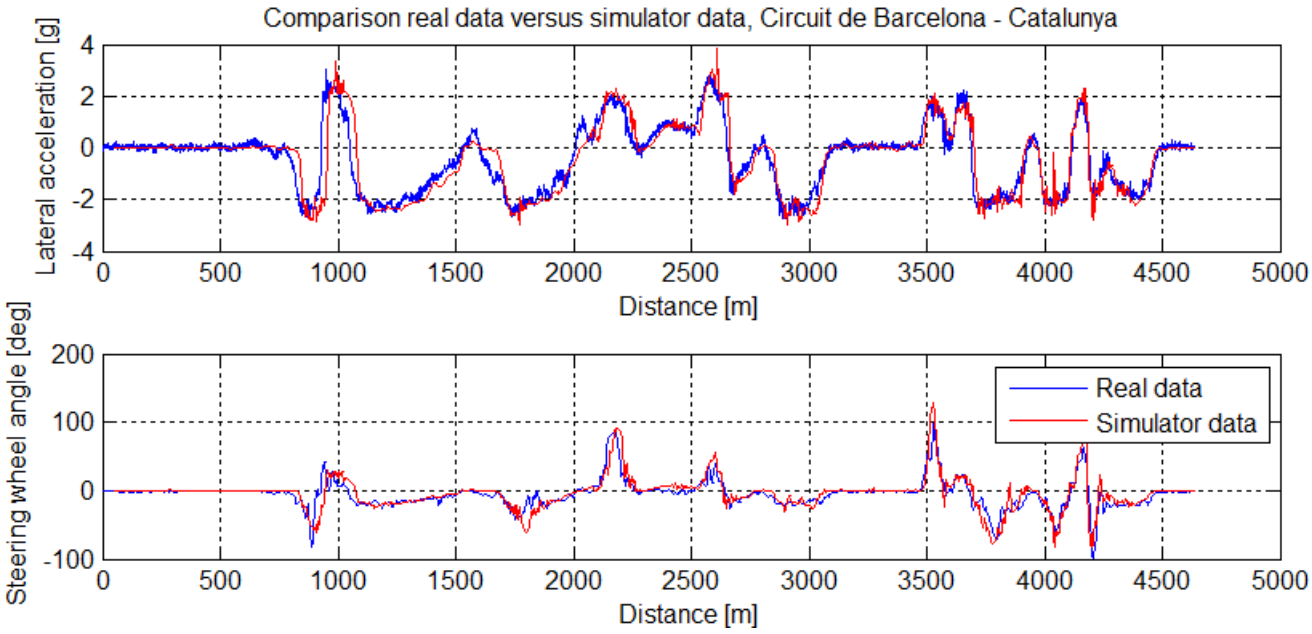

Figure 3.3: One lap compare. Lateral acceleration and steering angle shown. Source [35] & [53]

are similar in real and in the simulator. It seems however that the start finish straight is too long in the simulator. This can be seen by the fact that turn 1 starts later in the simulator than in the real data, whereas the distance from the exit of turn 15 to start finish is equal in both cases. The entry of turn 3 is tighter in the simulator than in real, since the corner radius is initially lower. The mid corner section of turn 3 is equal, but the exit of the simulator turn 3 looks more tight given a smaller corner radius. For turn 4, the same properties as for turn 3 apply, tight entry and exit of the corner but an equal mid corner radius. After this section of tighter simulator corners the extended start finish straight is compensated for, since the overlay of corners is equal after this section.

All corners in the following section have a similar trend. The mid corner radii are equal, but in the simulator the exits are tighter given the smaller corner radius at every turn exit. Only turn 10 is different from this trend. This corner is more open in the simulator than in real given the larger corner radius, yielding lower later accelerations. Furthermore turn 14 is in the simulator tighter than in real. This can be seen given the fact that the duration of turn 15 is shorter in the real than in the simulator. This straight section between turn 14 and turn 15 is therefore longer in real.

All differences are made visible by making an overlay of the generated track layout for both situations. In most race data analysis software, functions are available in which a track map can be generated given recorded lateral acceleration and vehicle speed. The overlay of both track maps shows exactly where the tracks differ from one another. This result is shown in figure 3.5.

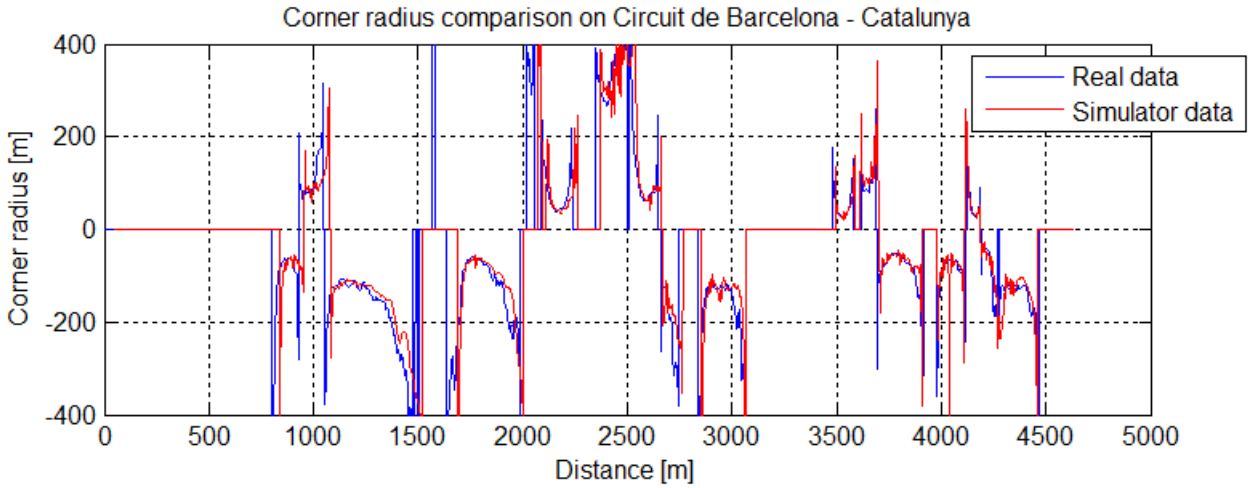

Figure 3.4: Comparison of corner radii for real car data and simulator data on Circuit de Barcelona - Catalunya.

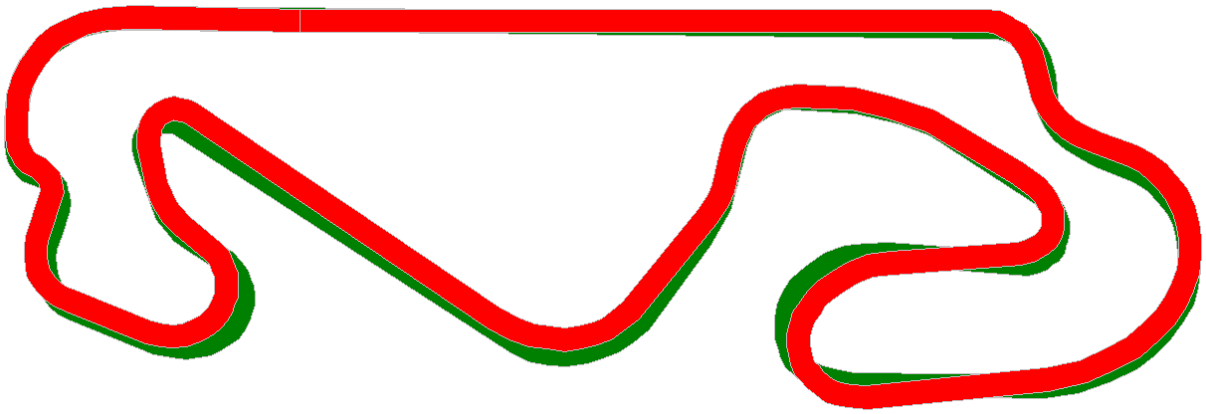

Figure 3.5: Overlay of track maps generated with real recorded data and simulator recorded data.

3.3 Vehicle behavior

In this section, the behavior of the car is analyzed. This analysis should give an insight at where the differences between the real car and the simulator model exist. The turns of the track are divided into three separate categories having specific properties to address car performance. These categories are high speed corners, low speed corners and chicanes.

To assess the differences and similarities of the simulator data compared to real car data, tests are required which show characteristics of both vehicles. A useful way of capturing properties and behavior of both vehicles is determining the steering metrics [56] according to Katzourakis (2012). These steering metrics consist out of the steering sensitivity and the steering torque gradient. The steering sensitivity is the gradient of lateral acceleration

per 100 degrees of steering wheel angle, given by equation 3.2.

$$\text{Steering sensitivity} = \frac{\partial \text{ lateral acceleration}}{\partial \text{ steering angle}} \cdot 100^\circ = \frac{\partial\ a_{lat}}{\partial\ \delta_{steer}} \cdot 100^\circ \tag{3.2}$$

The steering torque gradient indicates the required steering wheel torque to produce a certain lateral acceleration. It is determined by taking the gradient of steering wheel torque per lateral acceleration. In equation 3.3, the corresponding equation is shown.

$$\text{Steering torque gradient} = \frac{\partial \text{ steering torque}}{\partial \text{ lateral acceleration}} = \frac{\partial\ T_{steer}}{\partial\ a_{lat}} \tag{3.3}$$

Using these equations of steering metrics, a relationship can be found between the corresponding parameters, being lateral accelerations and steering angle and lateral acceleration and steering torque. These relations can be found using robust regression functions in MATLAB [56]. Using this regression technique, a characteristic equation of the first order is found. This equation is given by a gradient between the two parameters and an offset. Although the steering sensitivity is defined as lateral acceleration per 100° of steering wheel angle, the characteristic equation for steering sensitivity used in this report is actually the inverse steering sensitivity. In other words lateral acceleration is shown on the horizontal axis and steering wheel angle on the vertical axis.

3.3.1 High speed corners

The high speed corners are defined as the corners where the driver is able to keep the throttle (almost) full at relatively high speeds of approximately 200 km/h or above. In high speed corners, high lateral weight transfer plays an important role. In this category, turn numbers 3 and 8 are considered.

Turn 3

Turn 3 is the first high speed corner on this track. The turn starts directly after the exit of the second turn. The entry speed is approximately 170 km/h accelerating in the corner to the exit speed of 210 km/h. The turn is a right hand turn with full throttle applied through the complete corner. The real car is subjected to a lateral acceleration of 2.0-2.5 g.

Measurements performed both in the car as in the simulator are shown in figure 3.6. Here lateral acceleration, corner radius, steering wheel angle and steering torque are compared for both cases. As can be seen in the simulator data, the entry is tighter than for the real data given by a higher initial lateral acceleration. As discussed earlier, the exit opens more for the real car data given a larger corner radius. This was also shown in figure 3.5. Another observation is the magnitude of steering wheel torque. Simulator data shows that much more steering torque is present in the steering wheel compared to the real data. Furthermore, the real data show load variations of 10 Nm where the simulator data is more smooth.

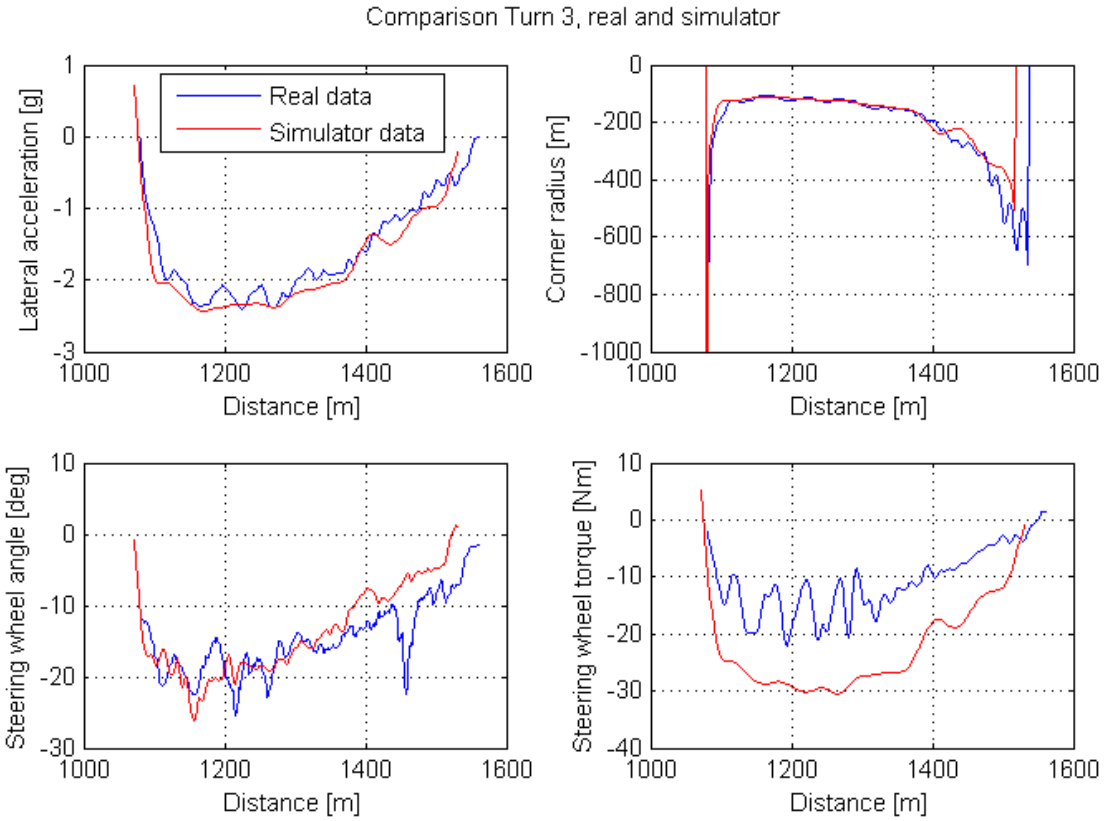

Figure 3.6: Overlay of data measurements with real recorded data and simulator recorded data of turn 3.

The steering metrics as discussed above are shown in figure 3.7. The regression line is also shown. The corresponding first order relations for the steering sensitivity are shown in equations 3.4 and 3.5, whereas the steering torque gradient is given in equations 3.6 and 3.7. Lateral acceleration is indicated by a_{lat}, steering angle δ_{steer}, and steering torque T_{steer}. The steering sensitivity is indicated by S and steering torque gradient by G.

$$S_{\mathrm{T3,real}} = 6.7780 \cdot a_{lat} - 3.4956 \tag{3.4}$$

$$S_{\mathrm{T3,sim}} = 10.5484 \cdot a_{lat} + 5.9618 \tag{3.5}$$

$$G_{\mathrm{T3,real}} = 7.1785 \cdot a_{lat} + 0.8414 \tag{3.6}$$

$$G_{\mathrm{T3,sim}} = 12.8303 \cdot a_{lat} + 0.7455 \tag{3.7}$$

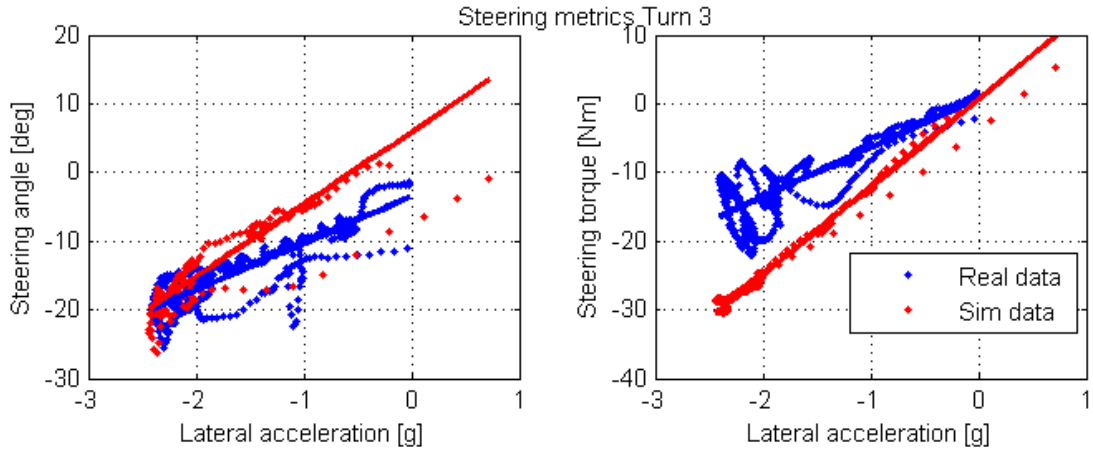

Figure 3.7: Steering metrics of turn 3.

Turn 8

Since turn 8 is located on a crest, it is blind and therefore a challenge for the driver. This difference in height throughout the corner has an effect on the balance of the car. The speed throughout the corner is approximately 200 km/h with full throttle for the complete turn. The steering metrics are shown in figure 3.8. In a similar fashion as for turn 3, the steering torque of the simulator data are higher than in the real car. Another important observation is the spread of steering angles for lateral accelerations of approximately -2.5 g. As can be seen at the left-hand side of figure 3.8, the simulator measurements show a spread of $-5°$ to $-30°$. This spread can be assigned to the imbalance of the car model in the simulator.

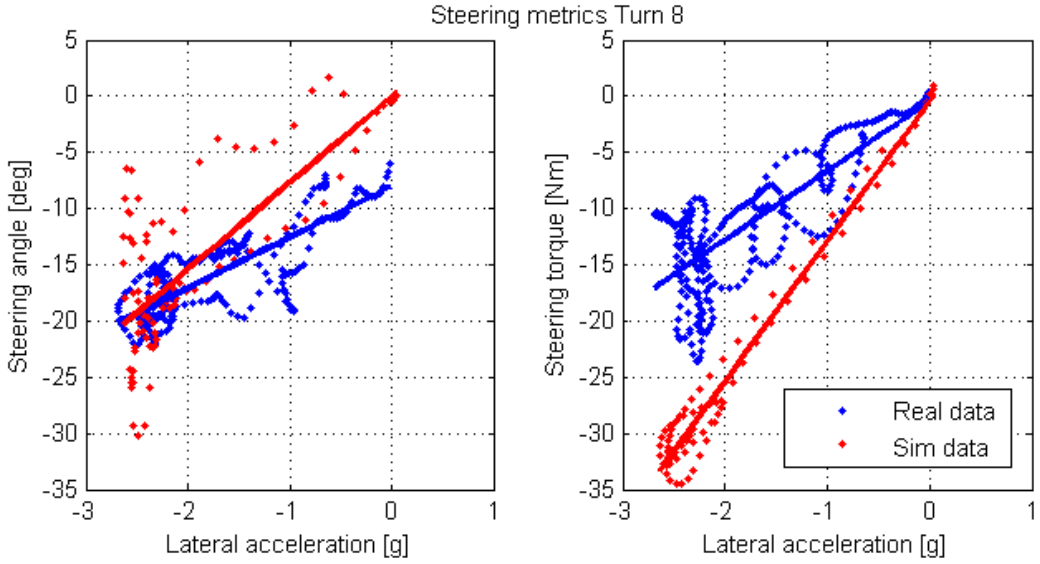

Figure 3.8: Steering metrics of turn 8.

The coefficients of the characteristic regression functions are given in tables 3.1 and 3.2.

These coefficients are based on the equations as demonstrated in equations 3.4 to 3.7. It also gives the percentual difference between the real measurements and the simulator measurements.

Table 3.1: Characteristic steering sensitivity equation coefficients for the high speed turns.

Turn	Gradient real	Gradient rFactor	Difference to real
3	6.7780	10.5484	55.63 %
8	4.4952	7.7149	71.63 %

Table 3.2: Characteristic steering torque gradient equation coefficients for the high speed turns.

Turn	Gradient real	Gradient rFactor	Difference to real
3	7.1785	12.8308	78.74 %
8	6.1363	12.4623	103.09 %

Although table 3.1 indicates that the steering sensitivity for turn 3 shows a difference of 50% with real measurements, the steering wheel angle for maximum lateral acceleration is equal as can be seen in figure 3.7. The measurement point for the simulation run are scattered, which is mainly caused by a bump in the road surface of the track model in rFactor. Apart from that, the steering wheel angle at maximum lateral acceleration is equal. Concerning the steering torque gradient, in general it can be seen that the gradient is higher in the simulator than in the real car. Higher steering torques are computed per lateral acceleration, which would require more effort of the driver to control the vehicle in the high speed turns. In the plotted steering metrics it is shown that the required steering torque per lateral acceleration is approximately twice as high in the simulator as in the real car, which is also mentioned in the differences in table 3.2.

3.3.2 Low speed corners

For the low speed corners, the driver has to brake hard in its approach and mid corner speeds do preferably not exceed 100 km/h. The challenge for low speed corners is to rotate the car as fast as possible. Low speed corners on this track are turn 5 and turn 9.

Turn 5

Turn 5 is a low speed, left-hand corner which is orientated downhill. The cars arrive with a velocity of approximately 200 km/h, braking into the corner to a mid corner speed of 100 km/h before going back on throttle. As can be seen in figure 3.1, turn 5 follows after the long right-hand turn 4. To go as fast as possible through turn 4, the cars end up completely at the left side of the track at the exit of turn 4. They bring back the car to the right-hand side of the track to prepare for the entry of turn 5. As a consequence, the driver needs to orientate the car straight before going into the corner. Therefore, there are two main lateral acceleration peaks found during turn 5. This phenomena is shown

in figure 3.9.

It can be concluded from the discussion above, that considering turn 5, not only the point at which the driver turns into the corner after the brake peak point has to be considered, but also the straightening maneuver that precedes the entry of the turn. If not, inaccurate results for the steering metrics yield, since the steering forces do not rise from neutral onwards as for the other turns, but start at their peak levels. These extended metrics are found in figure 3.10.

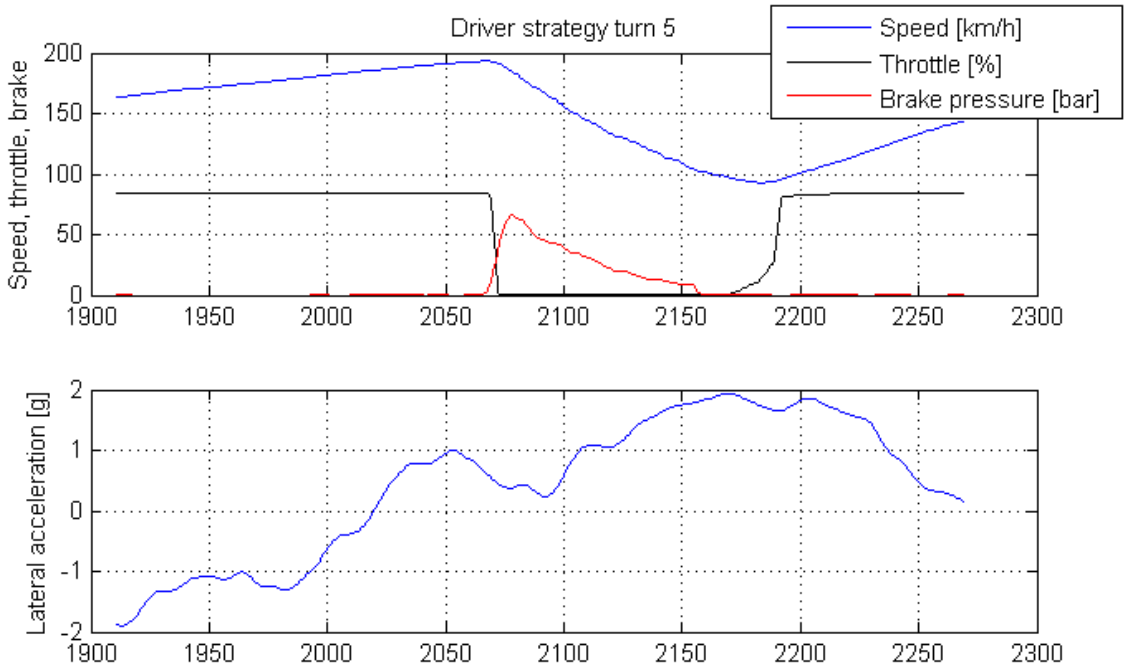

Figure 3.9: Driver strategy turn 5.

Turn 9

Contrary to turn 5, turn 9 is located at the end of a long straight. Therefore, the driver has already positioned the car to the most outer part of the track width. The driver approaches the corner with 225 to 230 km/h (the simulator vehicle having the higher top speed) and brake down to 75 km/h mid corner speed. Going too early on throttle may cause oversteer on the turn exit, which is visible in the steering metrics of turn 9, shown in figure 3.10. Looking at the steering sensitivity of the simulator vehicle, one can see that the steering wheel angle surpasses the $-20°$ angle. In a left-hand turn, only positive steering angles are expected for balanced cars.

Characteristic equations low speed turns

In tables 3.3 and 3.4, the characteristic equations for the low speed turns are given. The first observation which can be drawn from these tables is the inaccuracy of data for turn

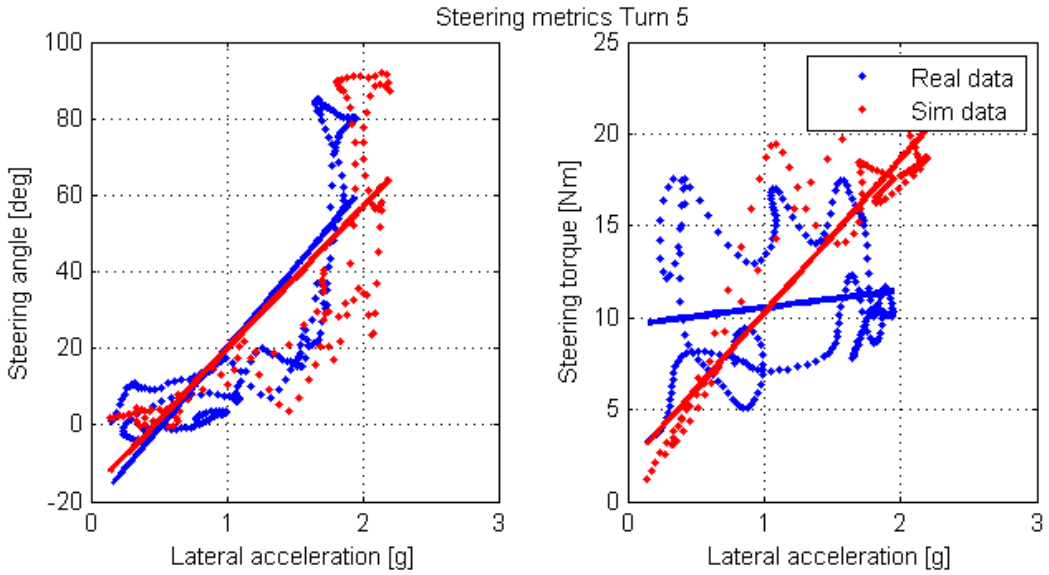

Figure 3.10: Steering metrics of turn 5.

5. As discussed in that section, the preparation for turn 5 makes it a difficult turn to consider. This is shown in the fact that, contrary to all other turns, the steering sensitivity of the real car for turn 5 has a higher gradient than the simulator vehicle. Considering the steering torque gradient, the gradient for the real car is low because of the spread of measurement points. Turn 9 however, confirms earlier found observations which showed that both the steering sensitivity and steering torque gradient are higher in the simulator than in the real car.

Table 3.3: Characteristic steering sensitivity equation coefficients for the low speed turns.

Turn	Gradient real	Gradient rFactor	Difference to real
5	41.8298	37.1699	-11.14 %
9	47.2414	54.7821	15.96 %

Table 3.4: Characteristic steering torque gradient equation coefficients for the low speed turns.

Turn	Gradient real	Gradient rFactor	Difference to real
5	0.9406	8.3584	788.62 %
9	4.4486	9.3366	109.88 %

3.3.3 Chicanes

Chicanes are defined as a close combination of left-right or right-left turns. Usually, the mid corner speeds are average to low. The challenge of a chicane is to change the wheel loads as quick as possible from one side of the car to the other. Two chicanes are present on this track, being the combination of turns 1 and 2 and turns 13 and 14.

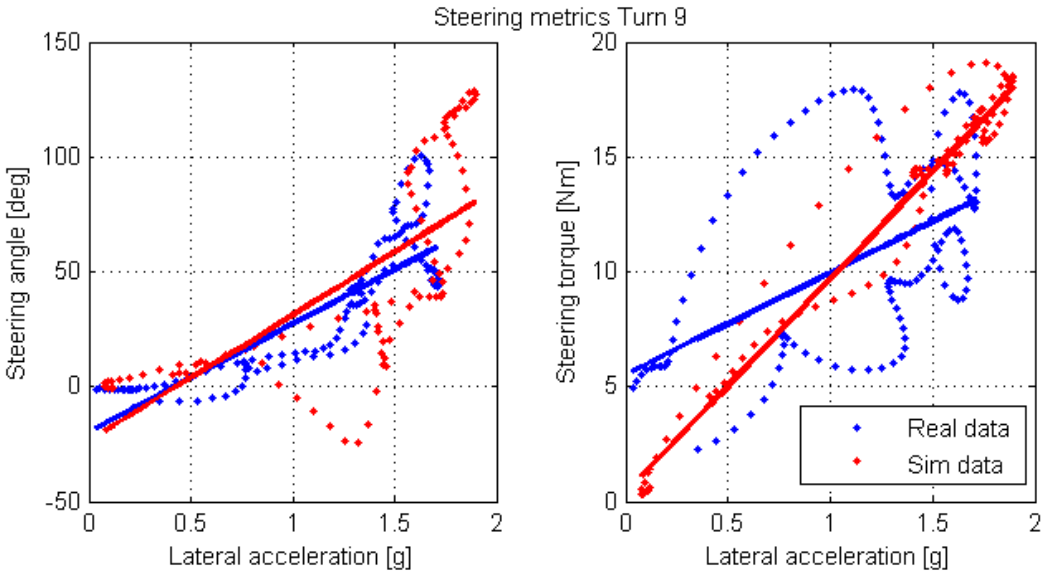

Figure 3.11: Steering metrics of turn 9.

Turns 1 and 2

The first turn of this track is where the cars arrive with high speed gained over the start/finish straight. The cars brake hard, reducing the speed from approximately 240 km/h to 150 km/h. On the entry of the turn, the drivers stays as much as possible to the left side of the track, steers into to corner and keeps the exit relatively tight to prepare for the left hand turn 2.

In figure 3.12, it can be seen that the steering angle for the real car is varying more than the simulator vehicle. This is demonstrated by the large negative steering angle at 910 meters and the large positive steering angle at approximately 960 meters. This suggests understeer in the car balance, since the steering angle is larger than the required steering angle to make the turn [54]. The simulator steering angle trace is more stable and does not show any large variations. This is also visible in the steering torque trace of both vehicles.

The steering metrics for turns 1 and 2 are given below. The understeering effect can be seen by the large steering angles, shown in the robust regression fit.

Turns 13 and 14

Turn 13 is preceded by the right-hand turn 12. This preparation is in a similar fashion as for turn 5. The exit of turn 14 merges with the entry of turn 15 as discussed earlier. The drivers approach turn 13 with approximately 150 km/h. The mid corner speeds of the real car and simulator car are not equal, the real car can only reach 70 km/h, where the simulator vehicle is able to reach 85 km/h as lowest speed in both turns. This has an effect of maximum lateral acceleration, which can be proved using equation 3.1. A larger speed yields a higher lateral acceleration, given a constant corner radius. The steering

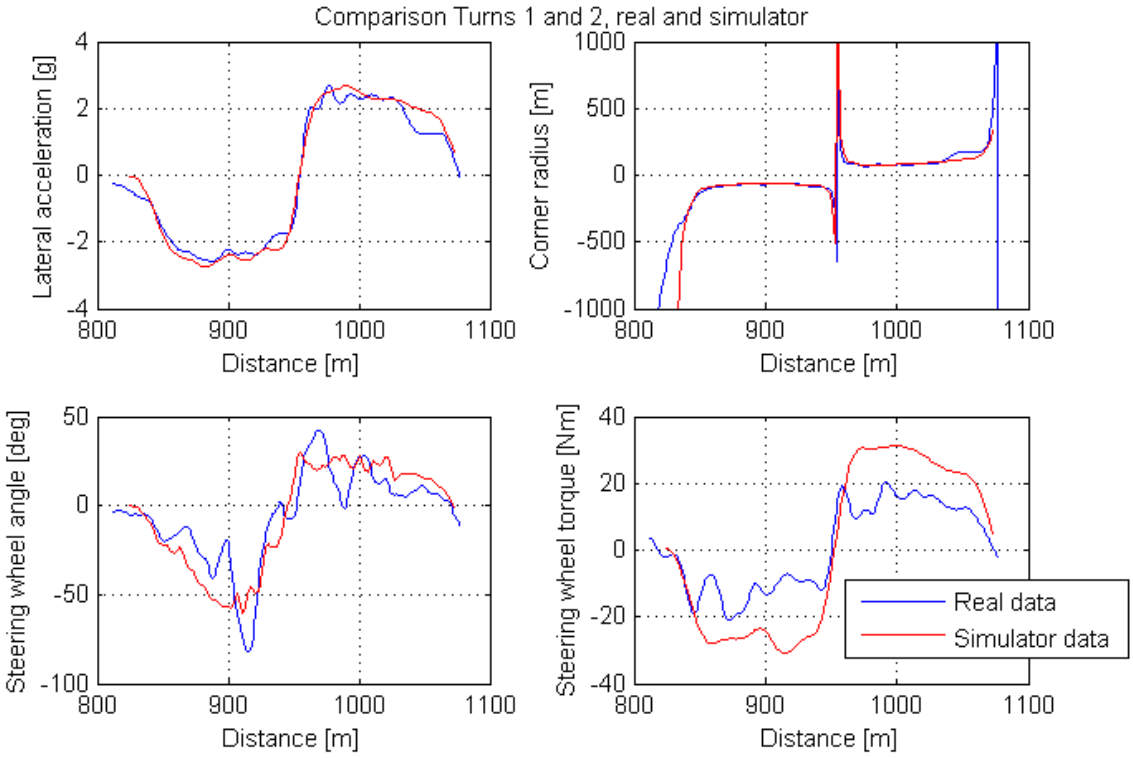

Figure 3.12: Driver approach for turns 1 and 2.

metrics for these turns are shown in figure 3.14. Here it is visible that the simulator vehicle attains a higher lateral acceleration.

Characteristic equations chicanes

Table 3.5: Characteristic steering sensitivity equation coefficients for the low speed turns.

Turn	Gradient real	Gradient rFactor	Difference to real
1 & 2	8.3192	12.7585	53.36 %
13 & 14	30.0544	28.4282	5.41 %

Table 3.6: Characteristic steering torque gradient equation coefficients for the low speed turns.

Turn	Gradient real	Gradient rFactor	Difference to real
1 & 2	6.1401	11.5384	87.92 %
13 & 14	7.1500	9.7153	35.88 %

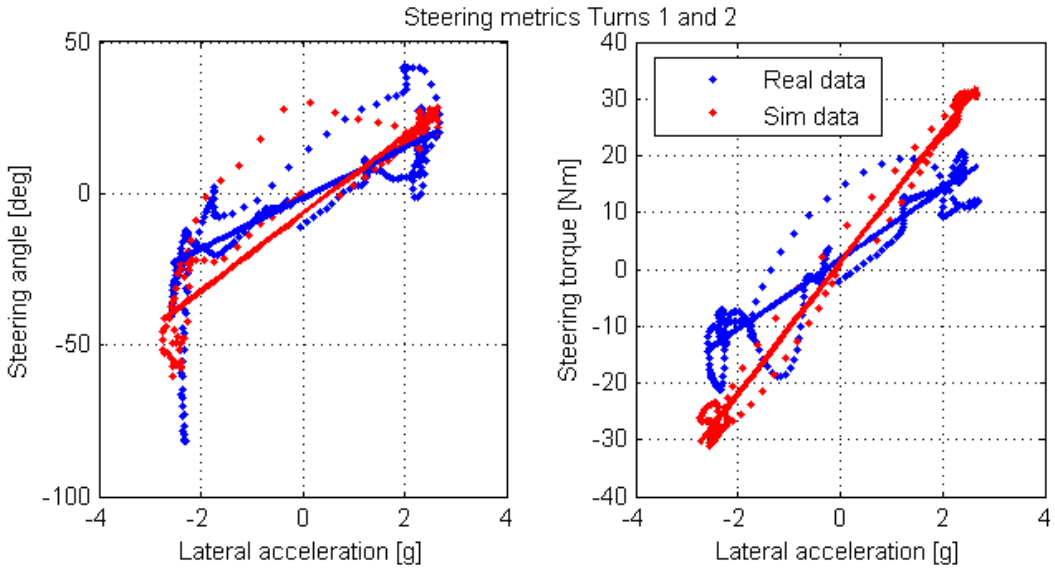

Figure 3.13: Steering metrics for turns 1 and 2.

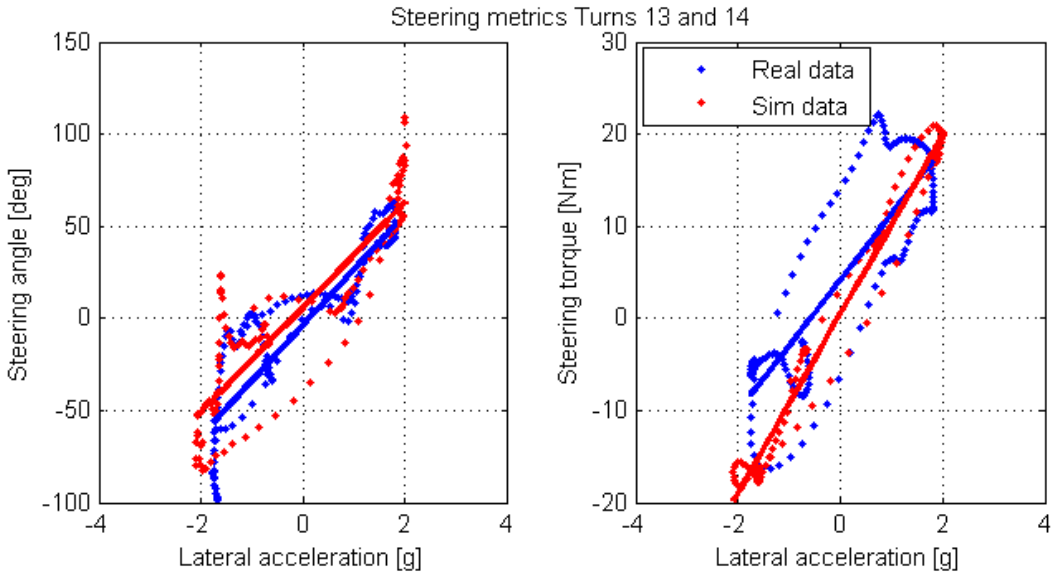

Figure 3.14: Steering metrics for turns 13 and 14.

3.4 Conclusion

In the previous sections, the steering metrics for the three classes of turns have been determined. These tests should give a framework for improvements of the simulator vehicle model. In this section the observations of the steering metrics are discussed.

The gradient of the steering sensitivity shows the steering wheel angle required for 1 g lateral acceleration. As concluded from equation 3.1, the lateral acceleration increased with increasing speed, given a constant corner radius. Therefore, a low gradient is expected for

the high speed turns as the speed is high. This is true comparing turn numbers 3 and 8 with the low speed turns 5 and 9. Comparing the real car data with simulator data, it is obvious that in the simulator more steering angle is required to gain a lateral acceleration, as the gradient in the simulator is higher. Consequently, the simulator vehicle is not as sensitive to a steering input as the real car.

Steering torque gradient is a measure of the magnitude of steering torque required to gain a lateral acceleration of 1 g. When the speed increases, the driver has to put in more effort to rotate the steering wheel. Therefore it is expected to have a higher steering torque gradient for the high speed corners. It is indeed true that the high speed turns require more steering torque since the gradients for high speed turns are higher. An observation made in all previous sections is that the steering torque gradient for the simulator is much higher than for the real car. That means that the simulator driver has to put in more effort to gain a lateral acceleration than the real driver. However, it must be noted from section 2.3.2 that the forces felt in the simulator do not reach the values as computed by the simulation software.

It can be concluded that there is room for improvement in both steering sensitivity as steering torque gradient. In this following chapters, an updated rFactor Formula 3 model is created by improving the tyre model and suspension model.

Chapter 4

Tyre models

In this chapter, a closer look is taken at the tyre model used in the rFactor vehicle model. The method of modeling of tyres is analyzed to understand the effect of typical tyre parameters on the tyre model. Furthermore, coefficients of a Pacejka tyre model of the Hankook Formula 3 tyre is available and are used to generate a new rFactor tyre file. At the end of the chapter, the effect of the new tyre file is analyzed using simulator data from both tyre files. The comparison with real data is performed in a later stadium.

4.1 rFactor tyre model

As discussed in chapter 2, rFactor is based on separate submodels. The complete model consists out of multiple files, each describing a section of the complete vehicle model. The tyre model is captured in one file, called the TBC file [60]. The TBC file of the baseline rFactor Formula 3 tyre model is given in appendix A. The rFactor tyre model is explored and elaborated in this section.

4.1.1 Slip curves

The rFactor tyre model consists mainly out of normalized slip curves with a peak value of 1.00. Individual slip curves for lateral tyre forces and longitudinal tyre forces are possible, although the tyre model used in the current Formula 3 vehicle model only uses a single slip curve both for lateral and longitudinal slip. The slip curve is a vector containing 237 values which are connected using a cubic spline [57].

A step parameter is defined, assigning a certain slip value to a data point in the slip curve vector. In the current tyre model, each step in the vector is an increase of 0.00900 in slip value. In case of longitudinal slip, this value corresponds to the SAE definition of slip as

shown in equation 4.1 [58]. The lateral slip value is converted to a slip angle by applying the inverse sine on the slip value.

$$S = -\frac{V - R_e \cdot \omega}{V} \tag{4.1}$$

The slip curve defined by the vector given in the tyre file of rFactor, is normalized to have a peak value of 1.00. The first step into converting it to lateral slip or longitudinal slip curves is multiplying the slip vector with coefficients of the vector called *DryLatLong*. This vector defines the coefficient of friction, which is the unitless ratio of friction force over normal force [59] shown in equation 4.2, where F_z is the normal tyre force. This equation shows the friction coefficient for lateral grip, replacing the lateral force F_y with F_x, yields the longitudinal friction coefficient. The two values in this vector determine the friction coefficient value both for lateral as longitudinal slip.

$$\mu_y = \frac{F_y}{F_z} \tag{4.2}$$

4.1.2 Tyre load sensitivity

Tyres are load sensitive, which means that the coefficient of friction decreases with increasing wheel load [34]. In other words: the ratios of Fy/Fz and Fx/Fz decrease with increasing load [34]. This effect in tyre dynamics is also applied to the rFactor tyre model by defining the *LoadSens* vector. This vector contains three values which are used to determine a multiplication factor to the coefficient of friction for a given load. This relation is given in equation 4.3, provided by rFactor developer ISI [60]. They define the change of friction coefficient as a grip multiplier. In other words, increasing wheel loads affect friction coefficients which is computed by the grip multiplier. By filling in equation 4.3, the grip multiplier as a function of wheel load is computed. This multiplier is then multiplied by the friction coefficient to yield the tyre load sensitive coefficient of friction.

$$TLS = \frac{2 + FL * IS - 2 * FM}{FL^3} * F_z^3 + \frac{3 * FM - 3 - 2 * FL * IS}{FL^2} * F_z^2 + IS * F_z + 1 \tag{4.3}$$

Equation 4.3 is built up out of the parameter *LoadSens* mentioned above. This vector contains three values, the first being the initial slope (IS) of grip multiplier as a function of wheel load. The second value is the final grip multiplier (FM) value which is present at the final load (FL) given as third value in the *LoadSens* vector. Furthermore, F_z is the normal load per tyre. To illustrate the load sensitivity behavior of the tyre, a plot is shown in figure 4.1.

The resulting grip multiplier determined by evaluating equation 4.3 given a certain tyre load, is multiplied over the complete slip curve as established in section 4.1.1. The higher the wheel load, the lower the coefficient of friction. To sum up the tyre model up to this point, figure 4.2 is given. It is clearly visible that the coefficient of friction is lower for

Figure 4.1: Modelation of tyre load sensitivity in rFactor, decreasing grip with increasing tyre load.

higher wheel loads.

Another effect of increasing wheel loads is the variation of peak slip angle. This is already illustrated in figure 4.2. According to Milliken [34], the peak slip angle increases with increasing load. In the rFactor tyre model, this effect is modeled by the usage of the *LatPeak* and *LongPeak*. These vectors consist out of three values. The first value indicates the peak slip angle (for lateral tyre forces) or peak slip ratio (for longitudinal tyre forces) at zero load. The second value of this vector indicates the peak slip angle or peak slip ratio at the wheel load given by the third parameter. In between these values of wheel load, the relation between slip angle or slip ratio and wheel load is described by half a sine wave, starting and ending level [60]. This relation is shown in figure 4.3. In this particular case, the lateral characteristics are shown. The peak slip angle versus wheel load are shown. In the same fashion, slip ratio versus wheel load can be constructed.

4.1.3 Camber

The camber angle of a wheel is defined as the angle between the tilted wheel plane and the vertical. A camber angle is defined positive if the wheel leans outward at the top relative to the vehicle [34]. Due to this camber angle, the contact patch is distorted which leads to an increase of lateral force for a specific slip angle compared to a normal orientated tyre. This effect is modeled in rFactor by using the vector *CamberLatLong*. This vector has three parameters. The first parameter is the peak camber angle at which a change in the coefficient of friction is present. The second parameter defines the increment of friction coefficient at the peak camber angle, whereas the last parameter represents the longitudinal friction coefficient loss of a camber angle of 90° [57].

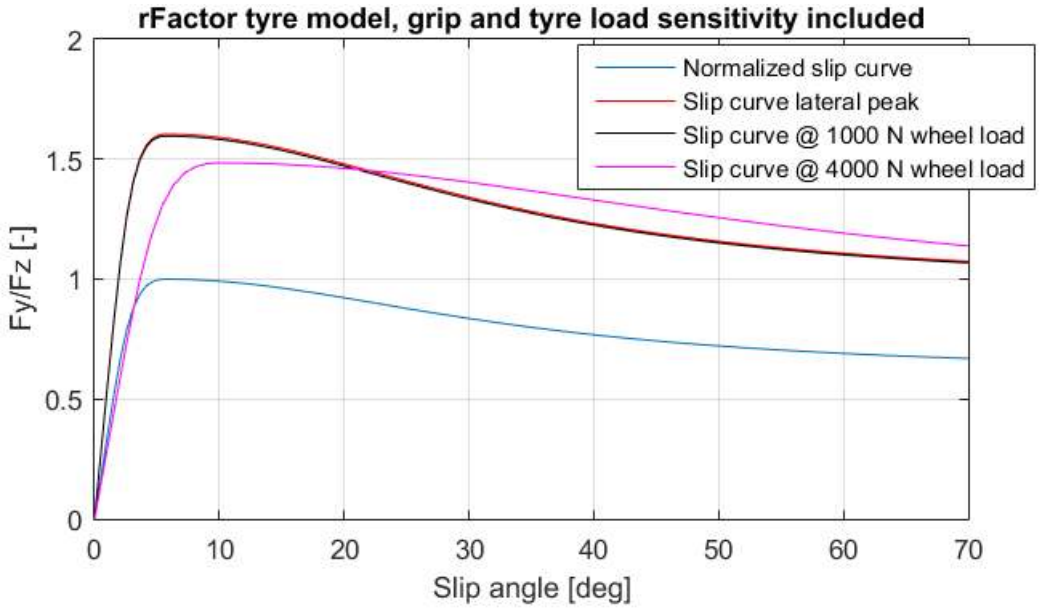

Figure 4.2: Construction of rFactor tyre model. Friction coefficient and tyre load sensitivity included.

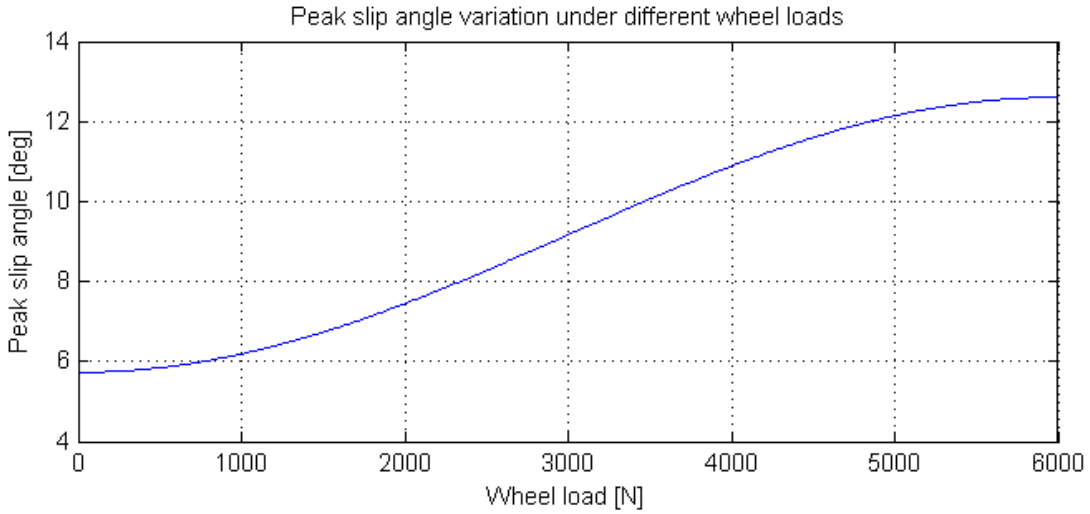

Figure 4.3: Relation between wheel load and peak slip angle.

The lateral coefficient of friction increment is a function of camber angle. The actual relation between these two parameters is given by a quarter of a sine wave, having a specific slope at zero camber angle and zero slope at peak camber angle. This relation is shown at the left hand side of figure 4.4 to clarify the influence of camber angle. After the peak camber angle, the friction coefficient increment drops-off linearly [60]. At the right hand side of figure 4.4, one can see the relation between camber angle and longitudinal grip loss. As one can image, decreasing the contact patch area (which happens by introducing a camber angle) decreases the longitudinal coefficient of friction.

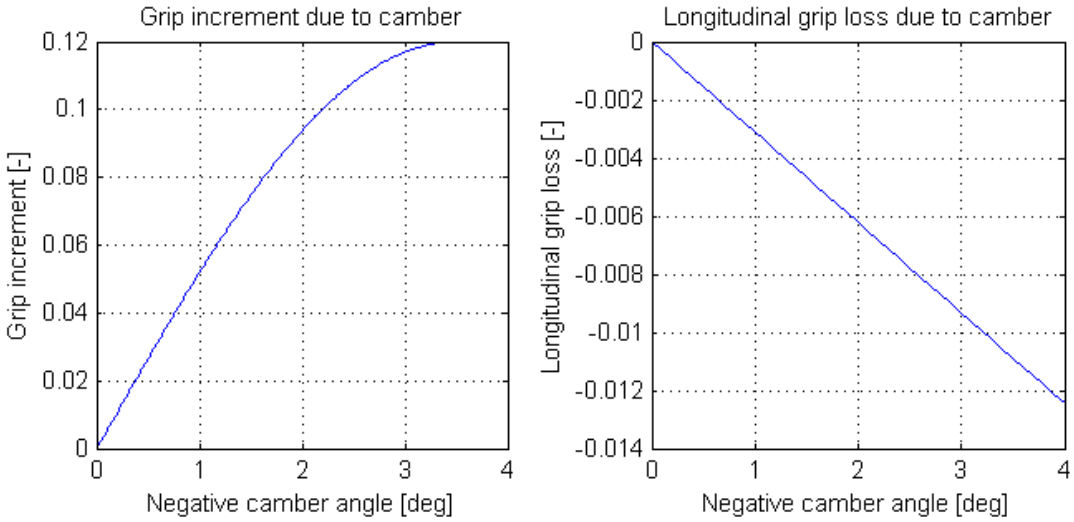

Figure 4.4: Effect of camber variation on lateral and longitudinal properties of the rFactor tyre.

4.1.4 Aligning moment

In the previous part of this chapter, the TBC tyre file of rFactor has been examined. In the TBC file, slip curves are defined and reshaped according to other parameters from this file. As discussed, the influence of weight on the lateral force generation capability has been examined, as well as the influence of camber. The effect of these parameters are directly related to the lateral and longitudinal slip curves.

The aligning moment of a tyre is an aligning property of a tyre. If the tyre is placed under a slip angle, the aligning moment generates a torque as such that the tyre aligns its heading with its path [34]. The origin of the aligning moment is the shape of the print of the tyre. Since print is triangular shaped, the point at which the resultant force works is not necessarily the center of the print. This offset is called the pneumatic trail and varies with slip angle.

Given the fact that the aligning moment is a consequence of the state of the vehicle, the rFactor programmers did not give a possibility to define a aligning moment curve in the same fashion as for longitudinal or lateral slip. The coefficient *PneumaticTrail* is defined in the TBC file which constructs, given the slip curves of the current tyre and its state, an aligning moment curve. However, the pneumatic trail of the TBC file is a single value. The relation between pneumatic trail and slip angle is undefined and hard coded into the rFactor source code. Therefore, research on aligning moment cannot be performed in the same manner as described in previous sections.

4.2 Hankook Formula 3 tyre model

The actual tyre used in the European Formula 3 Championship is the Hankook Formula 3 tyre. This tyre has been modeled into a Pacejka tyre model [64]. This model is used to compare the rFactor tyre model to the real Hankook Formula 3 tyre.

4.2.1 Pacejka tyre model

The Magic Formula is a semi-empirical tyre model used to calculate steady-state forces and moment characteristics. It is called the Pacejka tyre model, named after its developer, Hans Pacejka [61]. The Magic Formula model consists out of equations describing the characteristics of the tyre. These equations contain non-dimensional model parameters and scaling factors which are obtained by putting the tyre on a test bench.

The tyre model is then build by using the equations given by Pacejka [61]. These describe the tyre behavior in pure slip conditions as well as in combined slip conditions.

4.2.2 Slip curves

The slip curves of the Hankook tyre are constructed by inserting a vector of slip angles for lateral force production and a vector of slip ratios for longitudinal force production into the Pacejka tyre model. In contrast to the rFactor tyre model, it is not possible to generate a slip curve where normal load on the tyre does not play a role. Slip curves show the coefficient of friction for a range of slip angles. The friction coefficient is the ratio of generated lateral force over the normal force on that tyre. Ignoring the normal force or assuming it to be zero yields a non existing result.

By introducing static wheel loads, slip curves can be constructed both for the rFactor tyre as the Hankook tyre. These static wheel loads are determined by the minimum weight of car plus driver as stated in the Formula 3 regulations [62]. It is stipulated that the minimum weight of the vehicle including driver and fluids is 565 kilogram. The weight distribution of the car is determined to be 42.2% [63], which means 42.2% of the vehicle's weight is carried by the front axle. The remaining 57.8% is distributed over the rear axle. Calculating and rounding the static wheel loads yield a static front wheel load of 120 kilogram and a static rear wheel load of 165 kg.

Figure 4.5 shows the slip curves of the rFactor and Hankook tyres at the static wheel load as discussed. Similar to preceding simulations, the front tyre is considered here. Remarkable about the rFactor tyre is that the lateral and longitudinal properties are equal. The slip curves have the same shape, which already became clear from the TBC tyre file (one vector for both directions). Obviously, the curves are scaled to accommodate for slip angle and slip ratio. Comparing the shape of lateral slip curves of both tyres shows that the Hankook tyre possesses a peak friction force after which the friction drops more direct than the rFactor slip curve. A relatively lower peak slip angle is followed by a

sharp drop off in friction coefficient until an asymptote is reached. This is in contrast to the rFactor tyre which coefficient of friction drops off gradually after the peak, without a visible asymptote approach.

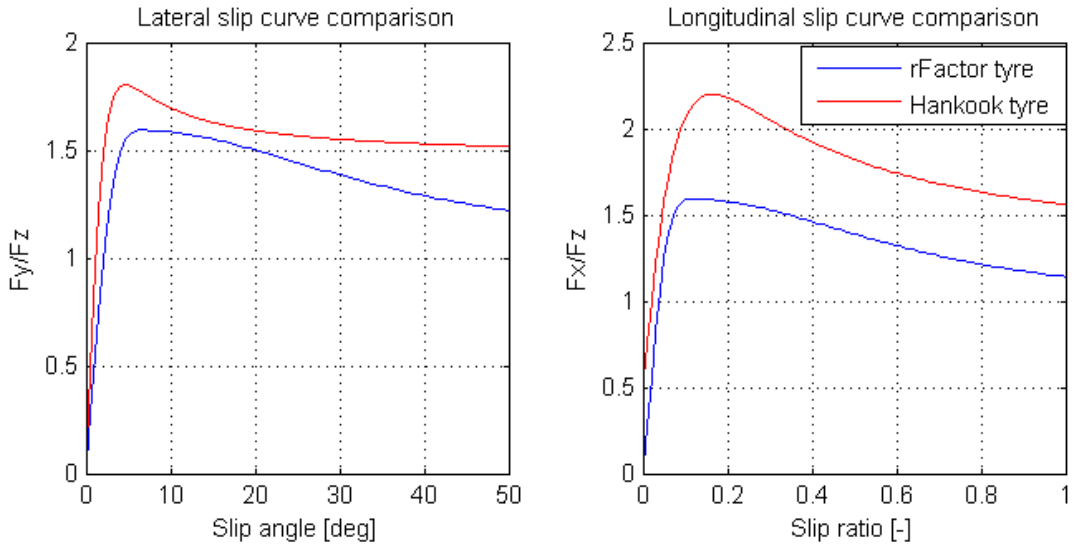

Figure 4.5: Slip curves for the rFactor and Hankook tyre. Static front wheel loads, no camber.

The peak friction coefficients of the Hankook tyre are higher than for the rFactor tyre, both lateral as longitudinal. The difference in peak friction coefficient is highest under longitudinal conditions. For the rFactor tyre, both peak friction coefficient values at static wheel load is 1.5926. The Hankook tyre has a peak value for Fy/Fz of 1.8018 and a peak value for Fx/Fz of 2.1982. It can be concluded from this observation that the grip of the rFactor tyre is lower than the Hankook tyre.

Slip curves consist out of three regions according to Milliken (1995). In the initial region, called the elastic region, is the region where a linear relation between slip angle (or ratio) and friction coefficient is found. The transitional region is where the transition between the linear relation and the peak slip angle is found. The last part, known as frictional region, starts from the peak slip angle and continues for the remaining possible slip angles. In the elastic region, the coefficient of friction is sufficiently high to prevent the tyre's footprint from sliding over the road surface [34]. This region can be approximated by a linear trend between slip angle and friction coefficient, where the slope of this relation is called the cornering stiffness. It can be seen in figure 4.5 that the cornering stiffness of the Hankook tyre is higher than the rFactor tyre.

4.2.3 Tyre load sensitivity

In the same fashion as for the rFactor tyre, it is useful to investigate the effect of normal load on the friction coefficient the tyre is able to generate. In figure 4.6, the effect of normal load on both the rFactor and the Hankook tyre is shown. On the vertical axis,

grip multiplier is used. This coefficient is the mulitplication factor added to the friction coefficient to incorporate tyre load sensitivity as explained in section 4.1.2. As stated above, zero load on a Pacejka tyre model is non existing, the reference normal load is 100 Newton. It can be observed that in contrast to the rFactor tyre, the Hankook tyre has a linear decrease in grip with increasing weight. Furthermore, the drop in grip is more severe for the Hankook tyre than for the rFactor tyre. In other words, the rFactor tyre is affected less by tyre load sensitivity. The weight penalty of reduced grip for additional weight is not as high as for the Hankook tyre.

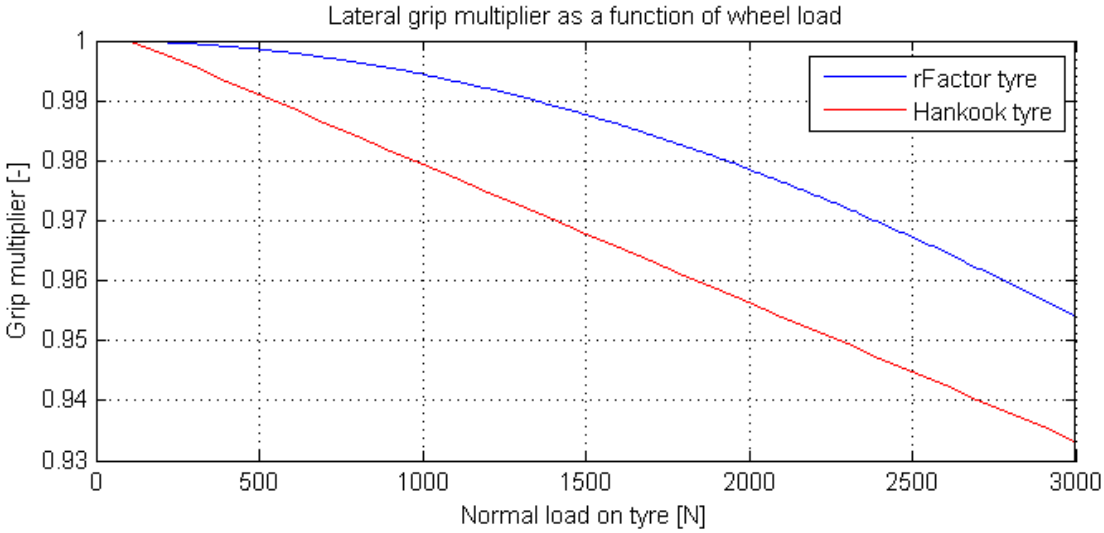

Figure 4.6: Effect of normal load on tyres on lateral grip producing capabilities.

The peak slip value is related to the normal load on a tyre as discussed for the rFactor tyre. Therefore it is investigated what the relation between peak slip values and normal load for the Hankook tyre is. Referring back to the discussion for this relation of the rFactor tyre: the modeling of this relation is represented by a half sine wave, starting and ending horizontal as can be seen in figure 4.3. In this figure, the load variation considered is between zero and 6000 Newton. The same analysis is done for the Hankook tyre. The result is shown in figure 4.7.

Remarkable about the lateral characterstic of the peak slip angles, is the shape of the Hankook tyre. For low normal loads, the peak slip angle is relatively high and drops to a minimum value at a normal load of 2000 Newton. Then it follows the same shape as the representation of the rFactor tyre. This is visualized in figure 4.8. The Hankook tyre reaches its maximum peak slip angle at a load of approximately 1900 kilogram, a load which will never occur with the current application of these tyres.

Longitudinally, both tyres behave completely different under increasing normal load. Where the rFactor tyre has a high peak slip ratio for higher loads, the Hankook tyre has a decreasing slip ratio peak for increasing load. It has to be mentioned that the horizontal shift in slip curve plays an important role for this specific case. The horizontal shift, known as S_{hx} in Pacejka's "Tyre and Vehicle Dynamics" [61], are introduced to have

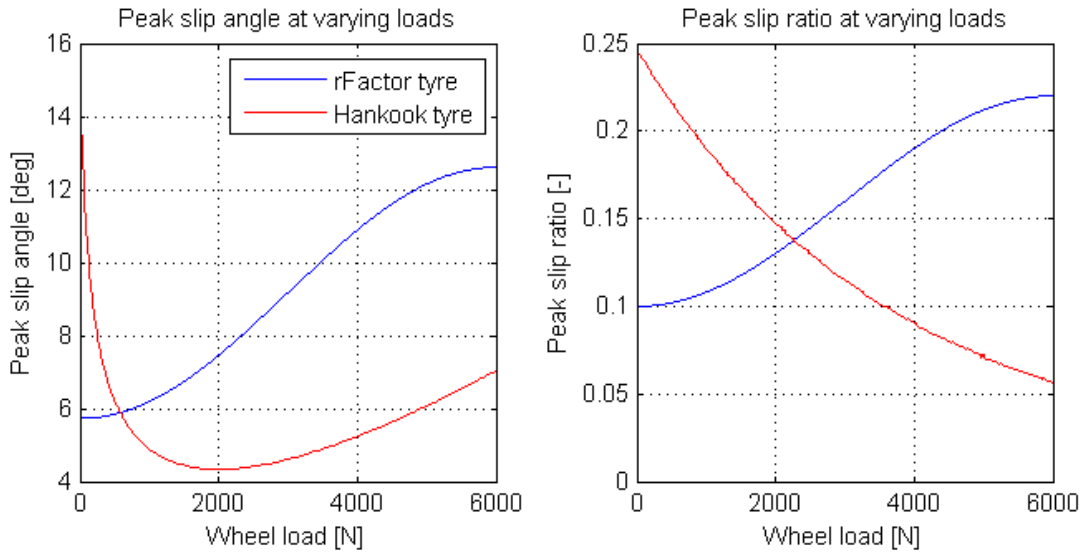

Figure 4.7: Shift of peak friction coefficient for increasing weight.

a offset from the origin. The offsets S_h and S_v appear to occur when ply-steer, conicity effects and possibly the rolling resistance cause the F_y and F_x curves not to pass through the origin.' [61], p174.

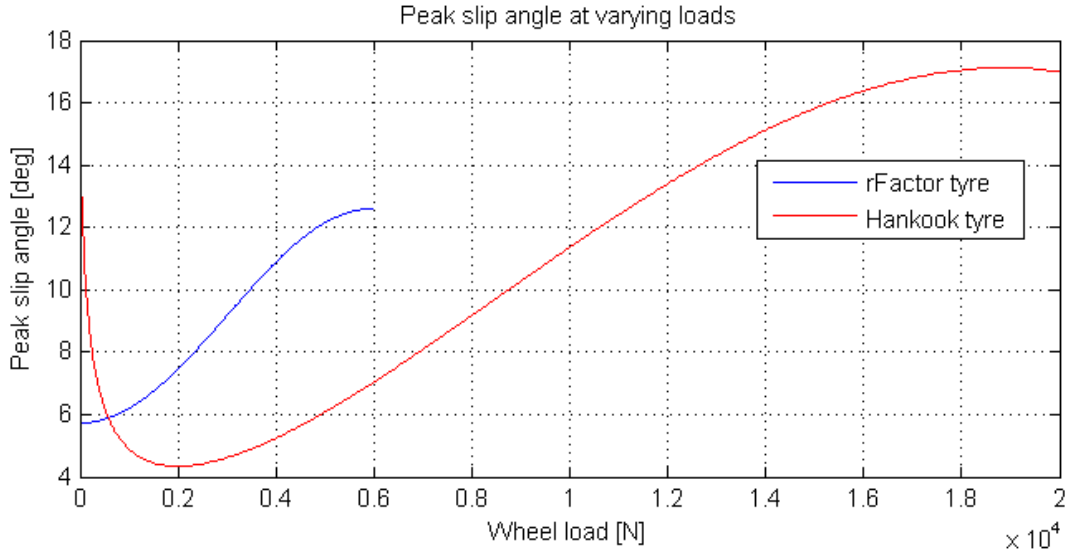

Figure 4.8: Peak slip angle shape comparison.

The governing equation calculating S_{hx} is given in equation 4.4. The two coefficients p_{hx} are weight related coefficients. The first coefficient p_{Hx1} is the horizontal shift parameter at nominal load. The second parameter p_{Hx2} is the variation of the horizontal shift with load. In other words: if nominal load is applied to the tyre, the horizontal shift depends of the p_{Hx1} coefficient. Every increment or decrement of weight introduces a horizontal shift larger than the horizontal shift at nominal load. Furthermore, a coefficient df_z is

present. This is the normalized change in vertical wheel load with respect to the nominal tyre load [61]. Lastly, the parameter λ_{Hx} is a scaling factor which equals zero for the given Pacejka data set [61], [64].

$$S_{Hx} = (p_{Hx1} + p_{Hx2} \cdot df_z) \cdot \lambda_{Hx} \tag{4.4}$$

The horizontal shift as discussed above, leads to the slip curves as shown in figure 4.9. It is stated that the closer the wheel load approaches the nominal load of 2244.4 Newton [64], the smaller the horizontal shift with respect to the origin. Smaller or larger wheel loads induce a horizontal shift. As expected, the slip curve corresponding to a normal force of 3000 Newton has the smallest horizontal shift as it is the curve with a wheel load closest to the nominal wheel load.

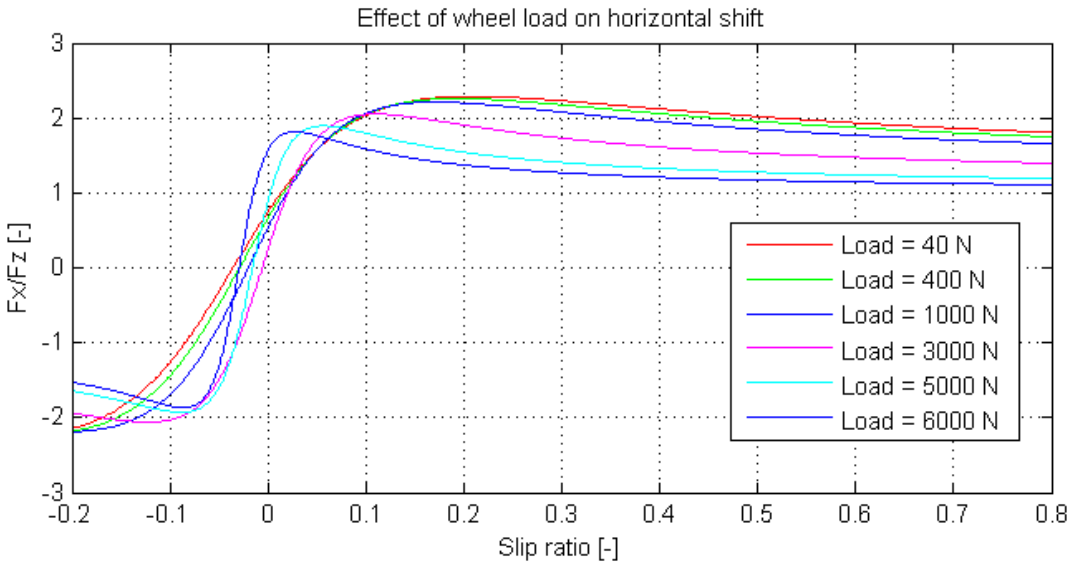

Figure 4.9: Horizontal shift introduced by changing wheel loads.

4.2.4 Camber

At the beginning of this chapter, the way camber is incorporated into the rFactor tyre model is elaborated. In the TBC tyre file, an optimum camber angle at which the grip increment is maximum is stated. The relation between grip increment and negative camber angle is given by a quarter of a sine wave, having zero slope at the optimum camber angle, as is displayed in figure 4.4. The longitudinal grip loss is also stated in the tyre file. This loss is related to the camber angle by a linear relation.

In order to compare the behavior of both tyres under varying camber angles, slip curves of both tyres will be constructed first. Since the optimum camber angle of the rFactor tyre is 3.5° [57], camber angles up to 4° are considered. The lateral slip curves are shown in figure 4.10. The first remarkable observation comparing both tyres is the sensitivity for camber changes on the rFactor tyre. The Hankook tyre is less sensitive to camber

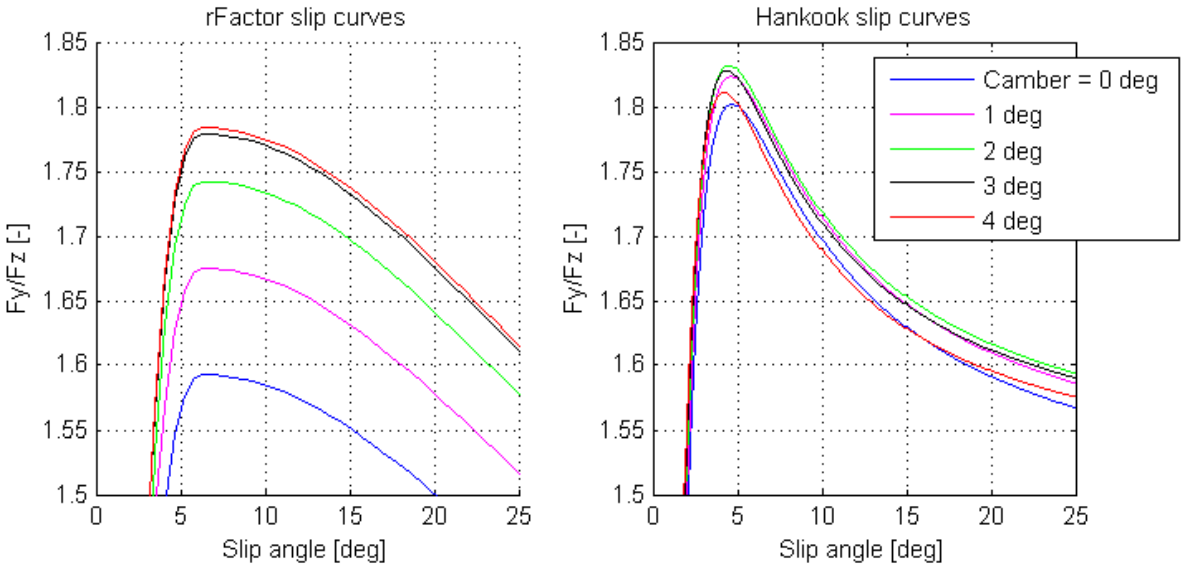

Figure 4.10: Influence of introducing camber angles on lateral slip curves of both tyres.

changes, where the peak friction coefficient is within a value of 0.05 range. Taking a close look at the Hankook slip curves, one can see the peak camber angle between 2 and 3 degrees having the two highest peaks. Higher and lower camber angles make the friction coefficient drop.

Longitudinally, the slip curves of both tyres also have a different behavior. In figure 4.11 it can be seen that the rFactor tyre is hardly effected by introducing a camber angle in longitudinal terms. The curves are nearly the same, where the Hankook slip curves clearly suffer from increasing camber angles.

The discussed differences about how both tyres react on camber angles is summarized in figure 4.12. Here it is shown what the effect of camber is on the overal grip of the tyre. In lateral sense, the rFactor tyre gains more lateral grip than the Hankook tyre. Furthermore, the peak camber angle for the rFactor tyre is higher than the Hankook tyre. Longitudinally, the rFactor tyre is less sensitive to camber angles than the Hankook tyre. The longitudinal grip loss is lower for the rFactor tyre.

4.2.5 Rear tyres

The differences between the rFactor front and rear tyre are limited. The basic slip curve for front and rear tyres are equal. In terms of friction coefficient, the rears have more grip. The *DryLatLong* coefficient increases with 0.06 to a value of 1.665. Furthermore, the variation of peak slip angles and peak slip ratios with wheel load is equal. The only difference is the effect of camber on the tyre. For the rears, the peak camber angle is lower than the front tyre, being at 3.0° in stead of 3.5°. Apart from the lower peak camber angle, the increase in lateral and drop in longitudinal coefficient of friction is the same

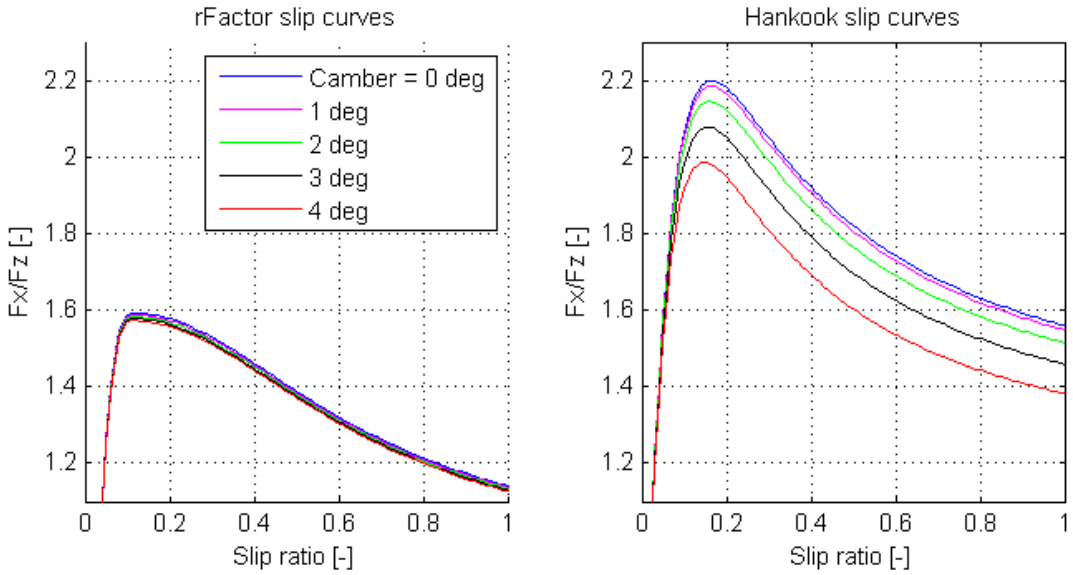

Figure 4.11: Influence of introducing camber angles on longitudinal slip curves of both tyres.

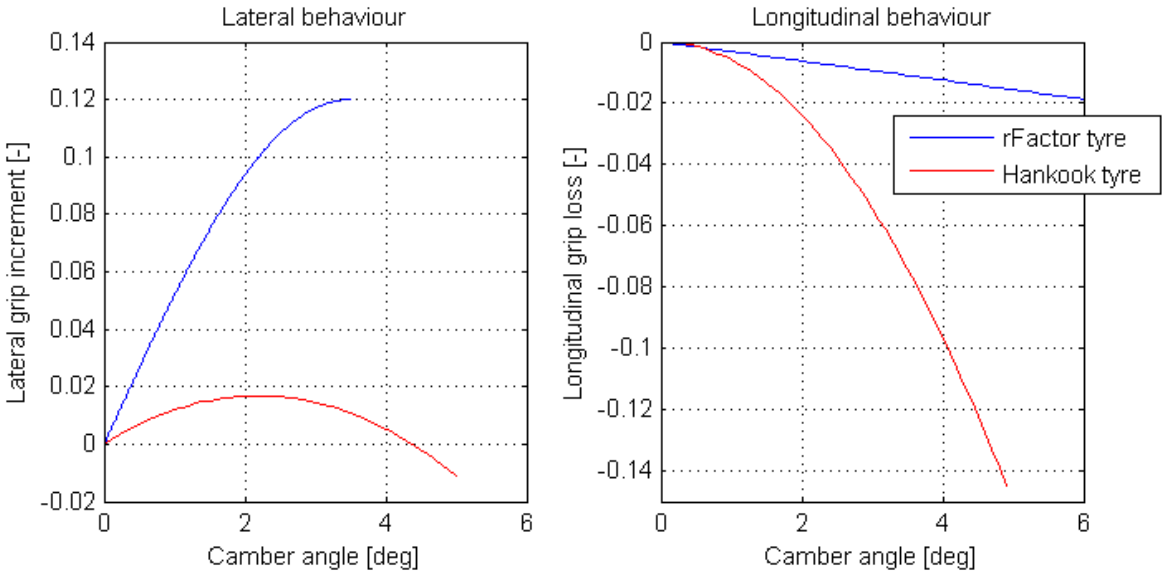

Figure 4.12: Influence of introducing camber angles on coefficient of friction of both tyres.

for the front and rear tyres.

The Hankook tyre model however, has more differences in front and rear tyre properties compared to the rFactor model. Starting with the basic slip curves of both tyres. The shape of lateral slip curve is totally different. Where the front tyres have a peak lateral force after which the grip decreases, the rear tyres have more constant grip with varying slip angle. This result is shown in figure 4.13.

The longitudinal behavior of the rear Hankook tyre is most remarkable. As can be seen

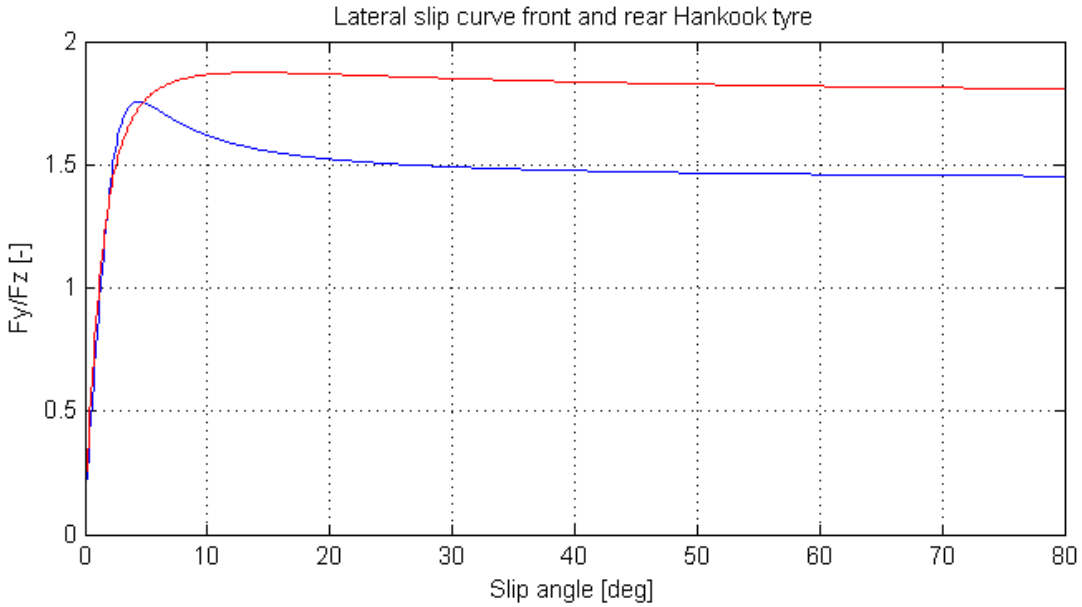

Figure 4.13: Lateral slip curve for the front and rear Hankook tyre model. The front tyre is shown in blue, the rear tyre in red.

in figure 4.14, the slip ratio where neutral grip (a friction coefficient of zero) is present is well below zero slip ratio. Therefore it is hard to generate a basic slip curve from this measurement. The shape of these slip curves is more similar, the coefficient of friction gradually decreases after the peak.

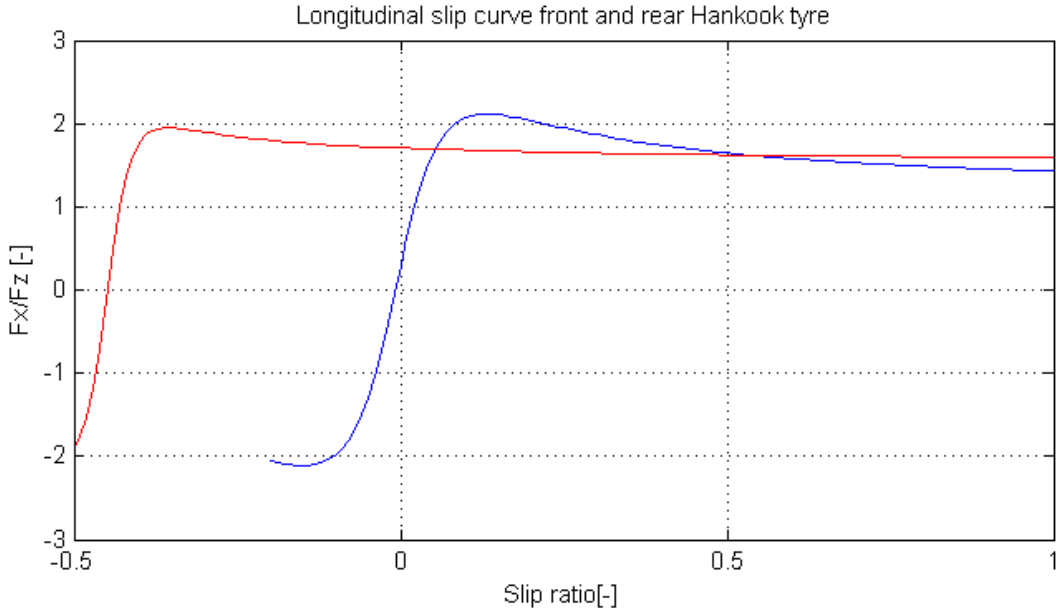

Figure 4.14: Longitudinal slip curve for the front and rear Hankook tyre model. The front tyre is shown in blue, the rear tyre in red.

In terms of tyre load sensitivity, the rear Hankook tyre model is more sensitive to wheel

load changes than the front tyres. In figure 4.15, lateral slip curves of the rear Hankook tyre is shown. The slip curves are built from a wheel load variation of 250 N to 4000 N. As can be seen at relatively high wheel loads, the friction coefficient of the rear drops drastically. The lowest green line which has the lowest friction peak even reverses sign at a slip angle of only 9°. In terms of longitudinal load sensitivity, no conclusion can be drawn due to the inaccurate level of longitudinal model capturing.

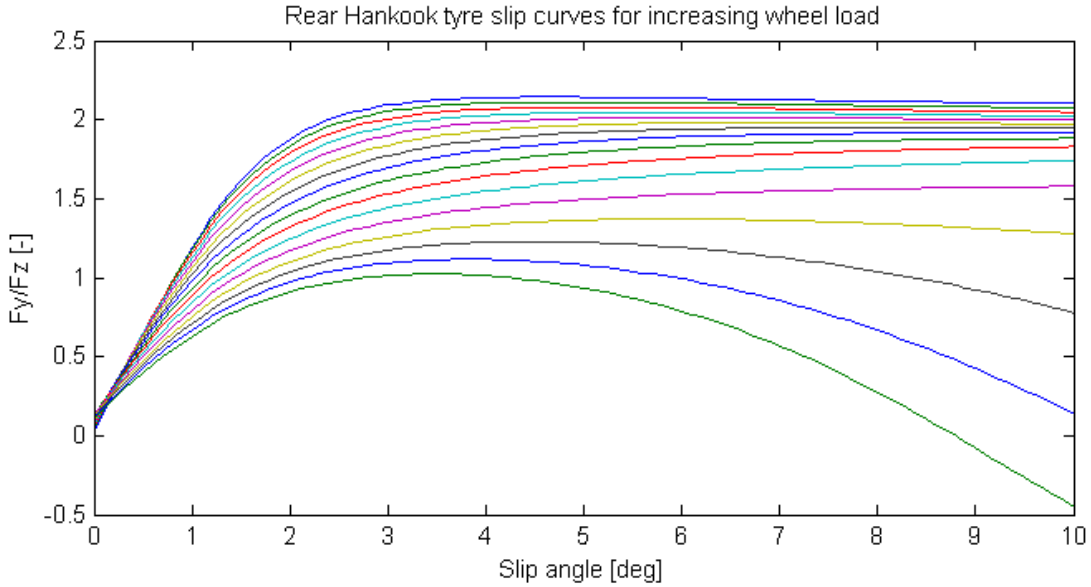

Figure 4.15: Lateral slip curves of Hankook rear tyre with increasing wheel loads.

Camber has the same effect on the rear tyres as on the front tyres. Simulations showed that the peak camber angle to have the highest lateral friction coefficient is 3.2°, which is 1° higher than for the front tyres. The grip increment itself is also higher for the rear tyres. Simulations for the longitudinal loss in friction due to camber show that camber has a higher effect on the rear tyres in longitudinal terms than for the front tyres.

4.3 Pacejka tyre model conversion

Now that the structure of both models are known, the rFactor tyre file can be updated with inputs from the Pacejka tyre model. After mathematical operations and construction of a new TBC file, the file will be tested in the simulator to analyse effects of the new tyre file in section 4.4. Furthermore, the test is used as input for the steering metrics analysis for chapter 6.

The precise generation of the rFactor tyre model based on the Hankook Pacejka tyre model is elaborated in appendix B.

4.4 Comparison of tyre models in rFactor

Both tyre files are used in rFactor to make a clear compare of how both models behave in the simulation software. The test driver for this test is Indian driver Arjun Maini, having considerable experience with Formula 3 cars. During the experimental laps, the exact same setup is used. The only difference is the tyre model in rFactor.

The first notable difference between both models is the tyre radius. As can be seen in figure 4.16, the top speed of the baseline tyre model is 234.5 km/h before it hits the RPM-limiter in 6th gear. For the Hankook tyre, having a larger wheel radius, the top speed is 241.7 km/h. This results from the difference in tyre radius of 0.01 meter.

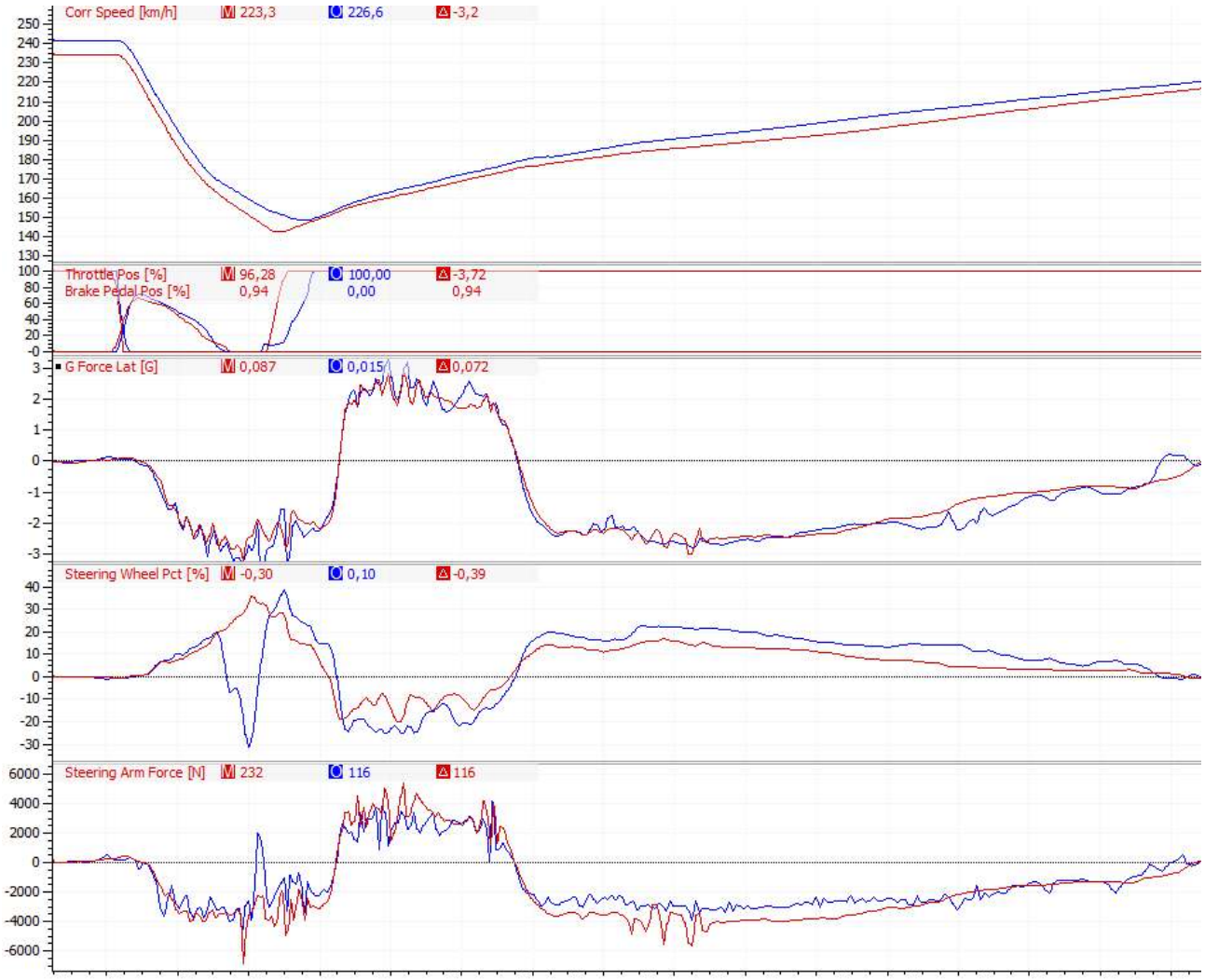

Figure 4.16: Comparison of tyre model in rFactor turn numbers 1, 2 and 3. Baseline model in red and Hankook model in blue.

Figure 4.16 also shows the first three turns of the Barcelona race track [66], [67]. It can

be seen that the vehicle has a higher corner speed with the Hankook tyres. Another observation is the correction in the blue steering trace corresponding to the Hankook tyre model, shown by a sudden sweep in which the steering angle becomes negative. Maini's comment on this oversteer correction is that the car has overall much more grip. However, on initial turn in, the car feels lazy in a way that small wheel angles does not influence the rotation of the car much. Then in the mid corner, the front suddenly grips which tends to his feeling to an oversteer balance due to which he corrects with the negative steering input. He admits however that this is not oversteer, but the sudden increase in front grip. The rear follows naturally because of the grip at the rear end of the car. The consequence of the correction of Maini, is that he is able to go on throttle later.

Remarkable about turn 3 is the overall higher lateral acceleration for the Hankook tyre model than the baseline tyre model. To get to this higher lateral acceleration however, a higher steering angle is required. The difference in in steering arm force is also noticeable. The Hankook tyre generates a lower force in the steering rack than the baseline tyres.

Turn 9 in figure 4.17 shows the effect of longitudinal grip of the Hankook tyres. Although arriving at a higher velocity, Maini is able to brake later and harder because there is more longitudinal grip available. It can be seen that the deceleration is higher. Due to the higher grip for the Hankook tyre, higher lateral acceleration is reached again with higher steering wheel angles. This causes the car to rotate faster and open the steering wheel earlier to go on throttle. Due to the higher longitudinal grip, he is able to go to full throttle more easily compared to the baseline tyre lap. This effects is confirmed by his comments afterwards. "I am able to brake harder without locking tyres. On power, the car sits. I am more confident to go on power early. The traction is better".

Answering the question which tyre model feels more realistic, Maini responds [68]: "The Hankook tyre model simply has too much grip compared to the real tyre for my feeling. Also the initial steering wheel input is not realistic. In real, the car responds more direct to small steering inputs."

The overall conclusion of the experiment is that the Hankook tyre model tyres have more grip both longitudinal and lateral. To reach higher lateral acceleration with the surplus of grip, a higher steering wheel angle is required. At low steering angles the tyres produce small forces, but increasing wheel angles suddenly increase lateral grip. The forces in the steering rack are lower with the Hankook tyres compared to the baseline model. The balance is unchanged according to driver feeling, although the sudden increase in grip in mid corners might feel as oversteer. Due to the higher tyre radius, the Hankook tyre model allows for higher maximum speed given the same gears.

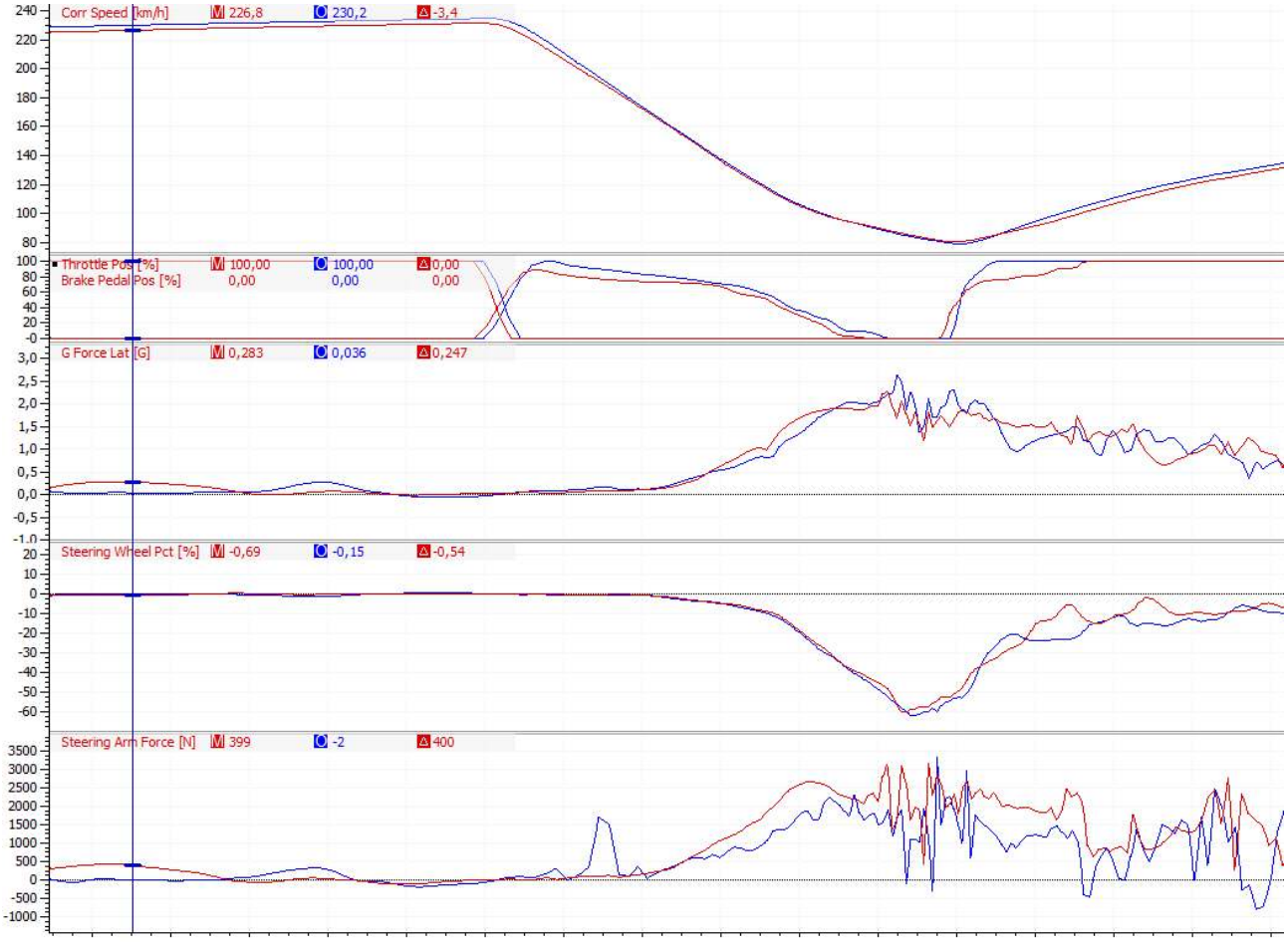

Figure 4.17: Comparison of tyre model in rFactor turn number 9. Baseline model in red and Hankook model in blue.

Chapter 5

Vehicle suspension and geometry

The geometry of the suspension of the Formula 3 car has influence on the steering forces the drivers feels while driving. The purpose of this chapter is to generate the exact geometry of the F312 Formula 3 car as input for the rFactor vehicle model. The information to construct the rFactor suspension model will be extracted from a Multibody Dynamic (MD) model which is generated given the exact data available of the F312 car. Since rFactor is a black box in terms of its physics, the generation of a MD model of the Formula 3 car might allow the team to perform simulations with new car setups or extra design features in a fully controlled environment. Ultimately, the MD model can replace rFactor as simulation platform if accurate results are achieved.

5.1 Multibody Dynamic Model

The development of a Multibody Dynamic model can help determining the accuracy of the rFactor vehicle model. It furthermore helps developing a fully controlled simulation environment. The MD model is constructed with the suspension data available and the Pacejka tyre model as used in chapter 4. Finally, the suspension model is converted to a rFactor model. Combined with the updated tyre model, this allows for at least two identical parts of the model when comparing the MD model and the rFactor model. In the following sections, the development of the MD model is described.

5.1.1 SimMechanics

The multibody simulation environment chosen for this specific task is SimMechanics. SimMechanics is an expansion for Simulink, a well known programming tool of MathWorks and is used throughout the TU Delft campus [70]. The biggest advantage of using SimMechanics is in the implementation possibility of Simulink models and other MATLAB based technologies in the SimMechanics multibody environment. This results in

a straightforward manner of implementing the Pacejka tyre model into the multibody model.

SimMechanics has two distinct versions, the First and Second Generation. According to MathWorks, the First Generation is a powerful tool to measure reaction forces which is important for the implementation of the Pacejka tyre model in the Multibody Dynamic model [71]. Apart from SimMechanics, other simulation packages are available such as Adams/Car or ChassisSim. SimMechanics is preferred as package to construct a Multibody Dynamic model of the Formula 3 car for this research, because it allows for full customization of the model and its environment and allows the engineers to post process results in MATLAB.

The basis of SimMechanics is defining Bodies by parameterization. The user can create a Body and specify its geometrical, mass and inertial properties [72]. These Bodies are connected to one another by Joints. These Joints can freely eliminate degrees of freedom to yield the requested type of joint. Joints and Bodies can be sensed by Body or Joint Sensors. This feature allows for measurements of specific reaction forces or motions of Bodies or Joints. Furthermore, motion or forces can also be externally applied to Bodies or Joints by using Actuators. An Joint Initial Condition block can also be used to generate an initial motion on a Joint, even before the simulation actually starts.

5.1.2 Body parts, dimension, weight and moment of inertia

The first step of developing the MD model is identifying all elements of the vehicle which will be present in the final model. The chassis of the car is seen as one single body. This body includes the monocoque, the engine, the gearbox, the wings and the driver. The wheels are split into three subparts being the wheel itself, the tyre and the rotating brake disc. The wheel is connected to the upright which allows the wheel to rotate about a lateral axis. The upright is then connected to the chassis by the suspension elements. All these parts are modeled as Bodies in SimMechanics. The connection between the Bodies is, as discussed, taken care of by specific Joints, with corresponding degrees of freedom.

The dimensions of the parts are determined either by available data or measurements. Dimensions of the wheels and tyres are given by the tyre manufacturer Hankook [73]. Since the Dallara F312 manual precisely define the location of all suspension members, the dimensions of these parts are known. Consequently, the location of the wheels follows from these data. Also the dimension of the chassis is a result of the location of the suspension pickup points.

According to regulations, the minimum weight of the car plus driver is 565 kg. The total mass of the vehicle will therefore be assumed to be 565 kg. Since the weight of the monocoque plus engine, gearbox and wings is impractical to measure, all other parts of the car are measured and subtracted from the total vehicle mass to yield the chassis weight. The masses of all considered parts are given in table 5.1.

Apart from the masses, also inertial properties are important inputs for the MD model. Since measuring inertial properties of car parts is not a straightforward method, the inertial values are determined by simplifying the geometry of the part and computing the moment of inertia of equivalent standard shapes such as hollow tubes and solid discs and cubes. The tyres, wheels and brake discs are considered as one solid discs, with known dimensions and weights. The chassis is seen as a solid tube, with an assumed radius of 0.6 meters and length of 4.351 meters according to the Dallara manual [69]. The suspension elements are solid tubes as well, having an average length of 0.23 meters (as computed from the known rod end points), a weight of 1 kilogram and a radius of 0.01 meter. The geometry of the upright is complex, therefore it is assumed that the upright is a solid disc with a radius of 0.13 meters and a thickness of 0.1 meter.

The front wheel inertia tensor is calculated as follows. The mass of the front wheel plus front tyre is 12.0 kg. The mass of the brake disc is 2.8 kg. The tyre has a diameter of 0.551 meters and a width of 0.2 meters. The moment of inertia about the spin axis therefore becomes:

$$I_{zz} = \frac{1}{2} \cdot m \cdot r^2 \tag{5.1}$$

$$I_{zz} = \frac{1}{2} \cdot 14.8 \cdot \left(\frac{0.551}{2}\right)^2 = 0.56\ kg \cdot m^2 \tag{5.2}$$

The other two moments of inertia are calculated as follows:

$$I_{xx} = I_{yy} = \frac{1}{4} \cdot m \cdot r^2 + \frac{1}{12} \cdot m \cdot l^2 \tag{5.3}$$

$$I_{xx} = I_{yy} = \frac{1}{4} \cdot 14.8 \cdot \left(\frac{0.551}{2}\right)^2 + \frac{1}{12} \cdot 14.8 \cdot 0.2^2 = 0.33\ kg \cdot m^2 \tag{5.4}$$

In the same fashion, all other moments of inertia are determined. The moment of inertia of the pushrod is assumed to have the same values as a single wishbone element or a tierod. Although its orientation is inclined and thus the moment of inertia different, the contribution of the pushrod is small compared to the chassis inertia. Since the upright is a combination of the upright itself, spindle, brake caliper and brake pads, the individual parts have no moment of inertia, but all contributions are summed up in the upright moment of inertia. All other values are given in table 5.1 below.

5.1.3 Suspension construction

As stated before, the geometry of the suspension members follow directly from the Dallara F312 manual [69]. The values are given in Appendix C. To construct the suspension layout of the F312 Formula 3 car, each member of the suspension is a separate Body block in SimMechanics. The starting and ending point simply follow from the provided table. The provided table shows the exact location for each point for one corner of the car. The

Table 5.1: Weight and inertia of all parts in the MD model.

Class	**Part**	**Weight** $[kg]$	I_{xx} $[kg/m^2]$	I_{yy} $[kg/m^2]$	I_{zz} $[kg/m^2]$
Chassis	Chassis	452.8	56.6	742.6	742.6
Wheel	Front wheel + tyre + brake disc	12.0	0.33	0.33	0.56
	Rear wheel + tyre + brake disc	14.0	0.46	0.46	0.69
Suspension	Upright	1.8	0.03	0.03	0.04
	Spindle	1.8	0	0	0
	Brake caliper	1.2	0	0	0
	Brake pads (set of 2)	0.5	0	0	0
	Wishbone	2.0	$8.8 \cdot 10^{-3}$	$8.8 \cdot 10^{-3}$	$2.0 \cdot 10^{-4}$
	Pushrod	1.0	$4.4 \cdot 10^{-3}$	$4.4 \cdot 10^{-3}$	$1.0 \cdot 10^{-4}$
	Tierod/Trackrod	1.0	$4.4 \cdot 10^{-3}$	$4.4 \cdot 10^{-3}$	$1.0 \cdot 10^{-4}$
	Rocker	1.0	0	0	0

other side of the car is constructed by mirroring the points in the longitudinal vehicle axis running through the center of gravity of the car. Apart from mirroring, an offset along the lateral axis is required to shift the rear corners to the right position. In the data table, the wheelbase is neglected. Therefore this is included in the model generation. The wheelbase is stated in the F312 manual [69] and is 2800 mm. In figure 5.1 the geometry of the suspension according the provided table is shown. The lower wishbones are shown in brown and the upper wishbones in red. The pushrods which transfer the vertical loads into the chassis are shown in blue while the tierods (front) and trackrods (rear) are shown in green.

The reference frame of the MD model is shown in the left bottom corner of figure 5.1. As can be seen, the longitudinal axis is the x-axis pointing in the direction of driving, corresponding to the convention of the Dallara F312 provided table. The z- and y-axis however are changed, with the y-axis pointing upwards and the z-axis pointing to the right.

There are four uprights which are located at the ends of the suspension elements. The uprights allow the wheel to be mounted and allow the wheel to rotate. To construct the uprights, all suspension element ends are connected. These points are indicated in figure 5.2 as numbers 6, 7, 8 and 11. The wheel rotation point, the spindle, is indicated with number 10 and is also part of the upright. The weight of the upright is the sum of the following components mentioned in table 5.1: upright, spindle, brake caliper and brake pads. The center of gravity of the upright is assumed to be at the spindle location, indicated by point 10 in figure 5.2.

The wheels are connected to the upright in point 10 shown in figure 5.2. The weight of the wheels is given in table 5.1. The center of gravity of the wheels is also assumed to be at location 10, their point of rotation. Any other location for the center of gravity would introduce an unbalance in the rotating wheel.

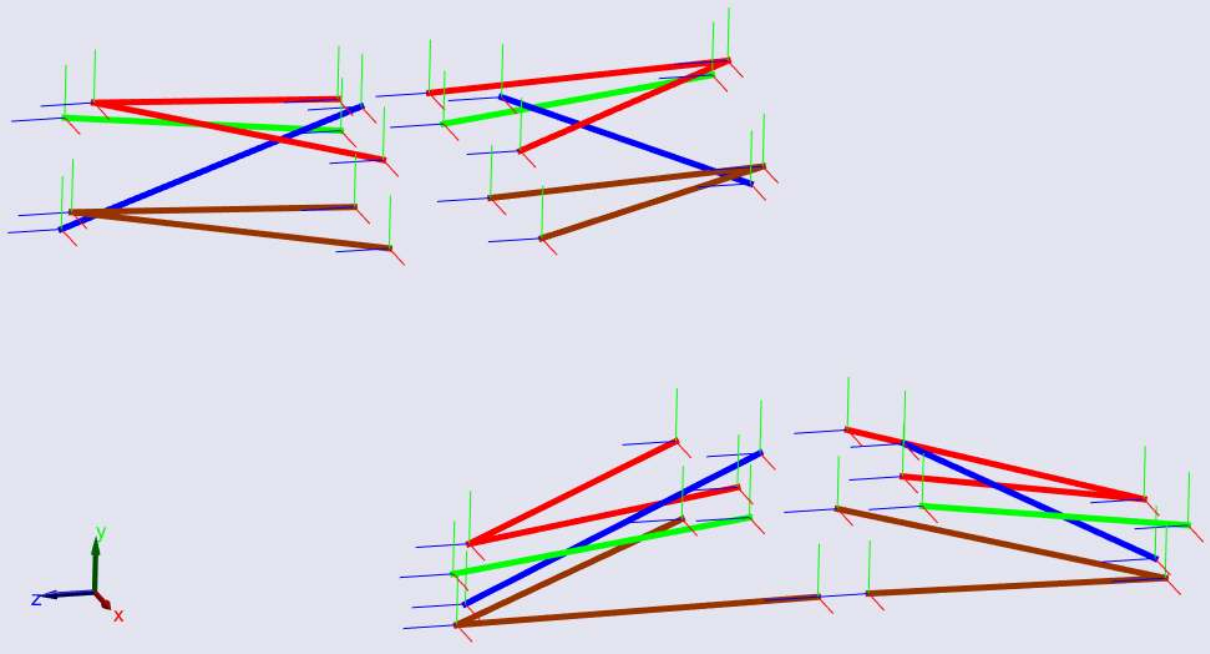

Figure 5.1: Suspension geometry according to Dallara F312 manual [69] in SimMechanics.

5.1.4 Chassis and suspension connection

The chassis is formed around the inner suspension element ends. The exact shape of the chassis is irrelevant for the MD model, since there is no aerodynamic model which requires the actual shape of the chassis. Furthermore, the weight, moment of inertia and location of center of gravity determine the required properties for the MD model. The chassis weight is computed by subtracting all known elements from the car total weight. The location of center of gravity is determined by the setup sheet available [63]. According to the setup sheet, the weight distribution of the car is 42.2%. That means 42.2% of the weight is on the front wheels and 58.8% on the rear wheels. The location of the center of gravity in a horizontal perspective is therefore located 42.2% of the length of the wheelbase behind the front upright center of gravity in x-direction, respecting the orientation shown in figure 5.1. In vertical sense, the height of the center of gravity is based on information provided by Dallara of their 2006 Formula 3 car, which states that the center of gravity is located 270 mm above ground height [79].

The suspension elements are linked to the chassis by spherical joints. The geometry of suspension and uprights automatically disable the redundant degrees of freedom. In figure 5.3 the car model is shown, where the suspension is linked to the chassis. Furthermore, the wheels and uprights are also shown.

The front tierods allow the vehicle to steer its front wheels. By pulling or pushing the tierods, a rotational moment about the kingpin axis of the wheels is generated, since the connection of the tierods to the upright is designed to have a specific offset [34]. In figure 5.4, the offset between the kingpin axis and the tierod location is shown. The other end

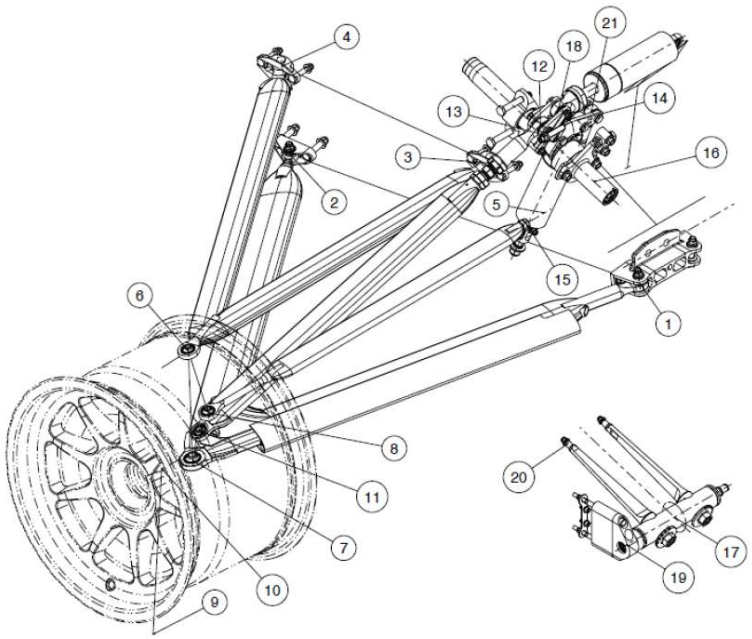

Figure 5.2: Front suspension geometry layout [69].

of the tierods are connected to each other at the steering rack. This is a horizontally actuated element which is part of the rack and pinion of the steering system. In the MD model, the steering rack is modeled as a horizontal Body connected to the chassis. This joint only allows lateral translations, similar to the real vehicle. In figure 5.3, the steering rack is seen at the front the vehicle colored red. The actuation of this element is elaborated in a later section.

The pushrod is connect to the chassis by a rocker. This rocker translates the motion of the pushrod in a direction in which the springs and dampers are placed. There is a difference in layout of front and rear suspension. The front suspension is equipped with rotational springs, whereas the rear is equipped with coilover (linear) spring-damper systems. The front rocker pivots around an axis parallel to the rotation axis of the spring. The rear rocker pivots around an axis perpendicular to a plane defined by the orientation of the pushrod and the spring-damper system. To find the vector orthogonal to the plane defined by the orientation of the pushrod and the coilover system, the crossproduct of both lines is used to compute the orientation of the normal vector [74]. In figure 5.3, the rear rockers are visible in yellow. As can be seen, the rocker has a triangular shape accommodating the pivot point, pushrod connection and the coilover connection. The springs and dampers are not shown in the figure, since the force generated by the springs and dampers are determined by Joint Spring & Damper systems available in SimMechanics. The front rocker is not visible, due to its location inside the chassis. However, this rocker also has a triangular shape to accommodate the pivot point (and spring connection), pushrod connection and the damper connection. The damper is, in contrast to the rotational spring, a translational damper equal as found at the rear of the vehicle.

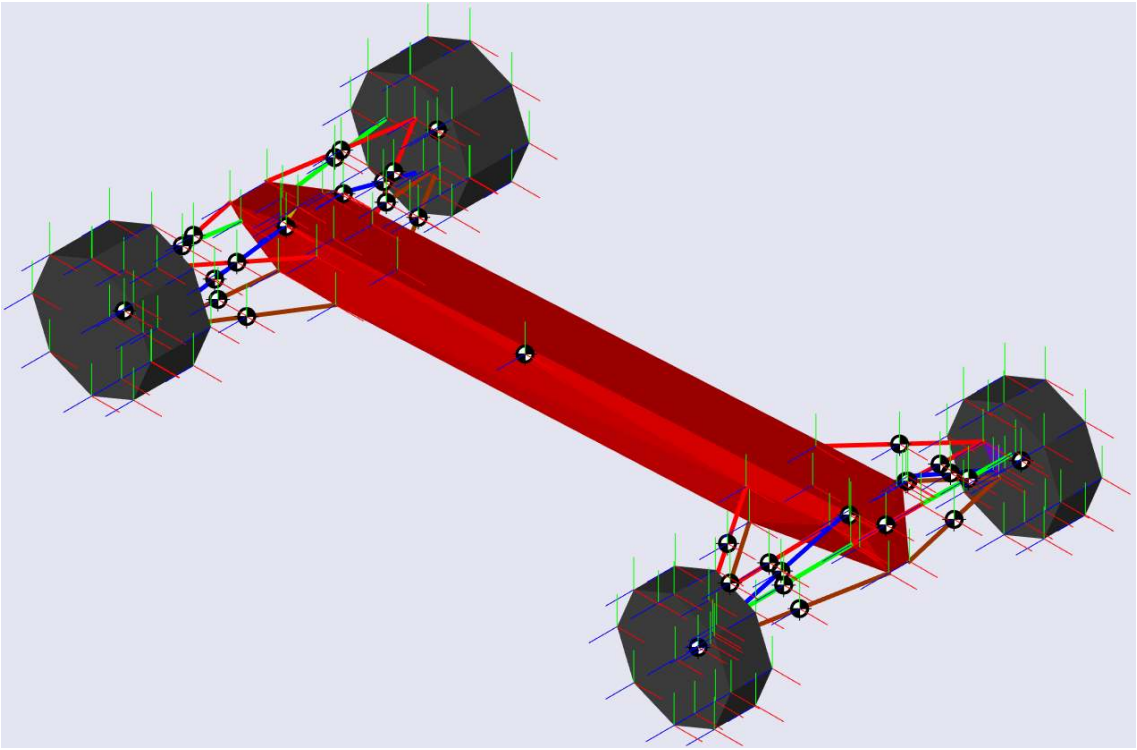

Figure 5.3: Car model. Chassis is shown in red, rockers in yellow, wheel plus tires in grey and upright in purple.

5.1.5 Springs and dampers

In SimMechanics, springs and dampers can be modeled by two interfaces: the Body Spring & Damper and the Joint Spring & Damper. The latter is chosen for the implementation in this MD model. As discussed in the previous section, the rocker pivots around its pivot axis. This pivoting motion is modeled by a rotational joint located at the pivot point of the rocker and having the pivot axis orthogonal to the plane defined by the pushrod and the coilover or damper system. The Joint Spring & Damper is then used to actuate the rotational movement of the rocker.

By using this rotational fashion of introducing springs and dampers, the properties of both should be converted from translational to rotational stiffnesses. The input for this block is the position of the rocker in degrees and the angular velocity in degrees per seconds. The output of the system is a torque. The front spring is easily adopted in the system as it is a rotational spring, the front damper properties and the rear springs and dampers require transformations.

Springs

According to the Dallara F312 manual, the 10 linear types of front springs vary from 11.0 Nm/deg to 24.5 Nm/deg, each increasing with a stiffness of 1.5 Nm/deg per type. The

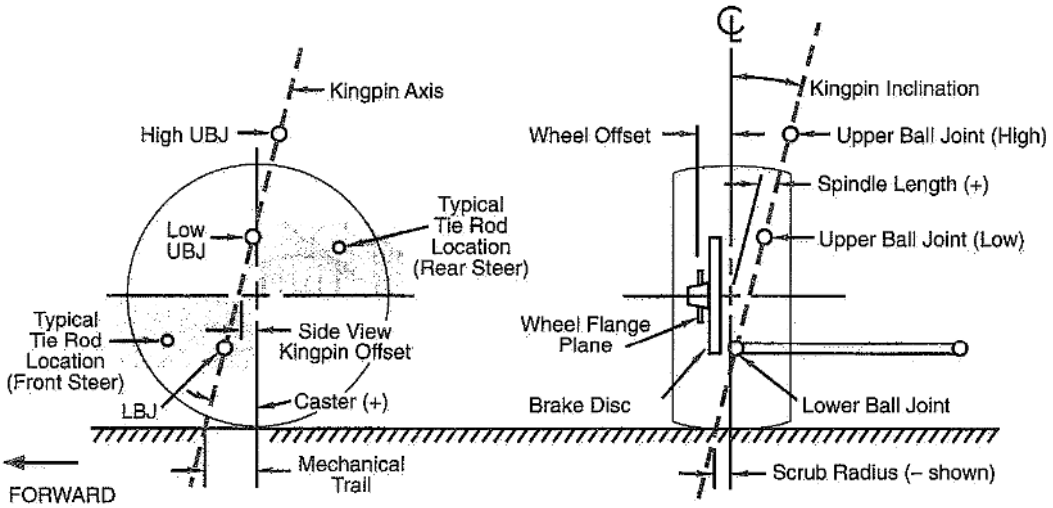

Figure 5.4: Tierod connection location. Offset between kingpin axis and tierod location visible. Source: Racecar Vehicle Dynamics [34].

springs used during the Barcelona test are the 17.0 Nm/deg springs. The rear springs used during this test were the 800 lbs/inch springs [75]. This stiffness is rewritten into N/mm as shown in equation 5.5.

$$800\ ^{lbs}/_{inch} = \frac{800 \cdot 0.45 \cdot 9.81}{25.4} = 139.0\ ^{N}/_{mm} \tag{5.5}$$

The modification of translation to rotation is dependent of the dimension of the rocker. From figure 5.2, it can be seen that the rocker pivot point is indicated by number 13. The pushrod connection point is number 12, where the spring connection is at point number 14. The rotation of the rocker due to pushrod actuation is completely determined by the geometry of the MD model. The displacement of the translational spring depends on the rotation of the rocker. It is computed that the distance from the rocker pivot to the spring connection is 76 mm. The assumption is made that this distance is the shortest separation between the rocker pivot point and the line parallel to the spring and damper system. Using the small angle approximation, in which it is assumed that the rocker will only have small rotation angles, the translational displacement of the spring connection given a rocker rotation of 1 degree is calculated as follows. In figure 5.5, the rocker with a 1° rotation is shown. Using the small angle approach, the transformation becomes:

$$sin\ 1^\circ = \frac{\delta}{0.076\ m} \tag{5.6}$$

$$\delta = 0.00133\ \ m \tag{5.7}$$

The rotation of 1° results in a displacement of 1.33 mm. With this figure, the force per degree rotation at the top of the rocker can be computed. Since the input for the

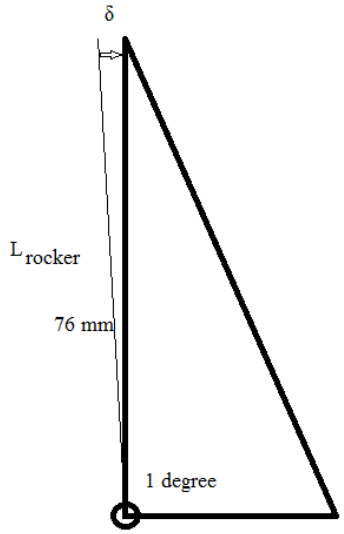

Figure 5.5: Spring transformation following from a 1° rotation on the rear suspension rocker.

SimMechanics block is a torque per rotation, this force is transformed into a torque in the rocker pivot point.

$$k_{rotation} = k_{translation} \cdot \delta \cdot L_{rocker} \tag{5.8}$$

$$k_{rotation} = 139.0 \cdot 10^3 \cdot 0.00133 \cdot 0.076 = 14.0\, Nm/deg \tag{5.9}$$

Dampers

The front dampers are in contrast to the front springs, translational dampers. Therefore, they have their own connection to the front rockers. This connection is indicated by number 14 in figure 5.2. The rear dampers are mounted in exact the same fashion as the rear springs. The Koni dampers mounted on the F312 Formula 3 car have different stiffnesses for varying damper speeds. Figure 5.6 shows the front damper characteristic. The stiffness of the dampers are indicated for the complete range of clicks, both for bump and rebound. Since there is one coefficient which can be used in the SimMechanics block, a linear approximation for the non-linear damper is chosen. For a damper velocity of 0.25 m/s, a reactive force of 1250 N is possible for both bump and rebound. The linear damping coefficient is therefore estimated to be 5000 Ns/m.

To transform the damping coefficient from a linear damper into a rotational damper, the same method as for the rear spring is used. The distance from the front rocker pivot point to the damper connection is 67 mm. This results in a rotational damping coefficient of 0.39 Nms/deg. The characteristics of the rear damper are similar, approximately 1250 N for a piston velocity of 250 mm/s [69]. Given the rear rocker geometry, this results in a rotational damping coefficient of 0.50 Nms/deg.

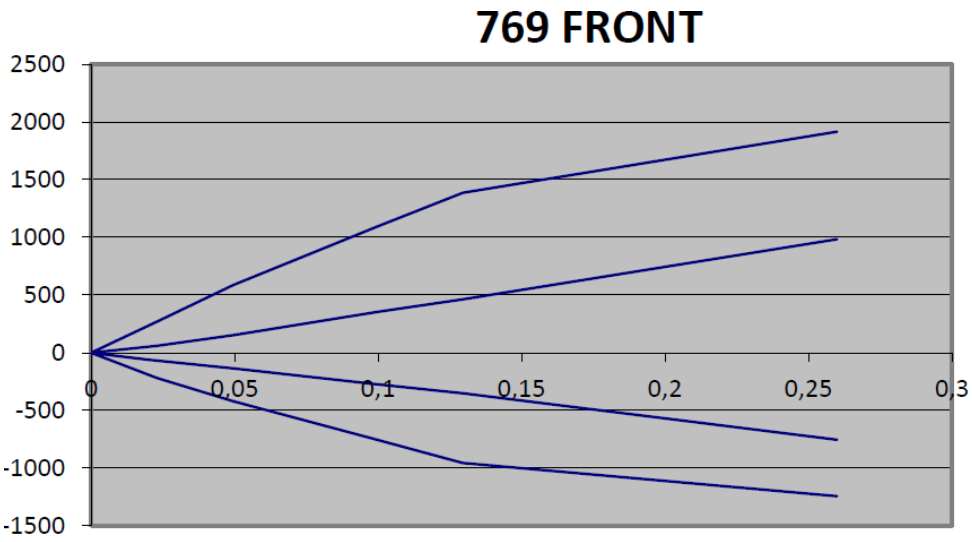

Figure 5.6: Koni 769 front damper characteristic. Vertical axis in N and horizontal axis in m/s. Source: Dallara F312 manual [69]

Roll stiffness

The height of the center of gravity above the ground has influence on the rolling moment caused by the lateral force produced by the tyres [80]. The higher the center of gravity, the higher the rolling moment on the vehicle. This rolling moment causes load transfer in lateral direction on the vehicle. In figure 5.7 it is shown that given the vehicle is in a right hand turn, the force produced by the tyres cause a load transfer towards the outside tyres. As discussed in chapter 4, tyres suffer from load sensitivity which means that the increment of tyre load is not linear with the increment of lateral force generated by that tyre. In this situation of load transfer, the gain of lateral force of the higher load tyre is lower than the loss of the unloaded inner tyre resulting in a lower lateral force produced on this specific axle.

To control the load transfer on an axle, anti roll bars influence the roll stiffness and thus the load transfer on an axle. Gergely (2008) [80] shows that higher roll stiffness cause higher load transfer and consequently a lower lateral force on that axle. It is important to note that anti roll bars influence the roll stiffness distribution over the axles, but never influence the total lateral load transfer on a vehicle. It only allows to shift the roll stiffness distribution and therefore lateral grip between front and rear.

Roll stiffness is controlled in the MD model by adding rotational springs on front and rear axles. By using the Dallara setup sheet, the roll stiffness influence of the anti roll bars is easily determined. For the favorable roll stiffness distribution of 63% [81], given the springs as discussed in the previous sections, the anti roll bars generate a roll stiffness of 184.6 kgm/deg at the front and 74 kgm/deg at the rear axle. These values are assigned to the rotational springs on each axle of the vehicle.

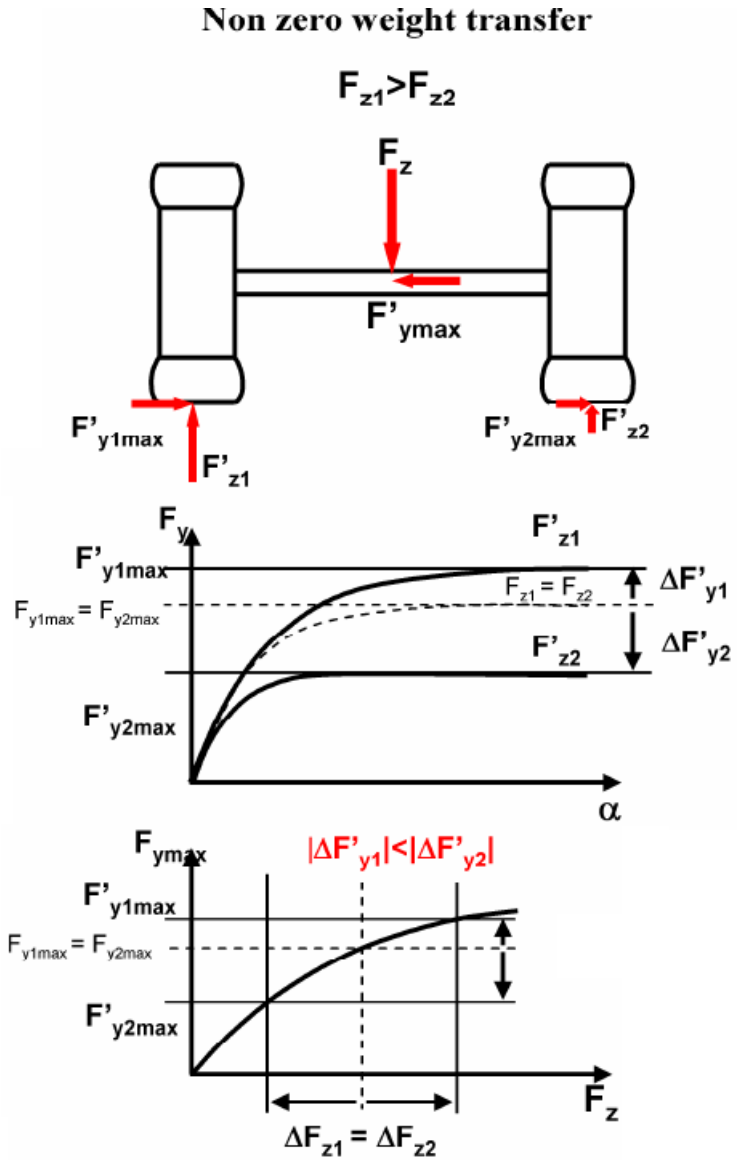

Figure 5.7: Lateral tyre load transfer due to lateral tyre forces in a right hand corner. Source: [80].

Aerodynamics

Formula 3 cars make use of their aerodynamic features to generate downforce, being their floors and front and rear wings. The information available about vertical aerodynamic forces are limited to the influence of the vehicle's floor. A lookup table is used which gives the C_z coefficient for the front and rear axle given a combination of front and rear ride height. According to personal communication with Van Leeuwen [82], a front ride height of 10 mm and a rear ride height of 20 mm would give a proper estimation of the aeroload at this track. The coefficient of vertical force at these ride heights are 0.8384 for the front axle and 1.3657 for the rear axle. These values are scaled with dynamic pressure to yield a vertical force on the vehicle body. The resultant force per axle is applied to the body

at the longitudinal center line of the vehicle.

The aerodynamic map of the Formula 3 car not only consists out of downforce, but also a drag force. Explicitly considering drag forces is unnecessary because of the actuation of the vehicle model. Since engine and brake characteristics are not adopted in the current state of the vehicle model, forward velocity is generated by an initial forward velocity. This initial forward velocity is maintained for two seconds until the vehicle is completely initialized, as will be discussed in section 5.1.6. After initialization, the forward velocity is controlled by the measurements performed on the real car, as described in the "Wheel and Body Actuation" paragraph in this section. The derivative of the real vehicle's velocity yields the body acceleration. This longitudinal acceleration multiplied by its total mass yields a longitudinal force applied at the center of gravity to control the forward velocity to the same magnitude as the real car. The main disadvantage of introducing forward velocity in this manner is the difference of longitudinal load transfer. On the real car, longitudinal forces are generated at the tyre contact patch with the road surface, which initiate a pitching moment about the center of gravity. Introducing the longitudinal force at the center of gravity eliminates the pitching moment about the center of gravity. However, since the main focus of this research concerns lateral response, this simplification adopted in the Multibody Dynamic model.

5.1.6 Ground definition

SimMechanics is a multibody dynamic model environment. Ground blocks are available to use, which are mostly used for robot applications having a fixed reference point of infinite mass [77]. Using a Joint, a Body block can be connected to the Ground. By elimination specific degrees of freedom, the user can block the vertical motion and have a vertically stationary Body. The Machine Environment sets the mechanical environment, thus defining gravity and its orientation in the model.

The application of the MD model requires normal (vertical) forces to be measured. However defining a Ground and attaching the vehicle by a Joint and restricting vertical motions does not yield vertical forces. In order to compute the normal loads, another solution of a horizontal ground is applied in the model.

The ground (or asphalt for the vehicle) with vertical gravity pointing downwards, prevents a body from infinitely falling down. As soon as the body is in contact with the ground, the ground exerts a vertical force on the body's contact point to prevent it falling through the ground. The body is in equilibrium. When the body is lifted up and the contact with ground is lost, there is no vertical force generated by the ground on the body. This principle can be simulated by a stiff, non-linear spring [78]. If the body falls through the ground, the spring creates a force pushing the body upwards. When the body is not in contact with the spring, the spring does not create any force on the body. The implementation of this spring is shown in figure 5.8. It can be seen that a damping effect is added to the system. The damping reduces the oscillations in the vertical displacement signal, as will be elaborated later in this section. Apart from defining the ground in this

manner, an additional vertical stiffness of the inflated tyre is incorporated. Although the stiffness of the ground spring is higher than the tyre vertical stiffness, it allows for a stiffness effect of the inflated tyre.

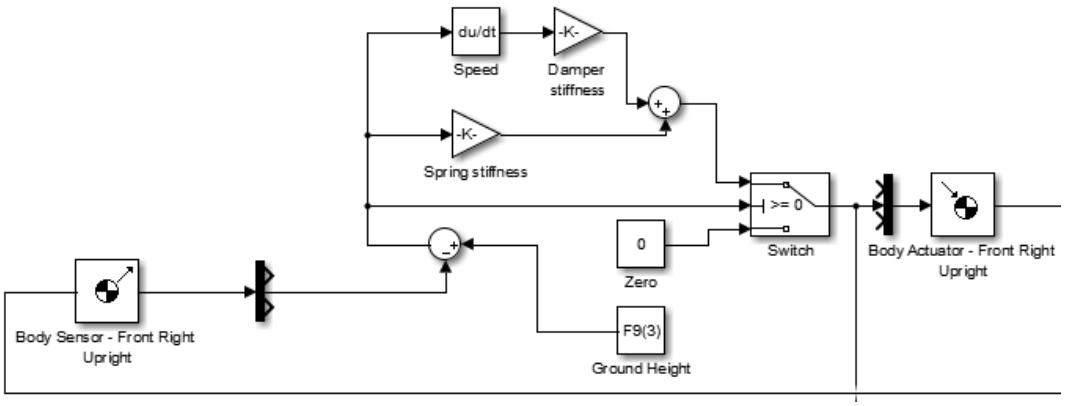

Figure 5.8: Ground defined as stiff, non-linear spring with damping.

The Body Sensor measures the position of the contact patch of the tyre. The vertical position is then compared to the actual level of the ground, defined by number 9 in figure 5.2. The Switch determines whether the spring is in operation due to the height of the contact patch or not. If the height of the contact patch is above ground level, the applied force by the Body Actuator is zero, else the computed force of the spring and damper is guided to the Body Actuator. The working principle of the activated ground (activated switch) is explained in equation 5.10 and filled in with actual parameters (in N and mm) in equation 5.11.

$$F_z = (h_{measured} - h_0) \cdot k_{ground} + \frac{d(h_{measured} - h_0)}{dt} \cdot c_{ground} \tag{5.10}$$

$$F_z = (h_{measured} - 26.5) \cdot 3620.5 + \frac{d(h_{measured} - 26.5)}{dt} \cdot 25.2 \tag{5.11}$$

The value of the ground spring and damper are chosen as such, that oscillations in normal force and contact patch height are minimal. The initial height of the contact patch according to the F312 manual is -26.5 mm [69]. As can be seen in figure 5.9, the initial sagging of the contact patch is approximately 0.33 mm. After 2 seconds, a vertical force of 700 N per axle pointing downwards is applied at the vehicle's center line per axle. Due to this force, the contact patch sags approximately 0.1 mm deeper. Although the tyre vertical stiffness is assumed to be 170 N/mm [79], the current stiffness of the ground spring allows for small normal force fluctuations. On the right hand side of figure 5.9, the step in normal force due to the extra load at t = 2 s, is exactly seen back. The normal force increases 350 N which is expected.

Another validation of working suspension is shown in figure 5.10. In this figure, the rocker rotation due to ground contact and the addition 700 N per axle is shown. Obviously, the

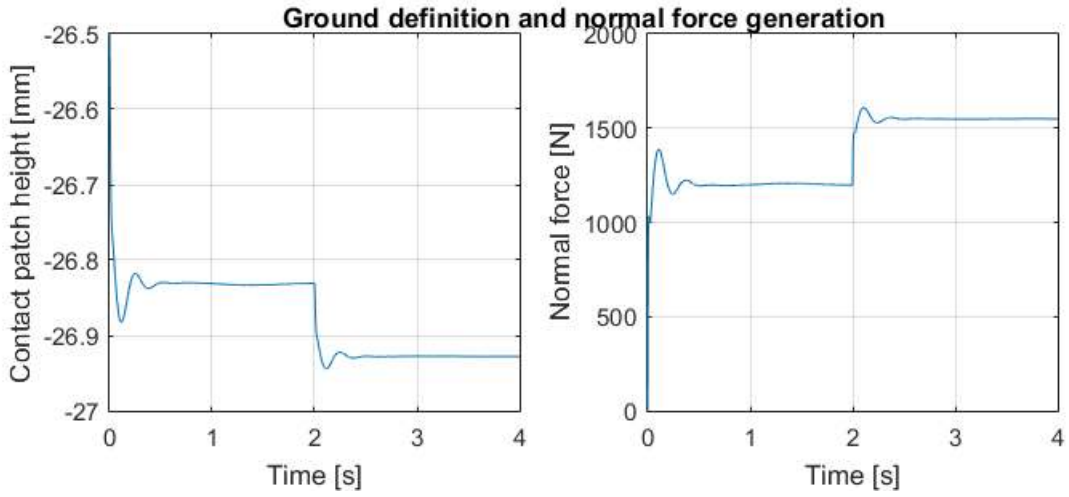

Figure 5.9: Reaction of ground being defined as stiff, non-linear spring and damper system.

rocker rotation is initially 0, but increases when the contact patch is in contact with the ground. Furthermore, the additional load rotated the rockers even further. An observation from this plot is that the front suspension is less damped compared to the rear, which is indicated by the extra oscillations at the front whereas the rear is damped after one oscillation.

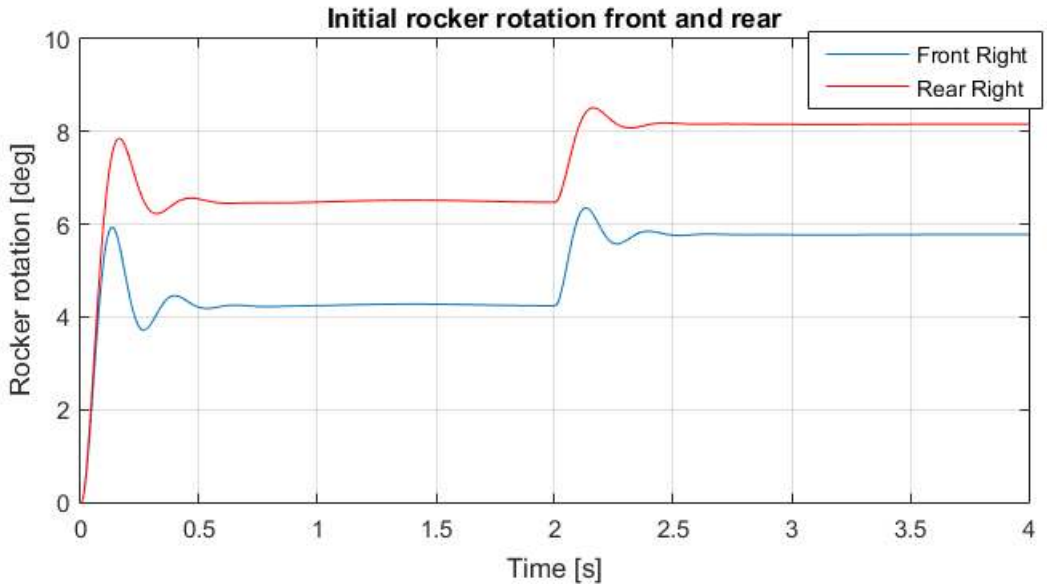

Figure 5.10: Rocker rotation under load.

5.1.7 Wheel and body actuation

The purpose of the MD model is to reproduce specific motions which were performed during the Barcelona test in 2013. From the track data available, the MD model can be actuated as such, that the motion should be reproduced in the same manner as the real

car. Since there is a strong focus on the steering rack forces produced in the MD model, certain states of the car are directly distillated from the track data and fed into the model.

From the track data, front wheel speeds are available. Furthermore, the wheel speed signals are converted to an overall vehicle speed within the Bosch data acquisition system [76]. By using the wheel speed signals of the front wheels and the computed vehicle speed, the MD model can be actuated in a longitudinal motion. This implementation eliminates the necessity of calculating longitudinal slip ratios. The advantage of this method is that there is no engine model or brake model required, which links throttle or brake signals to output torques on the rear and front wheels. Due to the absence of rear wheel speed sensors, determining slip ratios given a certain engine model would add considerable complexity to the MD model.

To make sure that the steering forces are influenced by the gyroscopic effect of rotating wheels, the individual wheel speed signals are actuated on the respective wheel. This follows from the fact that in corners, wheel speeds are different from in- and outside wheels. The rear wheels are actuated according to the vehicle speed and their radius.

5.1.8 Steering actuation

Apart from wheel speeds, steering rack motion is measured during operation of the real Formula 3 car. The steering rack can only move in a horizontal line, a linear potentiometer is therefore mounted on the steering rack to measure steer inputs. In the track data however, this signal is converted to a steering wheel angle. In the same fashion as performed in chapter 2, the rack and pinion primitive diameter of 15.60 mm [69] is used to convert the steering angle into linear motion of the steering rack.

The steering rack motion is then used to actuate the steering rack in the MD model, as shown in green in figure 5.1. As a consequence, the wheels are rotated about a vertical axis in order to steer the front wheels. This axis is the kingpin angle and is determined by the locations of the upper and lower wishbone connections to the upright, as seen in figure 5.4. The steering of the front wheels have effect on the slip angle computation, as will be shown in the next section.

5.1.9 Implementing the Pacejka tyre model

The Pacejka coefficients of the Hankook tyres have been studied in chapter 4, where a complete Pacejka tyre model has been developed in MATLAB. The advantage of creating a MD model in SimMechanics, a part of MATLAB, is the easy implementation of the Pacejka tyre model. The outputs of the tyre model are mainly the reaction forces in x- (longitudinal), and y-direction (lateral) and a reaction (aligning) torque about the vertical z-axis. The tyre model requires a tyre load, slip angle, slip ratio and a camber angle to generate the reaction output forces. In the currently designed model, no longitudinal tyre force are considered and thus no slip ratios need to be determined.

SimMechanics allows .m files to be run within the SimMechanics environment. For this, a Function Block is required. Opening the Function Block allows the user to copy the complete necessary .m script. The workspace however, is separate for all function blocks. Therefore, for each iteration, all Pacejka coefficients of the Hankook tyre (front and rear) have to be loaded. In figure 5.11, the implementation in SimMechanics is shown.

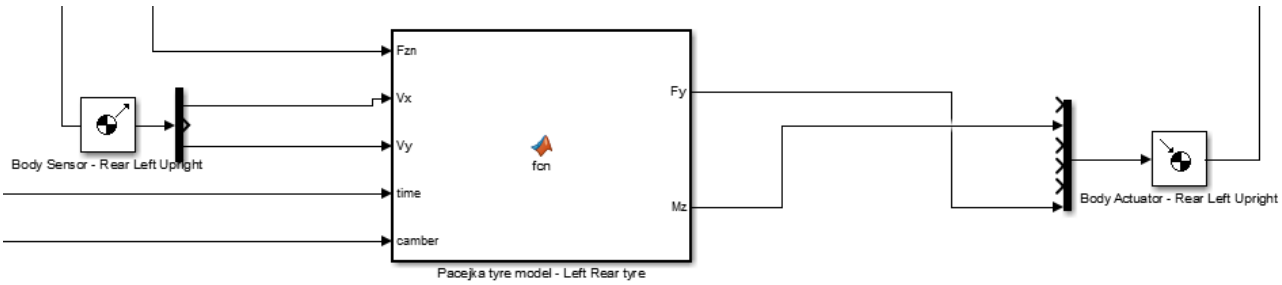

Figure 5.11: Implementation of the Pacejka tyre model into the SimMechanics Multibody Dynamic model.

The vertical tyre load is directly fed into the tyre model. This is the normal load which is computed by the Ground Spring as discussed in the "Ground Definition" section. To determine the slip angle of the tyre, the longitudinal and lateral velocity are required [61], which are measured using the Body Sensor of the particular upright. Using equation 5.12, the slip angle is determined for every time step within the Function Block. The time input is a necessity for the initial state of the vehicle. At t = 0, the ground does not produce a normal force yet, therefore the tyre model is assigned to use the static wheel loads in the initial phase of simulation. A body sensor measures the roll angle of the vehicle. This roll angle is fed into the Function Block as "camber". In the Function Block, this value is either added or subtracted from the static camber angle (dependent on the roll direction).

$$tan\ \alpha = \frac{V_y}{V_x} \tag{5.12}$$

The output of the Function Block is guided to the Body Actuator - Rear Left Upright. This Body Actuator exerts the lateral force and aligning moment on the tyre contact patch. Due to the fact that no slip ratio is used in this MD model, no longitudinal force is computed. Forward motion is determined by track data as discussed in section "Wheel and Body Actuation".

5.1.10 Lateral tyre force computation

The fact that there are no longitudinal forces computed in the tyre model, leads to errors in determining lateral tyre forces. The total capabilty of a tyre is visualized in a "g-g" diagram, where the maximum longitudinal and lateral forces are indicated [34]. A typical "g-g" diagram is shown in figure 5.12. This tyre in a given vehicle state is able to generate a maximum of 1100 lbs force. This force can be used as a tractive or braking force or lateral force, but also a combination both. The "g-g" diagram however shows that the

maximum performance of a tyre is always located on the outer circle. This means that if maximum lateral force is required, no longitudinal force can be requested simultaneously. The consequence of this fact is that when omitting longitudinal forces from the model, no trade-off between longitudinal and lateral force is made. The tyre will always generate the highest possible lateral force depending on the state of the vehicle.

5.2 rFactor suspension geometry

In the previous sections, the Multibody Dynamic model of the F312 Formula 3 has been developed. The geometry of the vehicle is defined using the information available by the car manufacturer Dallara. Using this information, the complete suspension is defined. This definition of the suspension, however, neglects set-up settings such as caster angle and ride height. Since set-up is dealt with separately in rFactor, the geometry as defined in the MD model is used as the input for the rFactor model. This conversion allows for fast adjustments on suspension geometry on the rFactor vehicle model.

In Appendix C, the information stated in the manual is given. Appendix D shows the way the rFactor suspension model is defined. This definition is given in the .PM file. For the rFactor model, all bodies involved in the suspension are defined. Apart from their location, also their mass and inertia is stated. The reference point is the center of gravity of the vehicle chassis. Then the locations of pickup points are defined according to the given conventions by rFactor. The chassis is connected to the spindles which in their turn are connected to the wheels. The connection elements are rigid bars.

The suspension elements which are defined in the .PM file are the two double wishbones per side, one upper and one lower wishbone and the steering arm for the front of the car and the track rods for the rear of the car. The pushrod element is defined in the .HDV file of the vehicle. An element is defined by the starting location and the ending location, indicated with the positive and negative side. Since the complete geometric model of the F312 car ha been built for the Multibody Dynamic model, an export script is written to generate the rFactor .PM file out of the MD model. This enables the user to adjust suspension geometry and rapidly convert this to an updated rFactor suspension model.

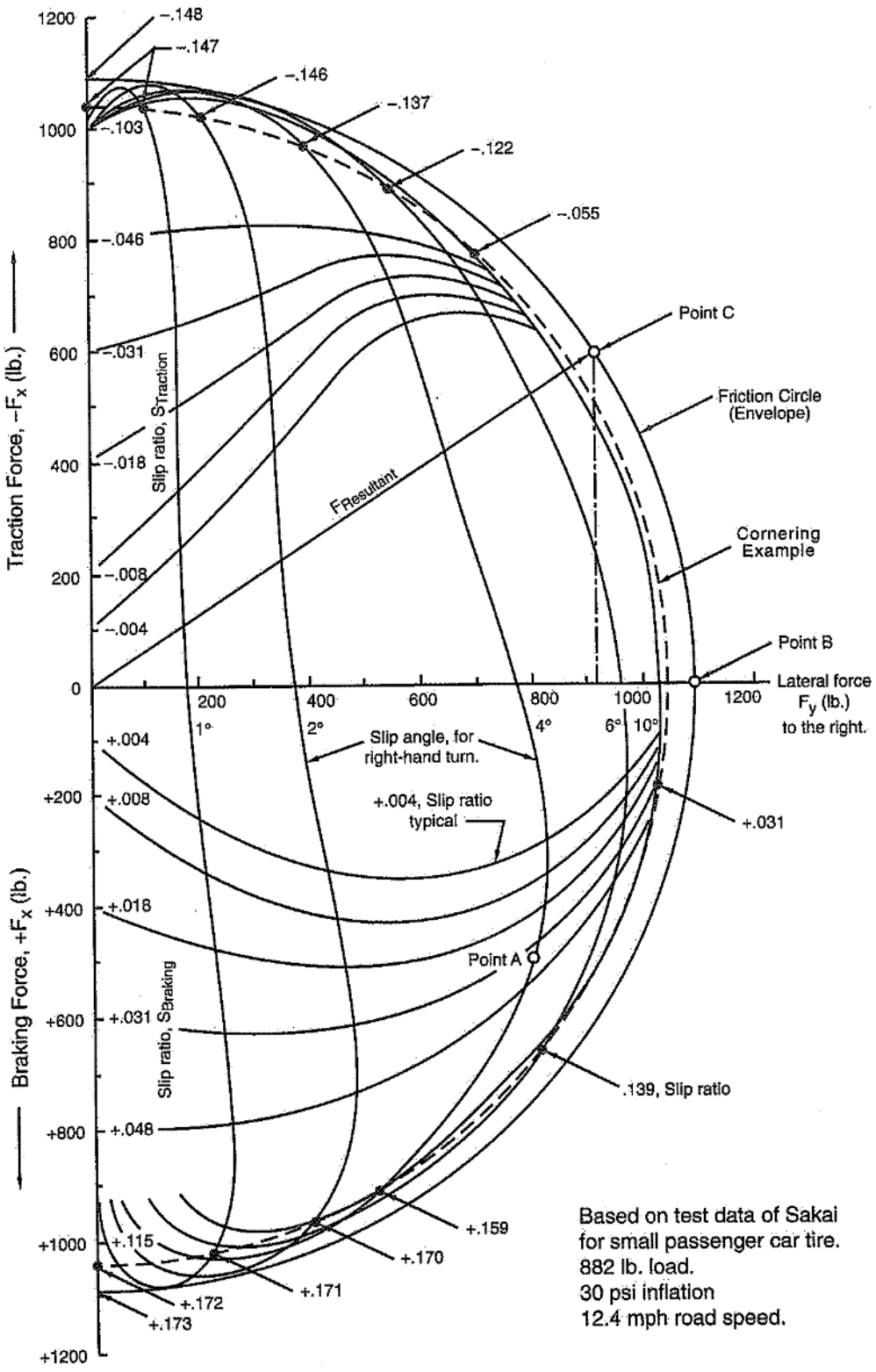

Figure 5.12: Typical "g-g" diagram indicating maximum performance of a tyre. Source [34].

Chapter 6

Dynamic simulations and results

In chapter 3 the measured differences in steering torque between the real Formula 3 car and the baseline rFactor Formula 3 model have been discussed. In a desire to reduce the differences in steering feel, the baseline rFactor model has been upgraded with a Pacejka model of the Hankook Formula 3 tyre and an accurately defined suspension model according to the data available from car manufacturer Dallara. In chapter 5 a Multibody Dynamic model of the same Formula 3 car has been developed using the same tyre and suspension model used in the updated rFactor vehicle model. The purpose of this chapter is to perform dynamic simulations to investigate the accuracy of both the Multibody Dynamic model as the physics of rFactor. This can lead to a new controlled simulation environment for Van Amersfoort Racing.

There are three cases which are considered for dynamic simulations. The first being weaving, slaloming from left to right. Furthermore a high speed corner is considered and a low speed corner. These three cases should give an insight in the accuracy of the updated rFactor model and the Multibody Dynamic model.

6.1 Multibody Dynamic Model setup and balance

Chapter 5 describes the development of the Formula 3 Multibody Dynamic model. During the development, the model is developed to be equal to the car driven during the Barcelona test to perform equivalent simulations. An example are front springs having a stiffness of 17.0 Nm/deg and rear springs having a stiffness of 800 lbs/inch. During initial simulations it became clear that the Multibody Dynamic model is unable to perform the prescribed motion with the same vehicle setup as the real car. The result of a trial-and-error sensitivity analysis showed that in order to complete the simulation maneuvers, the aerodynamic balance as computed from the available data should change to a balance in which the front downforce is decreased with 50% and the rear downforce increased with 50%. Apart from the aerodynamic balance, the mechanical balance also influences the simulation of the motion. This sensitivity analysis is elaborated in section 6.5.

6.2 Weaving motion simulation

Weaving is used in the real car to warm the tyres. Heat is essential for optimal tyre pressures and grip. During the winter test in Barcelona, Jack Hawksworth performed the best weaving motion in the car equipped with a strain gauge attached to the steering column. Therefore, his data is used as input for the Multibody Dynamic model. As described in chapter 5, the wheel speeds, vehicle velocity and steering wheel angle are used as inputs for the Multibody Dynamic model. Arjun Maini was told to reproduce the weaving motion of Hawksworth as best as possible in the simulator, trying to hold a similar velocity.

In the race simulator, no weaving is required to warm the tyre, neither to set a fast lap time. Therefore, weaving is not a part of simulator operation. It is however, a useful maneuver to assess and compare the vehicle response of the rFactor model, the Multibody Dynamic model and the real car. As described in section 6.1, the aerodynamic balance of the Multibody Dynamic model is changed to be able to successfully complete the prescribed motions. It is observed during simulations of the Multibody Dynamic model that a sudden loss in aligning moment is occurring surpassing a certain slip angle. This effect is discussed in more detail in section 6.5. To overcome this phenomenon, only 45% of the recorded steering wheel angle during the real Barcelona test is used as input for the Multibody Dynamic model. In this manner, the original balance of the real Formula 3 car is maintained and the actual model response of the Multibody Dynamic model is captured.

The average speed at which the weaving motion is performed by Hawksworth is 210 km/h. Related wheel speeds and steering wheel angles are extracted from the real recorded data. The steering input for the Multibody Dynamic model is shown in figure 6.1. The response of the model is shown in figure 6.2

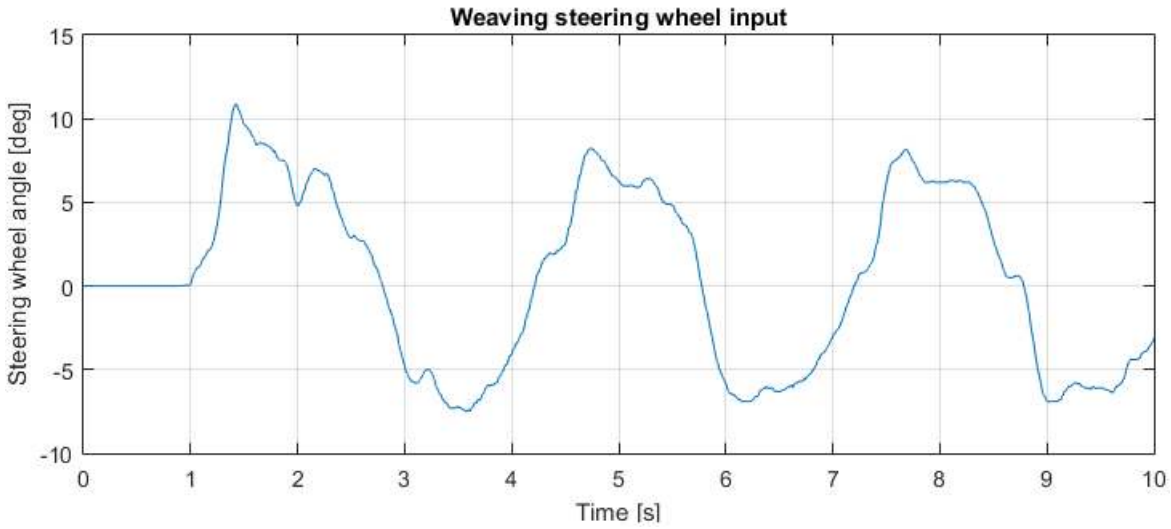

Figure 6.1: Steering wheel input for weaving motion of the Multibody Dynamic model. Extracted from Hawksworth's measurement data.

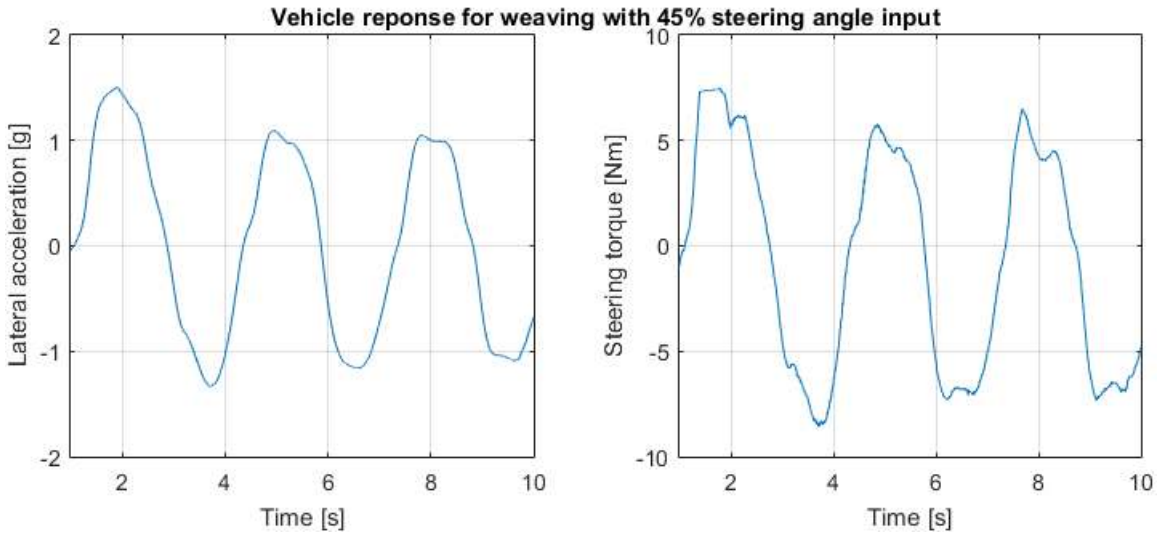

Figure 6.2: Multibody Dynamic vehicle reponse for weaving with 45% of the original steering angle input.

Steering metrics have been used in chapter 3 to make the steering characteristics of a vehicle measurable. Real data has been compared with the baseline rFactor model, which showed differences. These metrics will be used again to assess the performance of the updated rFactor model and the developed Multibody Dynamic model, using the same tyre and suspension model. In figure 6.3, the steering metrics for the weaving motion are shown. At the left hand side, the steering sensitivity is shown. It can be seen that the steering sensitivity of the real car and the multibody dynamic model show more similarity than the rFactor model with the real car. Despite reaching higher lateral accelerations, the rFactor model needs a higher steering angle to generate lateral accelerations. This trend has been seen in chapter 4, where Arjun Maini tested both vehicle models. Figure 4.16 shows that in turn 3 a higher steering wheel angle is required to make the turn compared to the baseline vehicle model.

By using the robust regression method, a regression function is established for the steering metrics. Using this function, the gradient of both metrics are determined to give an numerical compare between the real car and the two vehicle models. In table 6.1, the steering sensitivity gradient is given for the three measurements and their relative difference to the real measurement. Table 6.2 show the steering torque gradients and their relative difference.

Table 6.1: Steering sensitivity gradient for weaving motion.

Measurement	**Gradient**	**Difference to real**
Real car	5.0434	
Updated rFactor model	11.8501	134.96 %
Multibody Dynamic model	2.5568	-49.30 %

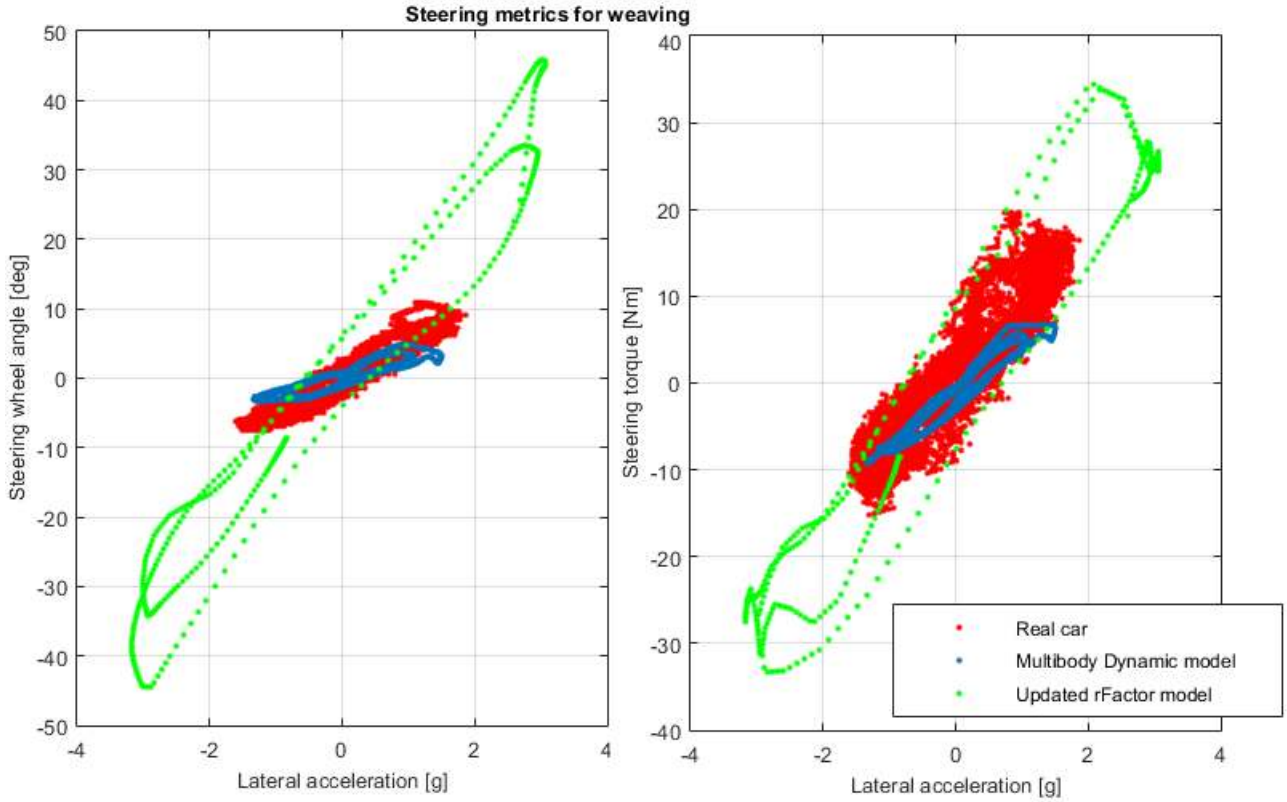

Figure 6.3: Steering metrics for weaving. Note the 45% steering input magnitude for the Multibody Dynamic model.

Table 6.2: Steering torque gradient for weaving motion.

Measurement	Gradient	Difference to real
Real car	8.0317	
Updated rFactor model	9.0389	12.54 %
Multibody Dynamic model	5.6075	-30.18%

From the tables above it can be seen that if one of the models is assigned to perform a weaving motion in the same fashion as the real car, the rFactor vehicle mode requires a 135% higher steering angle than the real car and the Multibody Dynamic model a 49% lower steering angle. Furthermore, the resulting steering torque felt by the driver is 13% higher in rFactor, on the condition that the steering motor is able to generate the required steering torque (see chapter 2 for more information), and the steering torque is 30% less in the simulation of the Multibody Dynamic model.

6.3 High speed turn simulation

In this section, a single high speed turn is considered. One of the turns with the highest velocity on the Barcelona race track is turn 3, a full throttle right hand corner. By simulating this corner, an additional compare can be made between the baseline rFactor

Formula 3 model and the updated Formula 3 model resulting from the implementation of the Hankook tyre model and the Dallara F312 suspension geometry.

In the previous section, it has been discussed that the original setup is not suitable for the Multibody Dynamic model to yield a correct vehicle response. To adjust the setup, the aerodynamic balance of the car is changed, since lowering steering wheel angles would in this case not result in the same trajectory. In other words, lowering the steering angles changes the layout and corner radius of turn 3. As discussed before, 50% decrease in front downforce and 50% increase in rear downforce allows the model to simulate prescribed motions. The average velocity for this turn, 230 km/h, is used to determine the aerodynamic load with the aid of the axle load table as discussed in chapter 5. Figures 6.4 and 6.5 show the input and responses for the Multibody Dynamic model for this simulation.

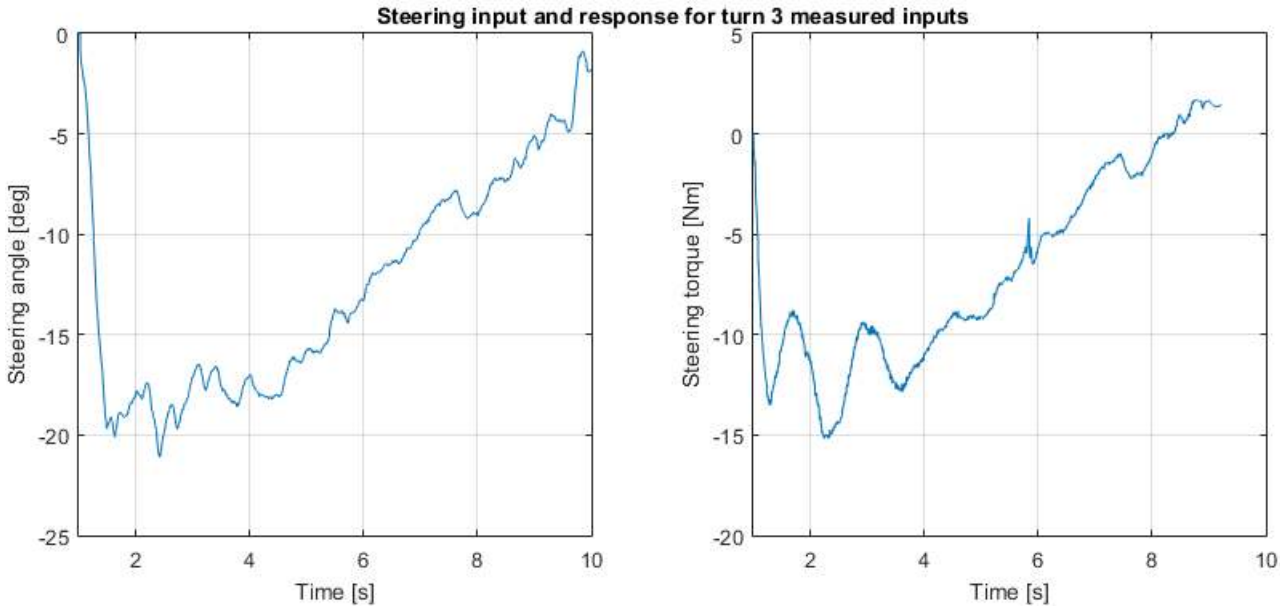

Figure 6.4: Multibody Dynamic model steering input and response for turn 3 measured inputs.

The right hand side of figure 6.5 shows the yaw rotation angle of the vehicle due to the steering input. As can be seen, the angle decreases to a value of -90° before it increases. This is caused by the way the SimMechanics model handles rotations over 90°, where the initial longitudinal velocity is completely exchanged into lateral velocity as seen from an fixed frame of reference. Considering the exchange of velocities due to rotation from a body frame of reference, the longitudinal velocity remains at its initial value and increases according to the external longitudinal acceleration as extracted from real data as described in chapter 5. The differences in measured velocities per reference frame in the Multibody Dynamic model is shown in figure 6.6.

The steering metrics for turn 3 are shown in figure 6.7. It can be observed from the steering sensitivity at the left hand side of this figure that the steering wheel input for the

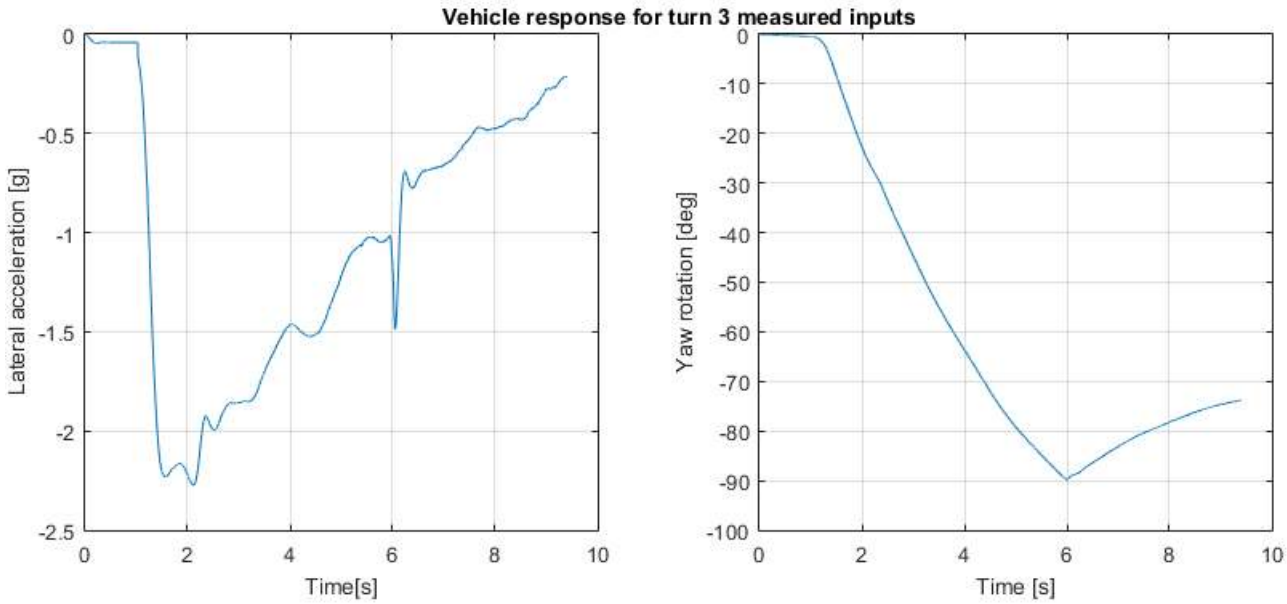

Figure 6.5: Multibody Dynamic vehicle response for turn 3 measured inputs.

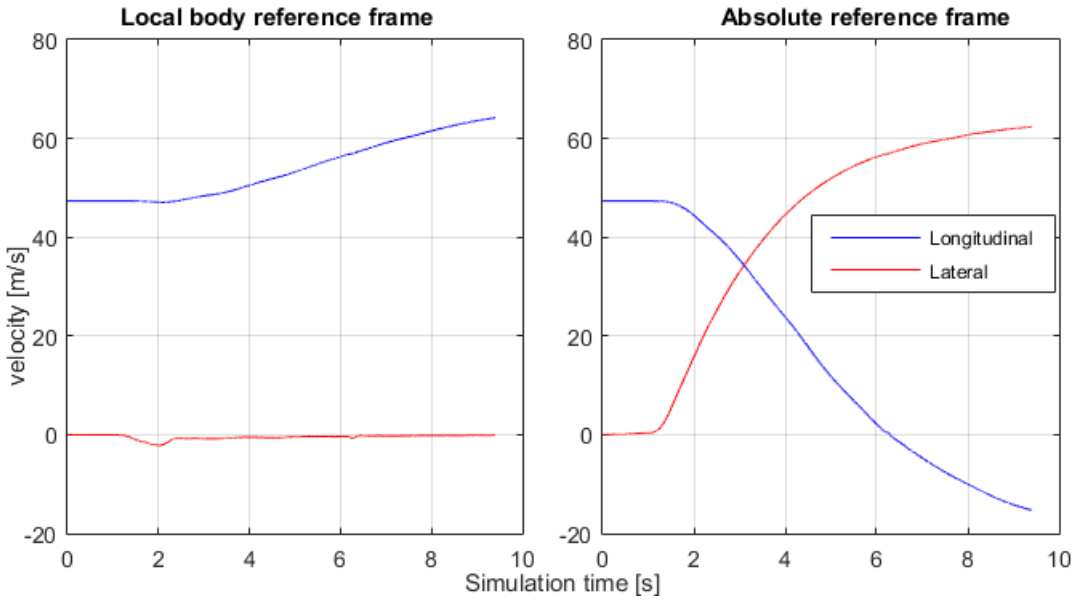

Figure 6.6: Longitudinal and lateral velocity of Multibody Dynamic model. Difference between local body reference frame and absolute reference frame is shown.

Multibody Dynamic model is corresponding to the real measured data as the range of the steering wheel angle is equal. To the same extend as for the weaving motion, the required steering wheel angle for the rFactor model to yield a certain lateral acceleration is higher than the real car and the Multibody Dynamic model. The results of the regression fit are shown in tables 6.3 and 6.4. Additional to the weaving motion, the regression results for the baseline rFactor model are included as derived in chapter 3.

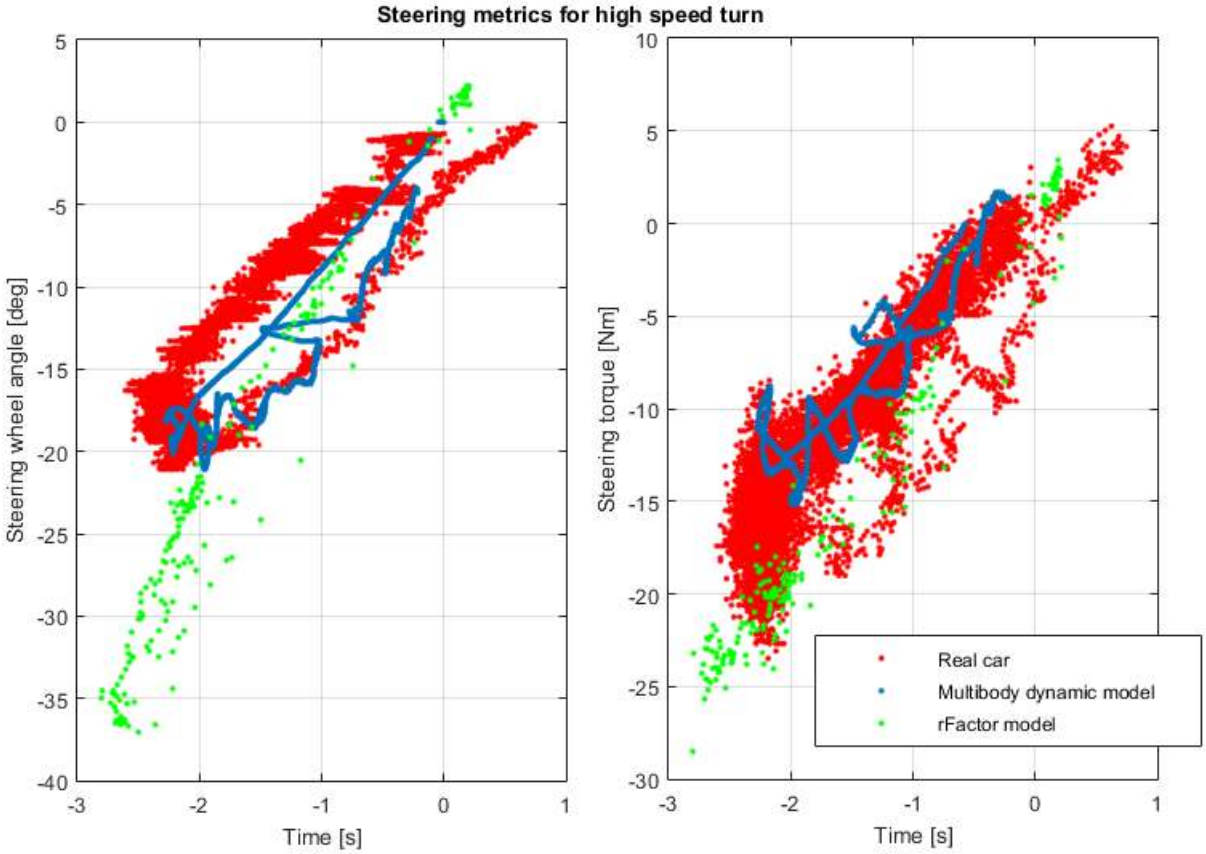

Figure 6.7: Steering metrics for high speed turn 3.

As expected, the steering sensitivity gradient for the updated rFactor vehicle model is not close to the real measurements. Compared to the baseline model, an additional 2° of steering wheel angle is required per lateral g. This indicates that the steering ratio (steering wheel angle to wheel rotational angle) has to be adjusted. By changing this ratio, the rotational angle of the steering wheel per lateral g can be decreased to match the real measurements. The Multibody Dynamic model shows close correlation with the real measurements, as the difference is 7%. The difference between both however, is that the real vehicle is able to reach a higher lateral acceleration given the same steering wheel angle and velocity input. Here the aerodynamic balance influences the understeer tendency created.

In contrast to the steering sensitivity, the torque gradient has been improved with the updated rFactor vehicle model. Per lateral g, the steering torque decreased from 12.8 Nm to 9.4 Nm, which results in a difference of 24.5% to the real measurement. The Multibody Dynamic model generates 3 % torque per lateral g to little to match the real measurement.

Table 6.3: Steering sensitivity gradient for high speed turn 3.

Measurement	Gradient	Difference to real
Real car	7.8128	
Updated rFactor model	12.5494	60.63 %
Multibody Dynamic model	8.3619	7.03 %
Baseline rFactor model	10.5484	35.01 %

Table 6.4: Steering torque gradient for high speed turn 3.

Measurement	Gradient	Difference to real
Real car	7.5340	
Updated rFactor model	9.3777	24.47 %
Multibody Dynamic model	7.2966	-3.15 %
Baseline rFactor model	12.8303	70.30 %

6.4 Low speed turn simulation

This section shows the results of low speed turn simulations compared to measurements performed in a low speed turn at the Barcelona race track. As Milliken (1995) [34] states: "An important principle of circuit racing, is that the velocity should never be constant unless held arbitrary for reasons of endurance, traffic, or safety, or limited by the maximum speed of the vehicle". In an ideal situation, the driver should apply the brakes until the apex of the corner after which the throttle should follow rapidly after. In the current research, the focus has been put on lateral properties of a Formula 3 car. This eliminated the research and development of accurate braking and engine models. Apart from driver influenced longitudinal controls, internal friction in bearings and aerodynamic drag is not considered in this study. Consequently, the longitudinal slip characteristics of the Hankook tyre has not been implemented in the Multibody Dynamic model. The longitudinal load transfer which follows from heavy braking and aggressive throttle application are therefore not part of the current model.

For the selection of low speed turn at the Barcelona race track, low longitudinal accelerations are the main focus points. Figure 3.2 of chapter 3 shows the throttle and brake application of the drivers in real and in the simulator. The corner with the lowest velocity is turn 9 at approximately 3500 meters from start/finish. However this turn is follows from a heavy braking zone into direct full throttle application. Turn 2 follows directly after turn 1. The transition comes, as can be seen at approximately 800 meters, with gentle throttle application going into turn 3. This fact makes turn 2 the best choice for low speed simulations given the model limitations.

The average speed in turn 2 where the downforce values are based on is 150 km/h. In the same fashion as the previous simulations, the same aerodynamic and mechanical balance is used. Figure 6.8 shows the steering wheel input and resulting steering torque for this turn. The reaction to this steering input is shown in figure 6.9, where the lateral acceleration and body yaw angle is shown. Finally, figure 6.11 shows the steering metric for the

low speed turn 2.

For the sake of clarity, the regression lines to measure the steering metrics are drawn. There are two observations which can be seen from the real measurements. The first is the difference in lateral acceleration for the steering sweep seen in the steering sensitivity at the left hand side. At a lateral acceleration of approximately 0 g, the steering angle is already between 10° and 15°. At the sweep back to a neutral steering angle, there is still a lateral acceleration of approximately 0.9 g present. Figure 6.10 shows that the steering wheel angle is already positive while the lateral acceleration is still near zero. At the exit of the turn, the opposite is seen: the steering wheel is neutral, but there is still a lateral acceleration of almost 10 m/s^2. This is caused by the follow-up turn 3, which is directly following up turn 2. The cause for this difference is the lag between steering wheel input and lateral acceleration This effect is known as tyre relaxation [83]. As discussed before, turn 2 follows from another low speed turn but in an opposite direction. Turn 1 is a right hand turn, where as turn 2 is a left hander. Since the transition between turn 1 and 2 is short, the driver aggressively turns the steering wheel to change directions. Tyre relaxation is a transient behavior of a pneumatic tyre and affects the dynamics of the vehicle at relatively low frequencies [84]. The tyre relaxation length can be described as the length the vehicle has to travel before the tyre lateral force is completely present. Relaxation effects are incorporated in the Pacejka tyre model. However, since a single turn is considered and not the combination of turn 1 and 2, no further investigation or validation on tyre relaxation is performed in the current research.

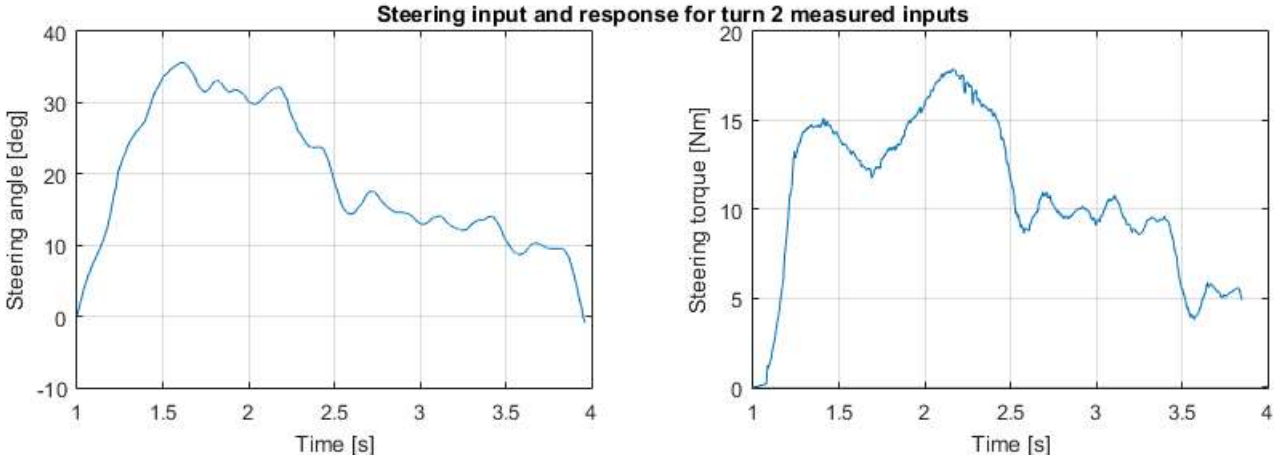

Figure 6.8: Steering input and response for the Multibody Dynamic model for low speed turn 2 inputs.

The gradients of the regression of the steering metrics are captured in tables 6.5 and 6.6.

Due to the tyre relaxation behavior in vehicle response in turn 2, it is hard to draw conclusions about similarities between real measurements and rFactor or Multibody Dynamic measurements. The steering sensitivity for the low speed corner for the updated rFactor vehicle model and the Multibody Dynamic model are in a close range to each other. In contrast, the steering torque gradient is higher for all simulation models than

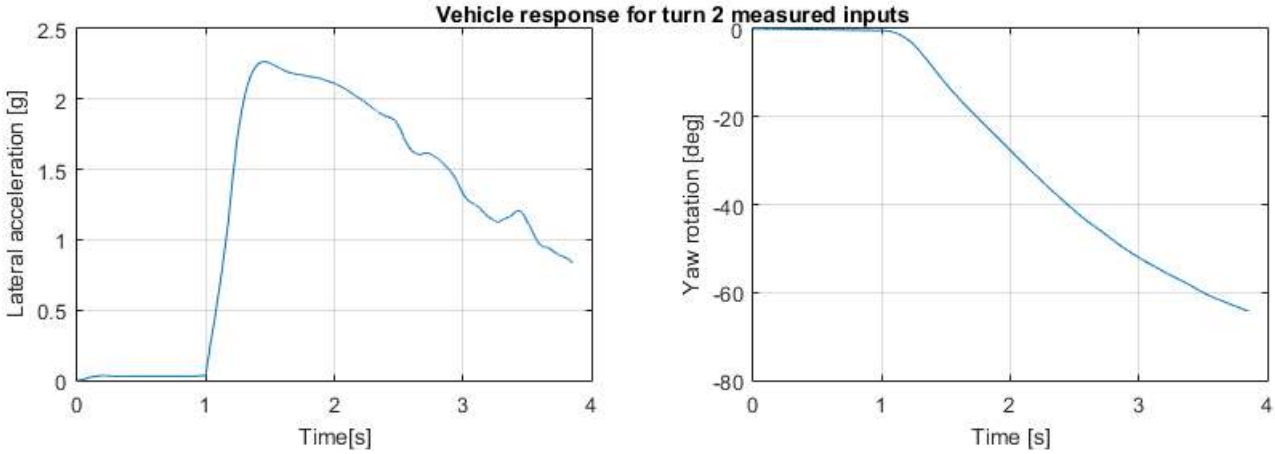

Figure 6.9: Vehicle response of the Multibody Dynamic model for low speed turn 2 measured inputs.

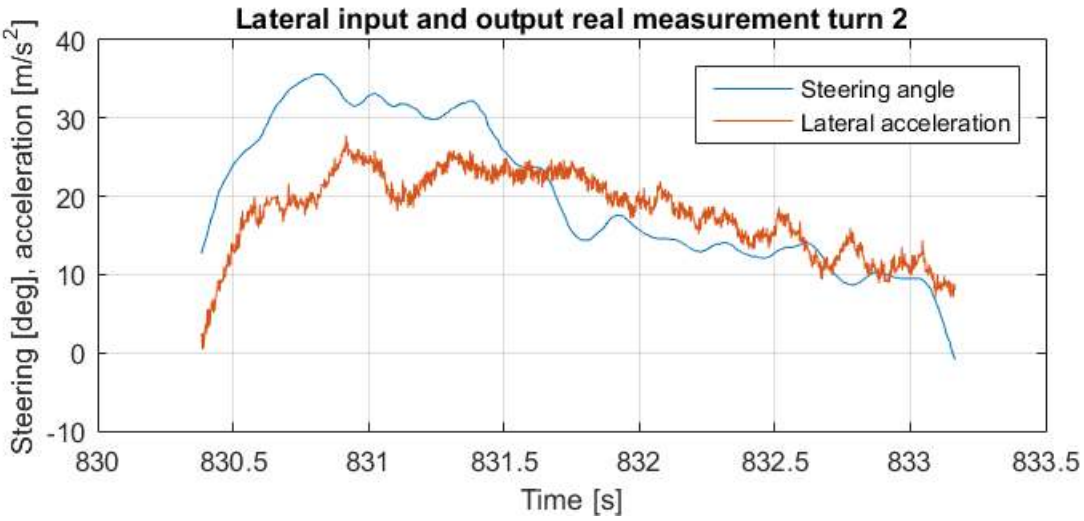

Figure 6.10: Steering input and resulting lateral acceleration in real measurement. Delay in lateral acceleration due to tyre relaxation visible.

for the real car measurement. As can be seen at the right hand side of figure 6.11, there is a large spread of measurement points of steering torque versus lateral acceleration. Fitting a robust regression through these widely spread points may have a small significance compared to the simulation measurements.

Table 6.5: Steering sensitivity gradient for low speed turn 2.

Measurement	Gradient	Difference to real
Real car	12.5804	
Updated rFactor model	12.7429	1.29 %
Multibody Dynamic model	13.8434	10.04 %
Baseline rFactor model	8.3192	-33.87 %

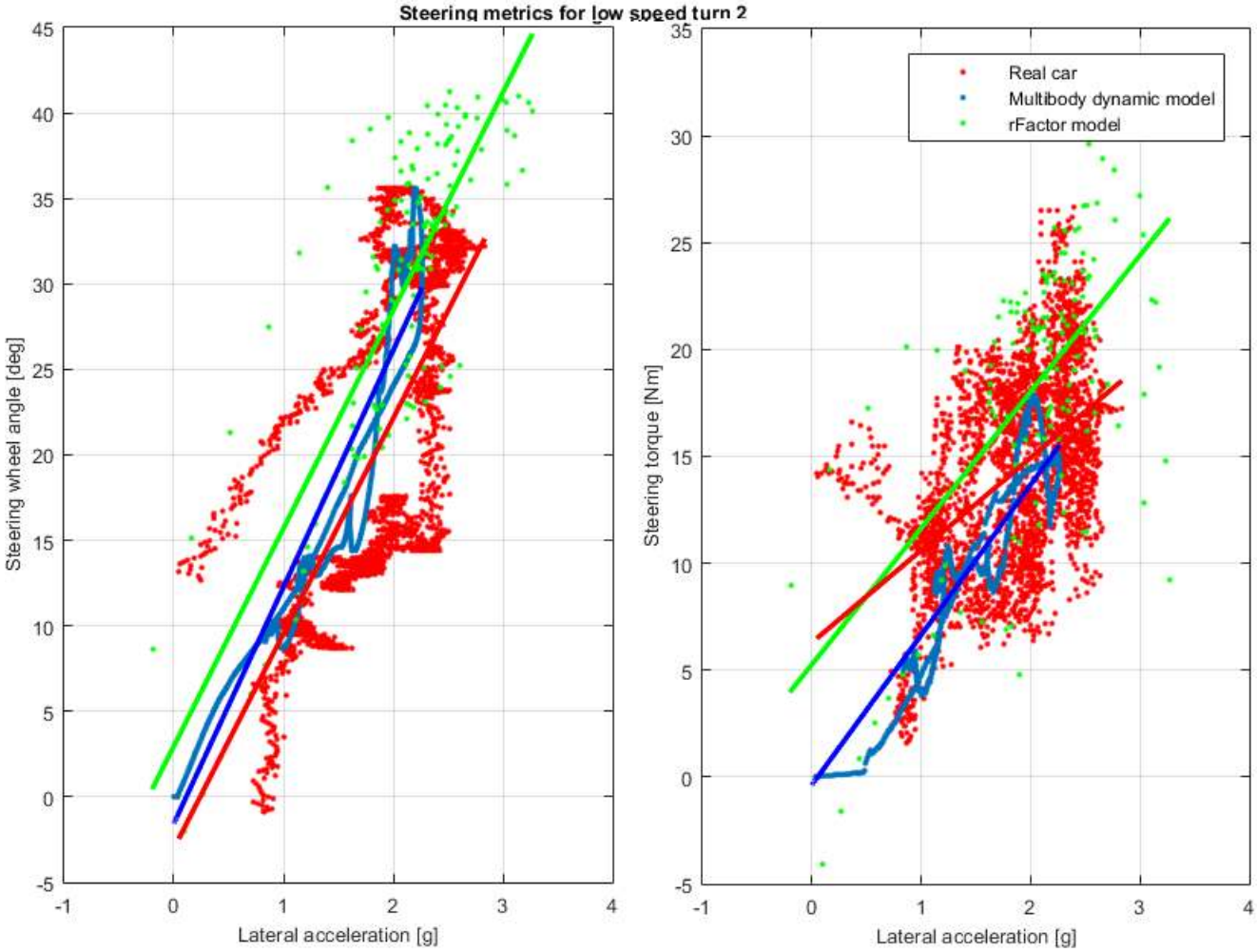

Figure 6.11: Steering metrics for low speed turn 2.

Table 6.6: Steering torque gradient for low speed turn 2.

Measurement	Gradient	Difference to real
Real car	4.3230	
Updated rFactor model	6.3817	47.62 %
Multibody Dynamic model	7.0235	62.47 %
Baseline rFactor model	6.4101	48.28 %

6.5 Multibody Dynamic Model balance sensitivity analysis

The need for a sensitivity analysis for the balance of the Multibody Dynamic vehicle is explained in section 6.1. The model which is generated having the same balance as the real car, was unable to perform the assigned simulation. This section elaborates on the

initial balance and the sensitivity analysis in balance to yield a suitable solution.

In chapter 4 comparing results between the baseline rFactor tyre model and the Hankook tyre model showed that the Hankook tyre model has more grip than the rFactor tyre model. According to Maini, the car feels lazy on initial turn in and suddenly grips, which feels like an oversteer balance. Furthermore, Maini corrects and anticipates on the oversteer balance when steering in. The fact that the Multibody Dynamic model is not able to correct for balance changes but follows a prescribed steering wheel angle trajectory (shown in figure 6.1), is the cause for the spin of the Multibody Dynamic model actuated with real data. In figure 6.12 at the left hand side, the lateral acceleration is shown for the steering wheel angle corresponding to the real measurements. It can be seen that the vehicle steers in initially, before the rear of the car loses grip, spins and loses all lateral acceleration. The right hand side of the figure shows the exponential increase in yaw rotation angle at approximately t = 1.7 seconds, where the lateral acceleration is lost.

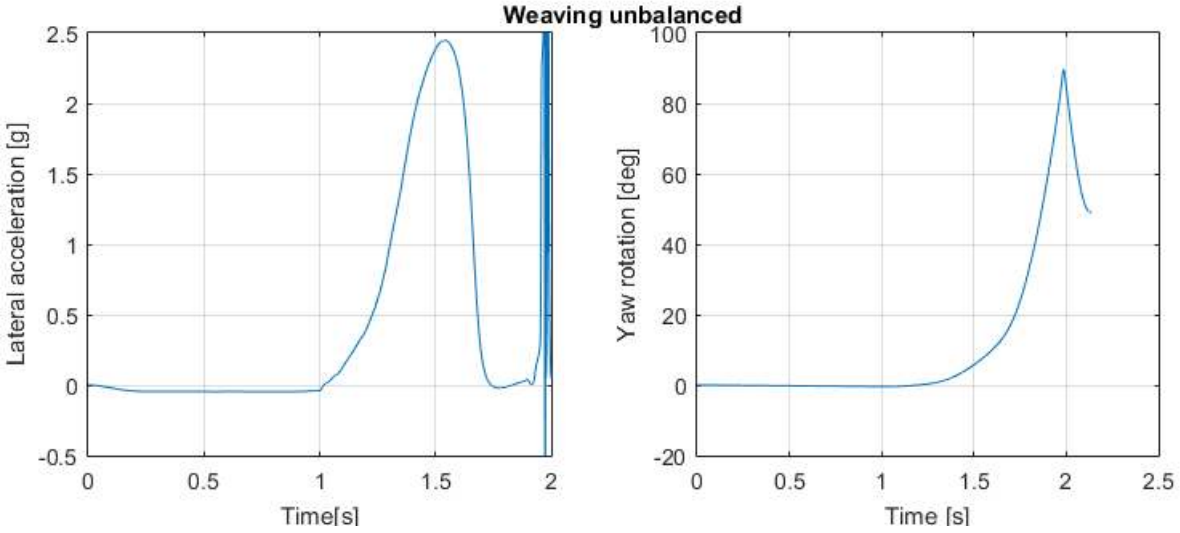

Figure 6.12: Multibody Dynamic model vehicle response to steering wheel input according to figure 6.1.

Apparently, the balance of the car is of importance for completing specific motions. In general, a chassis can be setup up for mechanical balance and aerodynamic balance. Mechanical balance is amongst others the result of spring stiffnesses, damper stiffnesses and anti roll bar stiffnesses. Aerodynamic balance is the distribution of front axle to rear axle downforce. To compensate the oversteer tendency of the Multibody Dynamic model, it is desired to make the balance more understeered. In terms of aerodynamic balance, this is achieved by lowering front axle downforce and increasing rear axle downforce. Mechanically, understeer is created by stiffer front springs and softer rear springs.

To test if both mechanical balance changes as aerodynamic balance changes influences the response of the vehicle, a sensitivity analysis is performed with which balance sweeps are performed in the weaving motion. The following setups (also shown in table 6.7)are used

in simulations to assess the capability of the model to performed the assigned motion:

- Front axle downforce is reduced to 50% of its original value while the other variables are kept equal did not yield a successful simulation.
- Front axle downforce is maintained to 50% while the rear axle downforce is increased to 150% of its original value. A successful simulation is performed.
- Front axle downforce is increased from 50% to 60% of its original magnitude. Rear axle downforce is kept at 150%. All other parameters remained equal. No successful simulation.
- Aerodynamic balance is maintained. Front spring stiffness is increased to 24.5 Nm/deg and the rear spring stiffness decreased to 600 lbs/inch. This choice is made in order to make the car more understeered to compensate the oversteered vehicle balance. The result was a successful simulation.
- The aerodynamic and mechanical balance are back to its original value, equal to the real Formula 3 car during the Barcelona test. The amplitude of the steering wheel angle is reduced to 45% of its original value. This option resulted in a successful simulation.

With the setup of the last analysis, the aerodynamic balance and mechanical balance of the Multibody Dynamic model is equal to the balance of the real car and is therefore useful to compare both. This option is chosen for performing the weaving motion with the Multibody Dynamic model. The adjusted aerodynamic balance of the Multibody Dynamic model of 50% of the original downforce at the front and 150% of the original downforce at the rear is chosen for the high speed and low speed corner simulation.

Table 6.7: Overview balance sensitivity analysis performing a weaving motion with the Multibody Dynamic model

	Aerodynamic		**Mechanical**		**Steering**	**Solution**
	Front %	**Rear %**	k_{front}	k_{rear}	δ_{steer}	
1	100%	100%	17.0 Nm/deg	800 lbs/inch	100%	No
2	50%	100%	17.0 Nm/deg	800 lbs/inch	100%	No
3	50%	150%	17.0 Nm/deg	800 lbs/inch	100%	Yes
4	60%	150%	17.0 Nm/deg	800 lbs/inch	100%	No
5	60%	150%	24.5 Nm/deg	600 lbs/inch	100%	Yes
6	100%	100%	17.0 Nm/deg	800 lbs/inch	45%	Yes

The reason of the required balance change can be found in the tyre model, especially the poor Pacejka model of the rear Hankook tyre. As discussed in section 4.2.5, the rear tyres are modeled in a way that the characteristics in longitudinal and lateral direction are not similar to the front tyres. Especially figure 4.15 shows the rear tyre response to increasing wheel loads. As can be seen by increasing the wheel load, the maximum friction coefficient decreases and occurs at higher slip angles. Even higher wheel loads cause the slip curve to collapse and even reverses sign.

Although the option for lowered front axle downforce and increased rear axle downforce while maintaining the initial mechanical balance did yield a successful simulation, another phenomenon occurs. Figure 6.13 shows the vehicle response for the weaving steering input. At the right hand side the resulting steering torque is displayed. An important observation is the sudden loss in steering wheel torque at t = 1.5 s. This effect is the result of decreasing aligning moment produced by the tyres when the slip angle surpasses the value at which the aligning moment is at its maximum. According to Milliken (1995) [34], the aligning moment can even reverse direction surpassing a certain slip angle. When the mechanical trail is small, most of the steering torque originates from the tyre aligning moment.

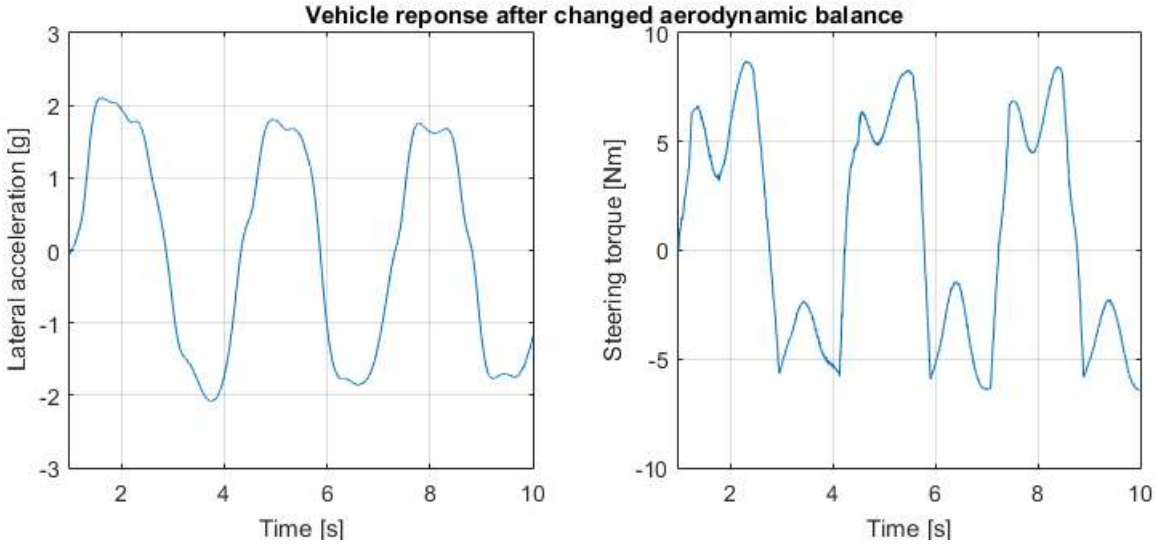

Figure 6.13: Vehicle response for weaving with a changed aerodynamic balance.

The sudden loss in steering torque can be addressed to two phenomena. The first is the lack of mechanical trail. The steering torque is dominated by the tyre aligning moment. Secondly, the maximum friction coefficient value and drop after the maximum friction coefficient occur at relatively low slip angles. Referring back to figure 4.10 in chapter 4, it is shown the the friction coefficient of the Hankook tyre model drops to a larger extend than the original rFactor tyres. Moreover figure 4.8 shows that the peak slip angle for the tyre load range the vehicle operates, is small compared to the baseline rFactor tyre. Apart from the change in peak slip angle, the lateral force produced by the tyre is influenced by the normal force on that tyre. In figure 6.14, the influence of normal force on the lateral tyre force is shown. As can be seen, if the inside wheel is lifted and is subjected to a smaller normal force, the lateral tyre force decreases considerably. These effects demonstrate the loss in steering torque as seen in figure 6.13.

6.6 Summary of simulations

Three test cases have been considered to analyze and compare vehicle response and steering metrics. Vehicle balance turned out to be crucial for the Multibody Dynamic model

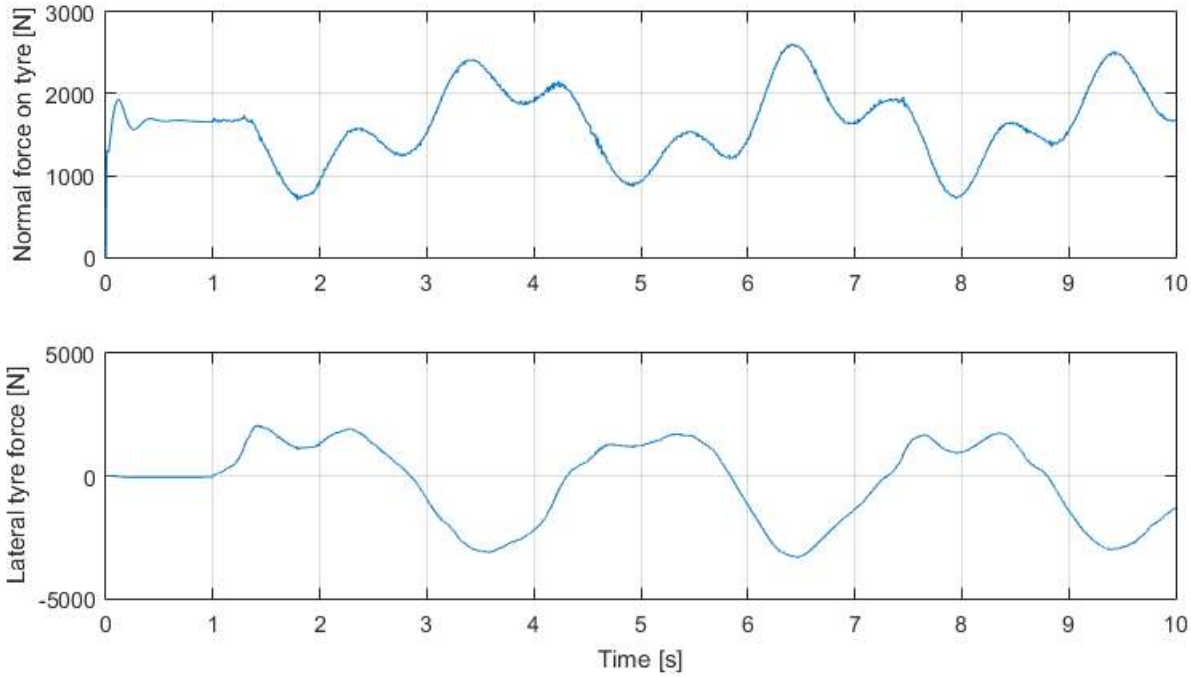

Figure 6.14: Tyre forces for simulated weaving motion with changed aerodynamic balance.

to complete the assigned task. For weaving, the steering wheel amplitude was reduced to 45% of its original magnitude in order to perform the motion with the same setup as the real Formula 3 car. It was shown that the Multibody Dynamic model is more sensitive to steering wheel input than the real car and generates less steering torque given a lateral acceleration. The updated rFactor model requires high steering angles to generate lateral accelerations, although the steering torque gradient showed correlation with the real car.

For the high speed turn, the Multibody Dynamic model performed the prescribed motion with the result of approximately equal steering metrics compared to the real car. The updated rFactor model showed an improved steering torque gradient compared to the baseline rFactor vehicle model in contrast to a decrease of steering sensitivity similarity to the real Formula 3 vehicle.

The updated rFactor model proved to be an improvement in the low speed corner, resulting in a closer match of steering metrics to the real car compared to the baseline model. The Multibody Dynamic model generated a higher steering torque gradient than the real car, however the wide spread of measurement points of steering torque gradient for the real car prevents a clear conclusion.

Chapter 7

Conclusion and recommendations

Van Amersfoort Racing decided to build a race simulator for training and development purposes. The simulation platform was based on the commercially available software named rFactor, which has proved its basis of simulations by the fact that half of the field of Formula One team utilizes the software for their racing simulators. Since there is no research available about the physical correctness of the software, the team wanted to investigate how well the software is able to give the drivers a high fidelity feeling in their simulator. Steering feel is a major aspect which helps drivers perform the driving task. Therefore the current study emphasizes on the steering feel of the real Formula 3 car and their virtual counterparts.

The first aspects which limits the fidelity in the simulator setup is the power supply of the steering motor. Since this motor combined with the current power supply is able to deliver 16 Nm of torque output, higher steering torques can not be generated in this setup. The impact of this limitation is that torque peaks well above 16 Nm are cut off as a constant output of 16 Nm. This reduces the ability for the driver to feel aligning torques and consequently the indication of level of grip at high steering torques.

To be able to compare steering torques computed by the commercial simulation software rFactor and the real car, measurements have been performed. The measurements on the real car and in the simulator took place at the same track, to make sure the corner characteristics are equal. It has been proved that the steering torques required to yield a certain lateral acceleration computed by rFactor are higher than the actual steering torques measured on the real car. Furthermore, the driver has to rotate the steering wheel in general to a higher angle than in the real car to generate a certain lateral acceleration.

The updated suspension and tyre model derived from the developed Multibody Dynamic model of the Formula 3 car have been tested by race driver Arjun Maini. His opinion about the updated model compared to the baseline rFactor model was that the initial turn-in feels lazy. Once the front tyres started to grip at higher steering wheel angles, the

balance would gently shift towards oversteer. Despite the sudden gripping of the tyres, the car was stable in the mid corner since the rear tyres simply follow the fronts. Overall, there is much more grip available. Not only in a lateral sense, but also longitudinally. This allowed him to brake harder and go more easily on power. The high level of grip was already noticed when generating the rFactor tyre model out of the Hankook Pacejka tyre model.

A disadvantage of the updated model is the fact that even higher steering wheel angles are required to turn the car as explained by Maini. This was also seen in measurements, where higher steering angles were required to make the corners. Apart from that, the resulting steering torque was lowered. Given the fact that changing the steering ratio is a straight forward procedure, the overall result of the update was positive in a way that it decreased steering torques. The driver however, did not experience the updated vehicle model as a step towards a more realistic driver feeling.

The Multibody Dynamic model is used to perform simulations in a high speed corner, a low speed corner and in a weaving motion. The standard setup as used during the test with the real Formula 3 vehicle, yielded an oversteered balance for the Multibody Dynamic model. After initial turn in, the front grips and the rear is unable to follow. A possible cause is the poor modeling of the rear Hankook tyre. There was one suitable solution to solve this imbalance: change the aerodynamic balance. For weaving the balance was not changed, but a decrease of amplitude of the steering wheel angle applied. The steering metrics showed that only small steering wheel angles are required to generate lateral accelerations. Also the updated rFactor model did not show good correlation to the real data as higher steering wheel angles were required. The steering torque gradient characteristic of the updated rFactor model had a close match to the real data. Also the Multibody Dynamic model showed good results in terms of steering torque gradient, despite the gradient being lower than the real measurements.

The steering sensitivity of the updated rFactor model did not show an improvement over the baseline model for the high speed turn, but for the low speed turn the difference to the real measurement was only 1%. The Multibody Dynamic model showed good correlation to the real measurements with a maximum relative difference of 10%. In terms of steering torque gradient, the updated rFactor model improved both in high as low speed corners over the baseline model. The Multibody Dynamic model steering torque gradient was nearly equal for the high speed turn, but lacked correspondence in the low speed corner. The correctness of the measurements for the low speed turn however, remain debatable due to the wide spread of measurement points.

The answer to the question about the physical correctness of rFactor can not be completely answered within this research. Although the model computes higher steering torques than measured in the real car, the model is controllable with the same balance as used on the real car. The high required steering wheel angles are adjustable by changing the steering ratio of the model. The Multibody dynamic model can be used to predict steering torques in corners according to velocity and steering wheel inputs, but given the remarkable aerodynamic balance it is not a complete virtual counterpart of the real Formula 3 car. As

a training tool, rFactor remains superior over the developed Multibody Dynamic model having a complete driver experience including audio and graphical features.

The current state of the Multibody Dynamic model is not sufficient to replace rFactor as simulation software. Apart from the missing graphical and audio implementation as stated above, the main aspect of not being able to run on the simulator is the absence of longitudinal dynamics. A following step in the process of developing a simulation platform is the implementation of longitudinal dynamics. If engine characteristics and brakes are implemented in the model, full control of the vehicle is possible. This allows the simulation of a wider variety of motions. The limiting factor in the current model is the fact that the absence of brakes and engine power restrict longitudinal load transfer and therefore influences performance. Low speed turns follow from a heavy braking zone into picking up throttle in the mid corner causes high longitudinal load transfers, which are now to a limited factor present.

Another reason why the current Multibody Dynamic model could not replace rFactor is the length of the computation time. Since the SimMechanics simulation is performed at a time rate lower than real time, the model can not be used in a real time environment. A change in solver and solver type influences compuatational time, however also influences stability of the simulation of running into singular motions. The implementation of Simulink Coder (formerly known as Real-Time Workshop) allows for real time simulation and should be considered for further investigation.

Improvements in the Multibody Dynamic model can mainly be made in the tyre model. As discussed, the rear tyre model of the Pacejka Hankook model is inaccurate. A possible improvement is the implementation of a proven tyre model instead of the Hankook tyre. Delft Tyre as developed by TNO Automotive provides a Magic Formula tyre model in a SimMechanics environment. Apart from the tyres, the aerodynamic model should have a significant improvement. Firstly, drag is not considered in this model, since the longitudinal actuation does not require drag computations. Van Amersfoort Racing has recently been conducting aerodynamic experiments and these could lead to an improved aerodynamic model. Also aerodynamic knowledge of former Formula 3 car could be used. Apart from the vehicle model, another aspect can be improved. Currently, there is no road input to the model. The implementation of a road surface with bumps, height changes and cambered roads add to the reality of simulation. These effects influence the load transfers in the vehicle and the tyre contact patch load variations.

The rFactor Formula 3 vehicle model can then be further improved with the aspects as discussed above. Currently only the tyre model and suspension model have been updated, but also other aspects of the rFactor vehicle model require further development. A successor in this subject will discover many aspects of improvements, both in the Multibody Dynamic model as the rFactor vehicle model.

References

[1] Webpage: Van Amersfoort Racing. Accessed on January 14th, 2015. http://www.vanamersfoortracing.nl/the-team.htm

[2] Webpage: FIA F3 European Championship: Sporting Regulations. Accessed January 14th, 2015. http://www.fiaf3europe.com/en/sporting-regulations/index.html

[3] S. de Groot, J.C.F. de Winter. (2011). *Car Racing in a Simulator: Validation and Assessment of Brake Pedal Stiffness*, Delft University of Technology

[4] Webpage: ADAC Motorsport: ADAC to stage Formula 4 in Germany in 2015. Accessed on January 14th, 2015. http://www.adac-formel-masters.de/uk/artikel/adac-to-stage-formula-4-in-germany-in-2015-adac-formula-4-will-replace-formel-adac-a

[5] S. de Groot, J.C.F. de Winter. (2011). *On the way to pole position: The effect of tire grip on learning to drive a racecar*, Delft University of Technology

[6] K. Koskela, V-M. Nurkkala, J. Kalermo, T. Järvilehto. (2012). *Low-cost Driving Simulator for Driver Behavior Research*, University of Oulu, Kajaani, Finland

[7] Webpage: SimHQ Motorsports: A visit to VirtualGT's Training facilities. Accessed on May 25th 2015. http://simhqmotorsports.com/feature-a-visit-to-virtual-gts-training-facility/

[8] F. Hoeberichts, F. Niewold (2013). *Moog Driving Simulator Speeds Dallara's Race Car Development and Enhances Driver Training*, Moog

[9] J.J. Slob. (2008). *State-of-the-Art Driving Simulators, a Literature Survey*, Eindhoven University of Technology

[10] P. Ciáurriz, I. Díaz, J.J. Gil. (2013) *Bimanual Drive-By-Wire System with Haptic Feedback*, University of Navarra, Spain

[11] T. Åkerstedt, B. Peters, A. Anund, G. Kecklund. (2004). *Impaired alertness and performance driving home from the night shift: a driving simulator study*, Karolinska Insitutet, Stockholm and Swedish Road and Transportation Institute, Linköping, Sweden

[12] S. Classen, C. Levy, D.L. Meyer, M. Bewernitz, D.N. Lanford, W.C. Mann. (2014). *Simulated Driving Performance of Combat Veterand With Mild Tramatic Brain Injury and Posttraumatic Stress Disorder: A Pilot Study*, University of Florida, USA

[13] J.C.F. de Winter, P.M. van Leeuwen, R. Happee. (2012). *Advantages and Disadvantages of Driving Simulators: A Discussion*, Delft University of Technology

[14] D. Toffin, G. Reymond, A. Kemeny, J. Droulez. (2003). *Influence of Steering Wheel Torque Feedback in a Dynamic Driving Simulator*, Renault Technocentre, Guyancourt cedex, France

[15] A. Liu, S. Chang. (1995). *Force Feedback in a Stationary Driving Simulator*, Nissan Cambridge Basic Research, Cambridge, USA

[16] G. Weinberg, B. Harsham. (2009). *Developing a Low-Cost Driving Simulator for the Evaluation of In-Vehicle Technologies*, Mitsubishi Electric Research Labs, Cambridge, USA

[17] Webpage: DrRacing's Blog: How close is close enough? Accessed on August 7th, 2015. https://drracing.wordpress.com/2014/01/03/how-close-is-close-enough/

[18] Webpage: F1 Simulators revealed. Accessed on January 16th, 2015. http://www.racecar-engineering.com/articles/f1/f1-simulators-revealed/

[19] H.B. Pacejka, E. Bakker. (2007). *The Magic Formula Tyre Model*, Delft University of Technology.

[20] Webpage: SimMechanics: Model and simulate multibody mechanical systems. Accessed on August 7th, 2015. http://nl.mathworks.com/products/simmechanics/?refresh=true

[21] H. Ljung. (1998). *System Identification.* Department of Electrical Engineering, Linköping University, Sweden

[22] J. Sjoberg, Q. Zhang, L. Ljung, A. Benveniste, B. Delyon, P. Glorennec, H. Hjalmarsson, A. Juditsky. (1995). *Nonlinear Black-box Modeling in System Identification: a Unified Overview.* Department of Electrical Engineering, Linkoping University, Sweden.

[23] Webpage Hubpages. (2012). *Whats the best PC-racing simulator?* Accessed on May 16th, 2013, from http://smoky08.hubpages.com/hub/Whats-the-best-PC-racing-simulator

[24] B. Lord. (2009). Inside Red Bulls Amazing F1 Simulator. *F1 Racing, August 2009.* Accessed via http://www.virtualr.net/driving-red-bulls-rfactor-pro-simulator on May 16th, 2013.

[25] Webpage: FIA Formula 3 European Championship. Accessed on January 13th, 2015. http://www.fiaf3europe.com/en/technical-regulations/index.html

[26] Webpage: Volkswagen Motorsport, *The engine concepts.* Accessed on January 13th, 2015. http://www.volkswagen-motorsport.com/index.php?id=312&L=1

[27] ES Admin (2013). *Racing cars in the new series equipped with Bosch technology.* Accessed on January 13th, 2015. http://automotive.electronicspecifier.com/drive/racing-cars-in-the-new-series-equipped-with-bosch-technology

[28] Renault Sport (2009). *Formula Renault 2.0 User Manual, A. Introduction.* Accessed on 15-11-2013. http://necup.com/index.php/regulations

[29] Dallara Automobili (2012). *Dallara F312 Manual*

[30] Webpage: RSC Forums, *The rFactor HDV file and it's role in defining the car.* Accessed on April 29th, 2014. http://www.ausfactor.com/rfc/HDV.htm

[31] Renault Sport. (2013). *Formula Renault 2.0.* Accessed on May 16th, 2014. http://www.tatuus.it/pdf/dp_formula_renault_2.0_2013.pdf

[32] Renault Sport. (2009). *Formula Renault 2.0 User Manual, E. Electronics.* Accessed on May 16th, 2014. http://necup.com/uploads/Manual%202012/E_ELECTRONICS.pdf

[33] K. Whittaker. (2013). *maxon motors in the Formula Renault 3.5.* Accessed on May 16th, 2014. http://www.maxonmotor.co.uk/medias/sys_master/8809608609822/2013-05-enUK-Formula-Renault-3.5.pdf?attachment=true

[34] W.F. Milliken, D.L. Milliken. (1995). *Race Car Vehicle Dynamics.* Warrendale, PA: Society of Automotive Engineers, Inc.

[35] Real data gathered during winter test at Circuit de Barcelona - Catalunya, Gustavo Menezes.

[36] Personal communication with R. Vernooij, February 11th, 2013)

[37] Renault Sport (2009). *Formula Renault 2.0 User Manual, B. Chassis.* Accessed on May 20th, 2014. http://necup.com/uploads/Manual%202012/B_CHASSIS.pdf

[38] Webpage: Hydaira dimension sheet. Accessed on January 19th, 2015. http://www.hydaira.ch/downloads/en/masse_ZU_G_Gz.pdf

[39] Webpage: Brake Fluid Explained. Accessed on January 19th, 2015. http://www.opieoils.co.uk/pdfs/tech-articles/Brake-Fluid-Explained.pdf

[40] Webpage: Leo Bodnar Electronics. Accessed on January 15th, 2015. http://www.leobodnar.com/shop/index.php?main_page=product_info&cPath=66&products_id=204

[41] Webpage: SimSteering. Accessed on January 15th, 2015. http://simsteering.com/products.html

[42] Webpage: CNET: *Input lag: How important is it?* Accessed on January 15th, 2015. http://www.cnet.com/news/input-lag-how-important-is-it/

[43] Webpage: Tweakers.net. Accessed on January 15th, 2015. http://tweakers.net/pricewatch/295217/optoma-3d-gt750-xl/specificaties/

[44] Webpage: Fly Elise-ng Immersive Display Desktop v1.4, User Guide. Accessed on January 15th, 2015. http://www.fly.elise-ng.net/images/products/ImmersiveDisplayDesktop/Immersive%20Display%20Desktop%20User%20Guide.pdf

[45] Optoma GT750XL User Manual, http://optomausa.com/webresources/files/support/2ff5b4d9a13e40619a44f7ca0f726588.pdf

[46] Philips Research Technology Magazine. Februari 2008. Accessed on January 15th, 2015.http://www.research.philips.com/password/download/password_31.pdf

[47] FIA. (2014). 2015 Formula 3 Technical Regulations. Accessed on January 19th, 2015. http://www.fia.com/sites/default/files/regulation/file/2015_R%C3%A8gleTech_F3_031214.pdf

[48] L. Bodnar. (2011). *Why Force Feedback In Computer Simulators Does Not Work.* Accessed on Januari 19th, 2015. https://dl.dropboxusercontent.com/u/17548791/FFBdontwork.pdf

[49] SimSteering User Manual. Accessed on February 28th, 2014. http://www.leobodnar.com/files/simsteering/SIMSTEERINGUSERMANUAL.pdf

[50] Webpage: Mathworks: Joystick Input. Accessed on February 28th, 2014. http://www.mathworks.nl/help/sl3d/joystickinput.html

[51] Webpage: Matlab Central: Real-Time Pacer for Simulink. Accessed on February 28th, 2014. http://www.mathworks.com/matlabcentral/fileexchange/29107-real-time-pacer-for-simulink

[52] Webpage: Race Department: Like you FFB strong? Think again.. Accessed on February 28th, 2014 http://www.racedepartment.com/forum/threads/like-your-ffb-strong-think-again.30763/

[53] Simulator data gatherer during simulator session at Circuit de Barcelona - Catalunya, Atze Kerkhof.

[54] P. Haney. (2003). *The Racing & High-Performance Tire*, United States of America

[55] http://www.mrwaynesclass.com/circular/notes/corner/home.htm 5-8-2014

[56] D.I. Katzourakis. (2012). *Driver Steering Support Interfaces Near the Vehicle's Handlin Limits*, Delft University of Technology

[57] TBC tyre file rFactor

[58] S.L. Miller, B. Youngberg, A. Millie, P. Schweizer, J.Ch. Gerdes. (2001). *Calculating Longitudinal Wheel Slip and Tire Parameters Using GPS Velocity*, Department of Mechanical Engineering, Stanford University, United Kingdom

[59] N.D. Smith. (2003). *Understanding Parameters Influencing Tire Modeling*, Colorado State University, USA

[60] Webpage: The rFactor TBC file and it's role in defining the car. http://www.ausfactor.com/rfc/TBC.htm. Accessed on December 15th, 2014.

[61] H.B. Pacejka. (2006). *Tyre and Vehicle Dynamics*, Delft University of Technology

[62] Webpage: FIA F3 European Championship: Technical Regulations. Accessed December 30th, 2014. http://www.fiaf3europe.com/en/technical-regulations/index.html

[63] Setup sheet car #30 for Norisring, 2014

[64] Test results (including Pacejka coefficients) of Hankook tyre on Flat Trac III CT test bench on March 19th, 20th and 21th, 2012.

[65] P. Stephens, H.J. Kohn. (1999). Influence of the tyre on subjective handling at the limit. Published in J.P. Pauwelussen (1999) *Vehicle Performance: Understanding Human Monitoring And Assessment* (p. 181). Meppel, The Netherlands: Swets & Zeitlinger B.V.

[66] Simulation data gathered during simulator test with baseline rFactor tyres at Circuit de Barcelona - Catalunya, Arjun Maini.

[67] Simulation data gathered during simulator test with Hankook tyres at Circuit de Barcelona - Catalunya, Arjun Maini.

[68] Personal communication with A. Maini, August 9th 2015.

[69] Dallara Automobili (2012). *Dallara F312 Manual*

[70] Webpage: SimMechanics. Accessed on May 12th, 2015. http://nl.mathworks.com/products/simmechanics/

[71] Webpage: SimMechanics First and Second Generation Comparison. Accessed on May 12th, 2015. http://nl.mathworks.com/help/physmod/sm/gs/simmechanics-first-and-second-generation-comparison.html

[72] Webpage: Modeling Multibody Systems. Accessed on May 12th, 2015. http://nl.mathworks.com/products/simmechanics/features.html#modeling-multibody-systems

[73] Webpage: Hankook Ventus F200. Accessed on May 12th, 2015. http://www.hankooktire.com/global/competition-cars-tires/hankook-ventus-f200.html

[74] Webpage: MATLAB Newsgroup: Plane equation. Accessed on May 19th, 2015. http://www.mathworks.com/matlabcentral/newsreader/view_thread/269355

[75] Personal communication with R. Vernooij, July 2nd, 2015.

[76] Bosch Motorsport, Datalogger C60, Manual, Page 95

[77] Webpage: MathWorks Documentation: Modeling Grounds and Bodies. Accessed on May 20th, 2015. http://nl.mathworks.com/help/physmod/sm/mech/ug/modeling-grounds-and-bodies.html

[78] Personal communication with M. Voskuijl, March 6th 2015.

[79] Dallara F306 setup sheet.

[80] B. Gergely. (2008). *Application of Active Anti Roll Bar Systems for Enchancing Yaw Stability*, Budapest University of Technology and Economy.

[81] Setup sheet car #30 for Imola, 2014

[82] Aeromap Dallara F312, personal communication with P.M. van Leeuwen, July 8th, 2015.

[83] M. Tidlund & S. Angelis. (2013). *Optimal steering control input generation for vehicles entry speed maximization in a double-lane change maneuver.* Masters Thesis. KTH Royal Institute of Technology.

[84] B. Niessen, S. Jansen, I. Besselink, A. Schmeitz & H. Niemeijer. (2012). *An enhanced generic single track vehicle model and its parameter identification for 15 different passenger cars.* TNO / Eindhoven University of Technology.

[85] Webpage rFactor-Leauge.com. Accessed on May 16th, 2013. http://www.rfactor-league.com/rFactor/rFactorFiles.html

Appendix A

rFactor file and model structure

The simulation software on which the simulator will operate is chosen to be rFactor. This game has proven to be one of the most realistic, open-endedness, fully modability [23] and easily available race simulation software in the current segment of racing simulators. Moreover, even Formula One teams base their simulators on rFactor [24] due to its open source character. Although the game has been developed and released in 2005, daily modifications are released by the game developer (Image Space Incorporated, ISI) or the immense community supporting the game. These facts made the decision to work with rFactor the logical step in the development of a high end race simulator for Van Amersfoort Racing.

As mentioned earlier, rFactor has full ability of customization. The files of rFactor are designed and organized as such, that so called modders (community members which develop extra content for the game in terms of cars or tracks) are allowed to have full access to car and track models. The real physics of the game however, are hidden to all people, as this is the intellectual right of the game developer (ISI).

A.1 File structure

All files concerning tracks and locations are stored in the following directory: rFactor\GameData\Locations. The minimum set of files required for a specific track consists out of 4 types of files. The first one, called Track.MAS is a compressed group of files containing all 3D geometric information of the track. Aspects like textures, skies and other objects are defined and drawn in these files. The second group of files is called Track.CAM, in which all camera positions at the sides of the track are defined. Track.AIW defines the coordinates of everything vital off-track. Examples are pitbox buildings and garage location. The last set of files is called Track.other. These files are mostly graphics used during loading sequences and are simply static images. On the other hand, there are vehicle files, in which the complete vehicle model is described and defined.

In contrast to track files, vehicle files are more complex and stored in different directories for the sake of overview. The first group of vehicle files can be seen as the master folder for each vehicle. The group is called Vehicle.RFM. In these set of files, general settings of the specific vehicle are defined. Environment settings, user settings, vehicle file paths and championship regulations are examples of these settings. These files are found in the rFactor\rFm folder.

The graphics of the vehicle are stored in files which define the group of Vehicle.VEH files. In these files, the general car of a specific class is defined, as well as liveries per team. That means each car in the class of vehicles has its own Vehicle.VEH file. The sound files of the cars are stored in the rFactor\GameData\Sounds folder. The group of files is called Vehicle.SFX, containing complete sets of sounds generating a realistic engine sounds for a specific vehicle.

The class Vehicle.VEH files defines what the car looks like while standing still. However, in most cases the car appears to be moving over the track. All details which help to make the car look like moving are defined in the Vehicle.GEN file class. Details like head movement and rotating rims are defined in the files of this class.

The most important physics file of a car is the Vehicle.HDV file. The extension HDV stands for High-detail vehicles parameters. In this file all core attributes of the vehicle is defined. Varying from engine, tyres and transmission parameters to setup and artificial intelligence (AI) parameters, all is described in the Vehicle.HDV file. In these files references are made to specific underlying files. Whereas the engine is defined in the Vehicle.HDV file, the details of that specific engine are described in the Engine.INI file. In this file torque curves are defined and other related parameters such as fuel consumption, engine lifetime and optimal operating temperatures for water and oil.

Another important file which influences the physics of the vehicle is defined in the Vehicle.PM file. In this file, the complete suspension geometry of the car is defined. The geometry is defined in a 3 axis system, where the x-axis of the reference frame is the lateral axis though the car, positive to the left as seen from behind. The z-axis is the longitudinal axis through the car with the positive end pointing backwards. Lastly, the y-axis is the vertical axis, positive upwards.

In figure A.1, the links between all files used by rFactor are shown. Most important for the current study, are the .ini files in the lower left corner, being the TBC-file and PM-file describing the tyres and suspension respectively. The combination of these six files define the parametric vehicle model. The six files in the lower right corner have the purpose of defining all graphical properties of the specific model.

A.2 Parametric model

The parameters used in rFactor are fully adjustable. These parameters are fed into the hidden physics engine of the game. These parameters have a simple nature. Most parameters are single value parameters, others may contain a matrix of values. Another type of parameter consists out of couples, whereas the first parameter defines the range which can be selected, while the second defines the setting within the given range to apply. In the table below, parameters concerning the tyre model are given for the baseline rFactor Formula 3 tyre plus its explaination. The suspension file is given in appendix D, where the values are corresponding to the suspension geometry of the real F312 Formula 3 car.

Parameter	**Value**	**Description**
SLIPCURVE		
Step	0.00900	Step increments in slipratio in the slipcurve
DropoffDunction	1.0	Describes how the slipcurve dropoff is affected when the peak of the slipcurve changes
Data		Slipcurve data per slipangle increment set in Step
COMPOUND		
DryLatLong	(1.605, 1.605)	Max friction coefficient on dry pavement in longitudinal and lateral direction
WetLatLong	(1.160, 1.160)	Max friction coefficient on wet pavement in longitudinal and lateral direction
Radius	0.265	Outer radius of the tyre
RadiusRPM	2.01 e-6	Increase in tyre radius per unit RPM
Width	0.180	Tyre width
SpringBase	59523.0	Spring rate with no pressure in tyre (1650lb/in @ 200kpsi) Springyness of the side carcass of the tyre
SpringkPa	1000.00	Spring rate per unit pressure. Total spring rate is SpringBase + SpringkPa * tyre pressure
Damper	1868.0	Damper rate tyre, pure damper rate of side carcass, air contribution to springyness is not considered. Higher damper leads to more rolling resistance (hysteresis) and higher heat build-up
SpeedEffects	(0.0, 0.0)	First parameter is speed (m/s) at which grip drops to half. Second parameter is equivalency parameter. Higher values makes speed a more dominant factor
LoadSens	(0.0, 0.5, 16000.0)	Tyre load sensitivity. First parameter is the inital slope at 0N vertical load. Second is grip multiplier, third final vertical load (multiplied*final load). LoadSens returns a value between 0.0 and 1.0, as mulitplier to grip level defined in DryLatLong
LatPeak	(0.100, 0.22, 12000.0)	First parameter describes at which slip angle (sin(value)) the peak slip occurs at zero load. The second parameters is the peak slip angle at the load given in the third parameter.

Parameter	Value	Description
LongPeak	(0.100, 0.22, 12000.0)	First parameter describes at which slip angle (sin(value)) the peak slip occurs at zero load. The second parameters is the peak slip angle at the load given in the third parameter.
LatCurve	'Default'	Assigns a specific SLIPCURVE for lateral forces generation
BrakingCurve	'Default'	Assigns a specific SLIPCURVE for braking forces generation
TractiveCurve	'Default'	Assigns a specific SLIPCURVE for tractive forces generation
CamberLatLong	(3.50, 0.12, 0.28)	Peak camber angle, lateral gain peak, longitudinal loss because the tyre is not flat on the ground. Value is gain at max camber angle
RollingResistance	2500.0	Resistance torque (Nm) per unit deflection (m) on ground
HeatBasePeak	(0.15, 0.00)	Base peak slip to compute friction heat, fraction of base to use (0.0=use dynamic peak slip only)
Heating	(7.40e-1, 7.20e-3)	First value creates heat linearly with rolling speed and vertical tyre deflection. Dependend on tyre radius and tyre pressure. Second parameter compared current slip to realtime peak slip (which changes wirh LatPeak and LongPeak), or a constant peak slip or a combination, depending on the values in HeatBasePeak. Adjustments by trial and error.
Transfer	(7.00e-3, 4.00e-3, 1.25e-4)	Heat transfer to road, static air, moving air, similar to Heating
HeatDistrib	(17.0, 130.0)	(Max camber angle/max off-pressure) that affects heat distribution (higher number is less temperature difference). Difference in temperature left, mid and right due to camber. Value is limit for amount of camber and off pressure
AirTreadRate	0.009	Heat transfer between tread and air inside tyre. Management if heat distribution across tyre. Increase in weight leads to increase in heat generation in sides of tyre.
WearRate	0	Wear rate constant
WearGrip1	(0.998,0.996,0.993,0.990, 0.985,0.978,0.969,0.954)	Grip at 6/13/19/25/31/38/44/50 % wear
WearGrip2	(0.934,0.904,0.864,0.810, 0.745,0.660,0.560,0.450)	Grip at 56/63/69/75/81/88/94/100 % wear
Temperatures	(90.0, 30.0)	Optimum operating temperature, starting temperature
OptimumPressure	(105.0, 0.0200)	Base pressure to remain flat on ground at zero deflection and multiplier by load to stay flat on ground. So first parameter is for normal shape of tyre with no load, second is kPa/N load to maintain shape
GripTempPress	(0.0, 0.0, 0.0)	Factors to change the grip when either below tyre optimal temp, above temp and off-pressure. The higher the value, the higher grip drop-off
PneumaticTrail	0.000012	Pneumatic trail per unit load (m/N). Responsible for self-aligning torque. Max self-aligning torque at half max slip angle.

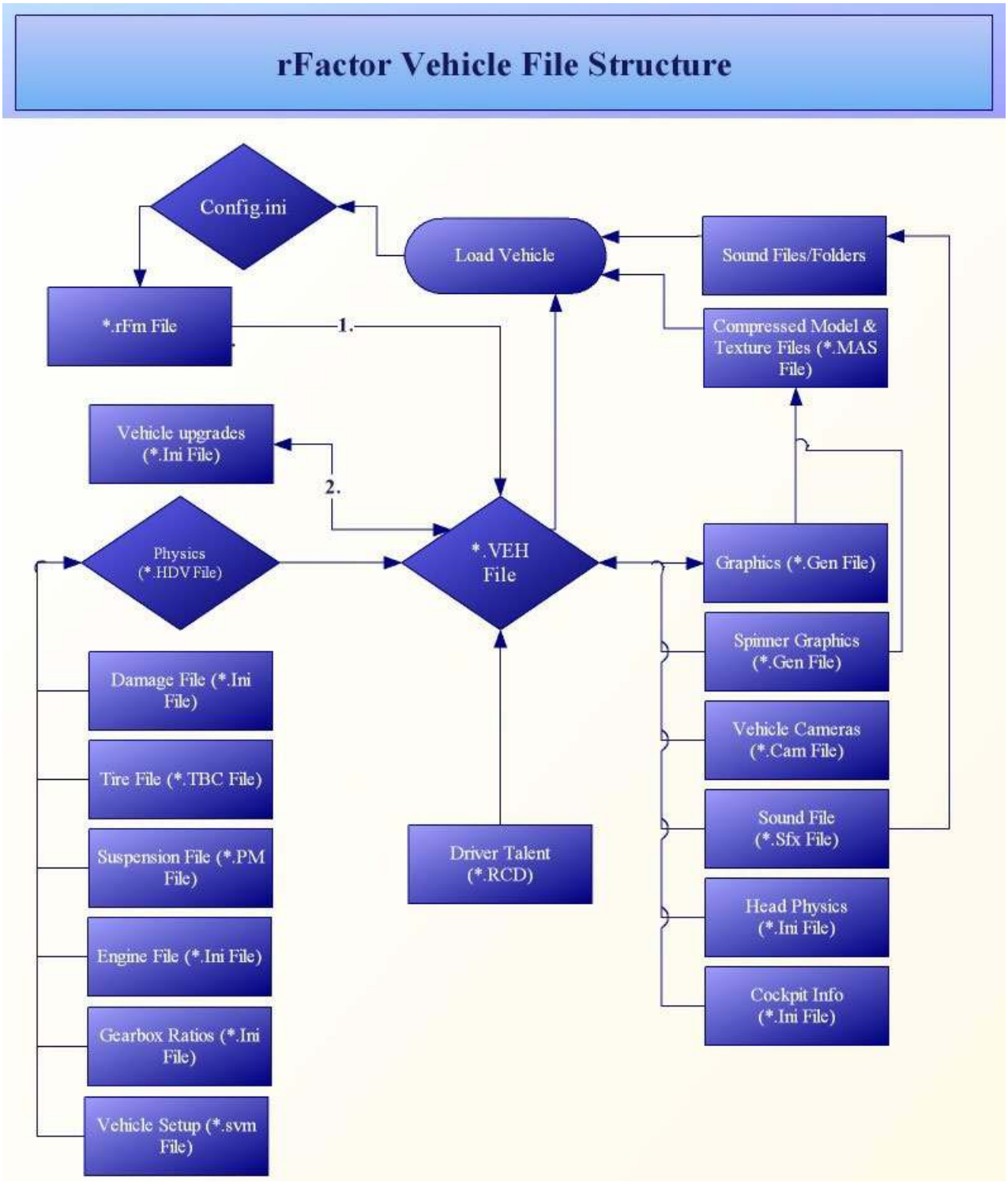

Figure A.1: File structure within rFactor to describe to parametric vehicle model. Source: [85]

Appendix B

Pacejka tyre model conversion

This appendix describes the method of converting the Pacejka tyre model of the Hankook Formula 3 tyre into a tyre model supported by rFactor.

B.1 Friction coefficients

The Hankook tyres which are used to develop the Pacejka model are tested at a specific normal wheel load. For the front tyres this wheel load is 2244.4 N, where the rear tyres are tested at 2339.0 N. In order to construct the slip curves as input for the rFactor model, slip curves are generated at these nominal wheel loads because this is the basis of the Pacejka model. At this nominal load, friction coefficients in longitudinal and lateral direction are determined. These friction coefficients can be recalculated to the normalized friction coefficients used by rFactor using the governing equation used for constructing a Pacejka tyre model. In equation B.1 is shown how the coefficient of friction for longitudinal slip is calculated.

$$\mu_x = (p_{Dx1} + p_{Dx2} \cdot df_z) \cdot (1 - p_{Dx3} \cdot {\gamma_x}^2) \cdot \lambda_{\mu x} \tag{B.1}$$

In this equation, the friction coefficient in longitudinal direction, μ_x, is a function of a base friction coefficient at nominal load, p_{Dx1}. The variation of friction coefficient with load is modelled by the parameter p_{Dx2}, which is multiplied by the weight related parameter df_z shown in equation B.2. The effect of camber is added by introducing the parameter p_{Dx3}, which is mulitplied by the camber angle γ_x squared. Lastly, scaling coefficient $\lambda_{\mu x}$ is multiplied, which is a scaling factor for the longitudinal force peak friction coefficient [64]. These scaling factors however, are all equal to one for these tyre tests.

$$df_z = \frac{F_{zn} - \lambda_{F_{z_o}} \cdot F_{z_0}}{\lambda_{F_{z_o}} \cdot F_{z_0}} \tag{B.2}$$

Filling in equation B.1 with all known values for nominal wheel load and zero camber from the test results yields for the front tyres:

$$\begin{aligned} \mu_x &= (2.111 - 0.16207 \cdot \frac{0 - 2244.4}{2244.4}) \cdot (1 - 19.902 \cdot 0^2) \cdot 1 \\ \mu_x &= 2.27307 \end{aligned} \tag{B.3}$$

In the same fashion, the longitudinal friction coefficient for the rear tyres can be determined. Furthermore, the lateral friction coefficient is determined by replacing the parameters which focus on properties in longitudinal direction by the lateral coefficients.

B.2 Slip curves

rFactor requires normalized slip curves. To generates these slip curves, operations on slip curves generated at nominal conditions are required. First, a slip curve is computed based on nominal wheel loads. To transfer to an slip curve which is independent of wheel load, use is made of the tyre load sensitivity property as discussed in section 4.2.3.

Apart from the effect of load on the magnitude of friction coefficient, the peak slip angle varies with wheel load. As shown in figure 4.8, the peak slip angle of the Hankook tyre starts with a relative high peak slip angle at low wheel loads. The peak angle decreases until a wheel load of 2010 N is reached. Increasing the wheel load further will shift the peak slip angle to a higher value. According to Stephens (1999) and Milliken(1995), the peak slip angle increases per definition with load. Therefore, the assumption is made that the peak slip angle at zero load is equation to the lowest peak slip value in of figure 4.8, being 4.3° at 2010 N. The effect of this correction is also shown in figure B.1.

To normalize the current slip curve, the maximum coefficient of friction in the curve should be determined. Next, the complete slip curve is divided by this maximum value to result in the normalized slip curve. Moreover, this peak value of friction coefficient is the lateral component of one of the parameters in the rFactor TBC file, being *DryLatLong*. The normalized slip curve is shown below.

B.3 Tyre load sensitivity

The tyre load sensitivity in rFactor is modelled by the parameter *LoadSens*. If the parameter *LoadSens* is used, the tyre is load sensitive equally in longitudinal and lateral direction. To add load sensitivity in both directions, use can be made of the following parameters: *LoadSensLat* and *LoadSensLong*. In section 4.2.3, it has been determined that the tyre load sensitivity of the Hankook tyre is a linear relation. Therefore, equation 4.3 is not required to construct the *LoadSens* parameters. The first value represent the

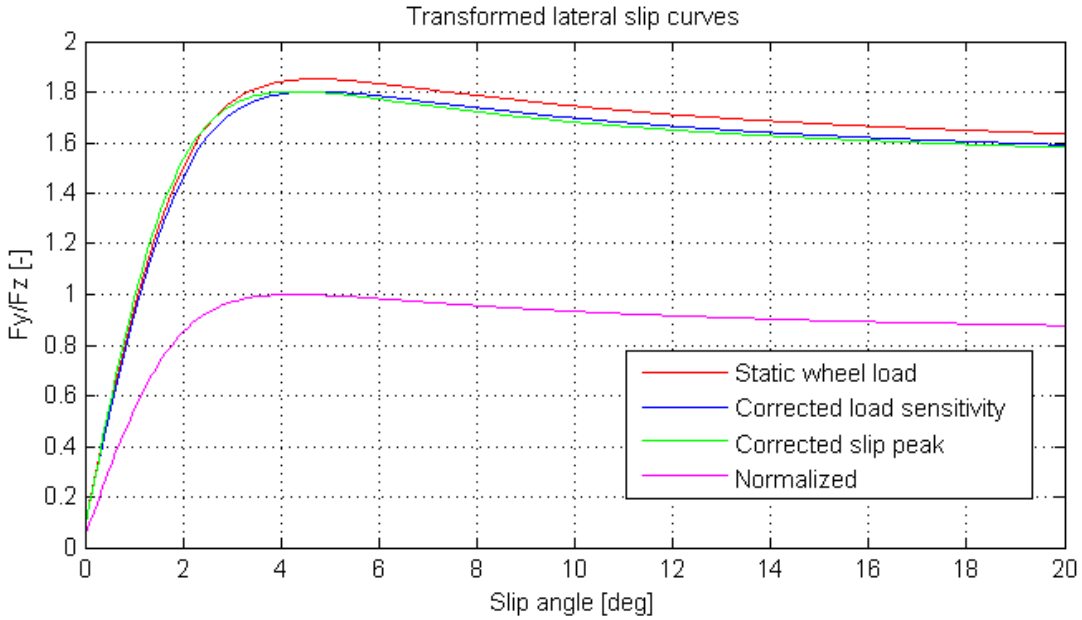

Figure B.1: Transformation of slip curve at static wheel load to normalized rFactor slip curve.

inital slope of the grip multiplier as a function of wheel load, where the second value is the grip mulitplier given at the wheel load as defined by the third value.

At zero wheel load, the grip multiplier equals 1. Increasing the wheel load will have a negative effect of the amount of grip. Decreasing linearly with increasing wheel load, it has been computed that the grip mulitplier reduced to a value of 0.8160 at a vertical wheel load of 8000 N. Given these facts, the *LoadSensLat* parameter is easily determinable. Computing the initial slope, the lateral tyre load sensitivity parameters results as given in equation B.4. The longitudinal load sensitivity parameters is given in equation B.5, determined in the same fashion.

$$LoadSensLat = (-0.000022, 0.8160, 8000.0) \tag{B.4}$$

$$LoadSensLong = (-0.000035, 0.7228, 8000.0) \tag{B.5}$$

B.4 Peak slip angles and ratios

rFactor uses the parameter *LatPeak* and *LongPeak* to determine the shifting of peak slip angle or peak slip ratio as a function of increasing wheel load. The exact definition of these parameters are clarified in section 4.1.2. To determine the relation between peak slip and wheel load, the peak slip is analyzed for a range of wheel loads. In lateral sense, the peak slip angle starts relatively high at low loads. Increasing the wheel load to 2000 N shifts the peak slip angle to a lower value. From that value for $F_{z,n}$ onwards, the peak

slip angle starts increasing again. The increasing peak slip angle is in line with theory as has been investigated. The behavior of slip ratio in the longitudinal sense is not in correspondance with the lateral slip angle behavior. If the wheel load starts to increase from its starting point, the peak slip ratio always decreases.

The *LatPeak* and *LongPeak* coefficients are determined by the wheel load variation as discussed above. These coefficients consist out of three values. The first value is determined by the slip angle of slip ratio at zero load. This value is easily extracted from the slip curves which were generated for the basic, normalized slip curve. The third value for the peak parameter is the maximum load at which the peak slip changes. Increasing the wheel load beyond this value, does not influence the peak slip which is given by the second parameter in the *LatPeak* and *LongPeak* coefficient.

The peak slip angle for zero load is, in contrast to figure 4.8, assumed to be the lowest value of the same figure. Since the relation between wheel load and peak slip angle is a half sine wave, the assumption is made that the minimum peak slip angle is present at zero load. Then the peak slip angle increases until the maximum value at 1900 kg is reached. The coefficient for the Hankook rFactor model is as follows:

$$LatPeak = (0.0781, 0.2944, 18700.0) \tag{B.6}$$

The decreasing peak slip ratio for increasing wheel load is incorporated into the *LongPeak* coefficient. Contrary to the lateral peak coefficient, the second peak slip ratio in the parameter is lower than the first peak slip ratio. The wheel load at which the second peak slip ratio is present is an arbitrary, high load. However, the peak slip ratio corresponds to that wheel load. The exact coefficient becomes:

$$LongPeak = (0.2104, 0.0279, 6000.0) \tag{B.7}$$

B.5 Camber

The influence of camber on the lateral and longitudinal performance of the tyre has been shown in figure 4.12. The lateral grip increment due to camber has its maximum effect at a camber angle of approximately 2.2°. The longitudinal loss increases exponentionally with increasing camber angle. The effect of camber has been modelled in rFactor with the *CamberLatLong* coefficient. The maximum grip increment is given by the second value at a camber angle provided by the first value (in degrees) in the *CamberLatLong* coefficient. The last value in this parameter is the longitudinal loss at a camber angle of 90°.

The determination of grip increment for changing camber angle is computed at static wheel load. From that starting point, the coefficient of friction is computed for zero camber. The camber is then increased to determine the difference in coefficient of friction until the peak camber angle. The highest coefficient of friction is then normalized

with the zero-camber coefficient of friction. The increment in friction coefficient is 0.0169.

Given the exponential decrease in longitudinal grip with increasing camber angle, the longitudinal loss is not computed over the entire range of camber angles (0° to 90°), but near the peak camber angle. This gives the most representative fraction of grip loss. It turns out if the trend as shown in 4.12 is linearized near the peak camber angle, the longitudinal loss at 90° would be 0.4862. This results in the following *CamberLatLong* parameter:

$$CamberLatLong = (2.1745, 0.0169, 0.4862) \tag{B.8}$$

B.6 Pneumatic trail

The aligning moment of the tyre is computed in rFactor based on the current state of the tyre. A separate input parameter has influence on the magnitude of the aligning moment, being *PneumaticTrail*. This parameter is indicated the pneumatic trail in meters per unit load. From the belt tests performed to construct the Pacejka model of the Hankook F3 tyre, pneumatic trail measurements are given in the test conditions and results. In test number 2012RT020007, the aligning moment at reference load of 980.7 N resulted in a pneumatic trail of 9.674 mm for a tyre pressure of 2.6 bar. Converting this to the rFactor definition of pneumatic trail for the front tyres yields:

$$\text{Pneumatic trail} = \frac{9.674 \cdot 10^{-3}}{980.7} = 9.864 \cdot 10^{-6} {}^{m}/_{N} \tag{B.9}$$

The rear tyres were measured a pneumatic trail of 14.894 mm in test number 2012RT020010. The reference load for the rear tyres was 1471.0 N. In the same manner, the *PneumaticTrail* coefficient for the rear tyres is computed to be $1.013 \cdot 10^{-5}$ ${}^{m}/_{N}$.

Compared to the original rFactor tyre model, the pneumatic trails for both the front and rear tyres are reduced from a value of 0.000012 ${}^{m}/_{N}$ to a value of 0.000010 ${}^{m}/_{N}$.

B.7 Rear tyres

As discussed in earlier sections, the Pacejka tyre model for the rear Hankook tyre is not completely accurate. Since there is no reliable information about the wheel loads at which the testing on the test bench took place, the modelling is performed in the linear areas of the Pacejka model for parameters which are not determinable in to same fashion as the front tyres. An example is the tyre load sensitivity. Referring back to figure 4.15, it has been concluded that at a certain load the lateral force capabilities of the rear tyres collapses. The avoid creating the model in this non-linear area, the tyre load sensitivity parameter is based on the wheel loads before the collapsing of lateral tyre force capability. This result is then extrapolated over a wide varity of wheel loads.

Appendix C

Suspension pickup points F312

This appendix contains two pages of the Dallara F312 car manual which show the exact location of all pickup points of the suspension on the car both for the front as for the rear.

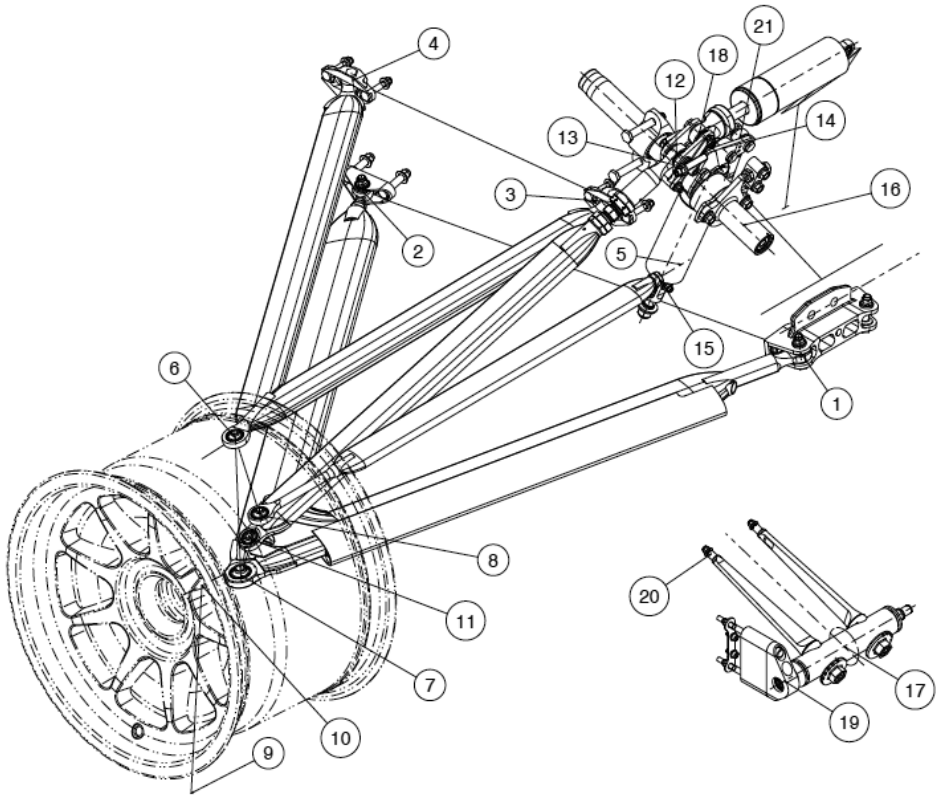
4
21
18
12
14
13
3
16
2
5
15
6
1
8
20
11
7
17
19
10
9

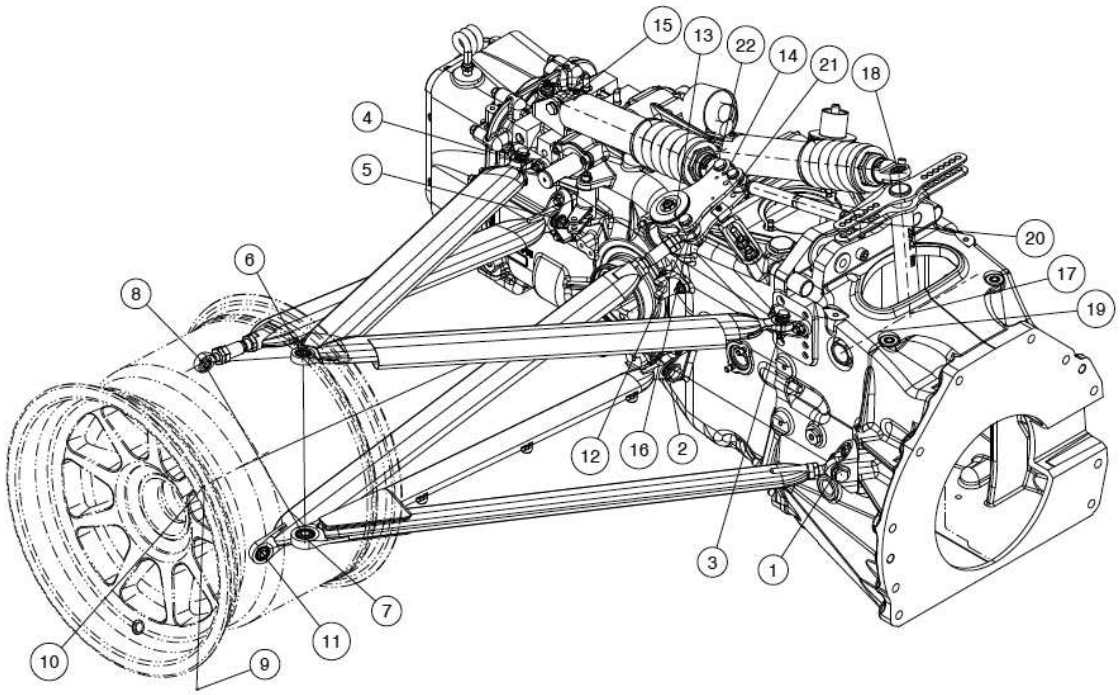
15
13
22
14
21
18
4
5
20
6
17
8
19
12
16
2
3
1
7
11
10
9

FRONT	X [mm]	Y [mm]	Z [mm]
P1	190,5	-50	282
P2	-380	-153	263
P3	17	-162,4	452
P4	-380	-168,8	418,5
P5	127	-170	427,5
P6	-65,9	-663,7	347,3
P7	-23,9	-697,2	201,8
P8	31,5	-723,0	322,3
P9	0	-797,5	-26,5
P10	0	-781,1	242,0
P11	-32,2	-678,6	239,4
P12	91,5	-141,6	542,0
P13	82,4	-125	512,9
P14	79,2	-58,5	502,7
P15	21,0	-96,5	317,3
P16	177,8	-125	482,9
P17 (int)	115,5	0	364,2
P17 (ext)	173,5	0	346,2
P17 (ext +40)	213.5	0	346,2
P18	96,3	-111,5	557,3
P19 (int)	115,5	-93,2	364,2
P19 (ext)	173,5	-93,2	346,2
P19 (ext +40)	213.5	-93,2	346,2
P20	45,6	-35	400,6
P21	79,6	-32	504,1

REAR	X [mm]	Y [mm]	Z [mm]
P1	415	-150	167
P2	121,9	-134	155,5
P3	309	-135	308,1
P4	-156	-90	279
P5	-92,5	-101	237
P6	25	-623,5	364,5
P7	85	-680	170
P8	-122	-637	289
P9	0	-770	-39,5
P10	0	-757,1	238,7
P11	12	-678	113
P12	164,5	-138,2	368,7
P13	129,1	-128,1	364,7
P14	142,4	-59,7	395,1
P15	-143,4	-37,7	339,2
P16	137,5	-113,5	328,4
P17	380	0	290
P18	361,7	0	477,1
P19	380	-50	290
P20	365	-66	443,108
P21	168,3	-65,2	398,9
P22	75,0	0	362,7

Appendix D

rFactor suspension file

The rFactor suspension file provided in this appendix shows the file structure of modeling the suspension in rFactor. The values are based on the pickup points provided by car manufacturer Dallara. Weights are measured and inertias computed or estimated based on the weight and dimensions.

```
//F1 Type suspension
////////////////////////////////////////////////////////////////////////
//
// Conventions:
//
// +x = left
// +z = rear
// +y = up
// +pitch = nose up
// +yaw = nose right
// +roll = right
//
// [BODY] - a rigid mass with mass and inertial properties
// [JOINT] - a ball joint constraining an offset of one body to an
// offset of another body (eliminates 3 DOF)
// [HINGE] - a constraint restricting the relative rotations of two
// bodies to be around a single axis (eliminates 2 DOF).
// [BAR] - a constraint holding an offset of one body from an offset of
// another body at a fixed distance (eliminates 1 DOF).
// [JOINT&HINGE] - both the joint and hinge constraints, forming the
// conventional definition of a hinge (eliminates 5 DOF).
//
////////////////////////////////////////////////////////////////////////
//
// Body including all rigidly attached parts (wings, barge boards, etc.)
```

```
[BODY]
name=body mass=(0.0) inertia=(0.0,0.0,0.0)
pos=(0.0,0.0,0.0) ori=(0.0,0.0,0.0)

// Front spindles
[BODY]
name=fl_spindle mass=(8.4) inertia=(0.0271,0.0452,0.0271)
pos=(0.781,0.0,-1.618) ori=(0.0,0.0,0.0)

[BODY]
name=fr_spindle mass=(8.4) inertia=(0.0271,0.0452,0.0271)
pos=(-0.781,0.0,-1.618) ori=(0.0,0.0,0.0)

// Front wheels
[BODY]
name=fl_wheel mass=(14.8) inertia=(0.3302,0.5617,0.3302)
pos=(0.781,0.0,-1.618) ori=(0.0,0.0,0.0)

[BODY]
name=fr_wheel mass=(14.8) inertia=(0.3302,0.5617,0.3302)
pos=(-0.781,0.0,-1.618) ori=(0.0,0.0,0.0)

// Rear spindles
[BODY]
name=rl_spindle mass=(8.4) inertia=(0.0271,0.0452,0.0271)
pos=(0.757,0.0,1.182) ori=(0.0,0.0,0.0)

[BODY]
name=rr_spindle mass=(8.4) inertia=(0.0271,0.0452,0.0271)
pos=(-0.757,0.0,1.182) ori=(0.0,0.0,0.0)

// Rear wheels (includes half of rear-axle)
[BODY]
name=rl_wheel mass=(16.8) inertia=(0.4637,0.6919,0.4637)
pos=(0.757,0.0,1.182) ori=(0.0,0.0,0.0)

[BODY]
name=rr_wheel mass=(16.8) inertia=(0.4637,0.6919,0.4637)
pos=(-0.757,0.0,1.182) ori=(0.0,0.0,0.0)

// Fuel in tank is not rigidly attached - it is attached with springs and
// dampers to simulate movement. Properties are defined in the HDV file.
[BODY]
name=fuel_tank mass=(1.0) inertia=(1.0,1.0,1.0)
pos=(0.00, 0.14, -1.20) ori=(0.0,0.0,0.0)

// Drivers head is not rigidly attached, and it does NOT affect the vehicle
```

```
// physics. Position is from the eyepoint defined in the VEH file, while
// other properties are defined in the head physics file.
[BODY]
name=driver_head mass=(5.0) inertia=(0.02,0.02,0.02)
pos=(0.0,0.7,-1.35) ori=(0.0,0.0,0.0)

////////////////////////////////////////////////////////////////////////
// Constraints
////////////////////////////////////////////////////////////////////////

// Front wheel and spindle connections
[JOINT&HINGE]
posbody=fl_wheel negbody=fl_spindle pos=fl_wheel axis=(-0.781,0.0,0.0)

[JOINT&HINGE]
posbody=fr_wheel negbody=fr_spindle pos=fr_wheel axis=(0.781,0.0,0.0)

// Front left suspension (2 A-arms + 1 steering arm = 5 links)
[BAR] // forward upper arm
name=fl_fore_upper posbody=body negbody=fl_spindle pos=(0.162,0.210,-1.635) neg=(0.664,0.105,-
1.553)

[BAR] // rearward upper arm
posbody=body negbody=fl_spindle pos=(0.169,0.176,-1.238) neg=(0.664,0.105,-1.553)

[BAR] // forward lower arm
posbody=body negbody=fl_spindle pos=(0.050,0.040,-1.809) neg=(0.697,-0.040,-1.595)

[BAR] // rearward lower arm
name=fl_fore_lower posbody=body negbody=fl_spindle pos=(0.153,0.021,-1.238) neg=(0.697,-
0.040,-1.595)

[BAR] // steering arm (must be named for identification)
name=fl_steering posbody=body negbody=fl_spindle pos=(0.170,0.186,-1.745) neg=(0.723,0.080,-
1.650)

// Front right suspension (2 A-arms + 1 steering arm = 5 links)
[BAR] // forward upper arm (used in steering lock calculation)
name=fr_fore_upper posbody=body negbody=fr_spindle pos=(-0.162,0.210,-1.635) neg=(-
0.664,0.105,-1.553)

[BAR] // rearward upper arm
posbody=body negbody=fr_spindle pos=(-0.169,0.176,-1.238) neg=(-0.664,0.105,-1.553)

[BAR] // forward lower arm
name=fr_fore_lower posbody=body negbody=fr_spindle pos=(-0.050,0.040,-1.809) neg=(-
0.697,-0.040,-1.595)
```

[BAR] // rearward lower arm
posbody=body negbody=fr_spindle pos=(-0.153,0.021,-1.238) neg=(-0.697,-0.040,-1.595)

[BAR] // steering arm (must be named for identification)
name=fr_steering posbody=body negbody=fr_spindle pos=(-0.170,0.186,-1.745) neg=(-0.723,0.080,-1.650)

// Rear left suspension (2 A-arms + 1 straight link = 5 links)
[BAR] // forward upper arm
posbody=body negbody=rl_spindle pos=(0.135,0.069,0.873) neg=(0.624,0.126,1.157)

[BAR] // rearward upper arm
posbody=body negbody=rl_spindle pos=(0.090,0.040,1.338) neg=(0.624,0.126,1.157)

[BAR] // forward lower arm
posbody=body negbody=rl_spindle pos=(0.150,-0.072,0.767) neg=(0.680,-0.069,1.097)

[BAR] // rearward lower arm
posbody=body negbody=rl_spindle pos=(0.134,-0.083,1.060) neg=(0.680,-0.069,1.097)

[BAR] // straight link
posbody=body negbody=rl_spindle pos=(0.101,-0.002,1.274) neg=(0.637,0.050,1.304)

// Rear right suspension (2 A-arms + 1 straight link = 5 links)
[BAR] // forward upper arm
posbody=body negbody=rr_spindle pos=(-0.135,0.069,0.873) neg=(-0.624,0.126,1.157)

[BAR] // rearward upper arm
posbody=body negbody=rr_spindle pos=(-0.090,0.040,1.338) neg=(-0.624,0.126,1.157)

[BAR] // forward lower arm
posbody=body negbody=rr_spindle pos=(-0.150,-0.072,0.767) neg=(-0.680,-0.069,1.097)

[BAR] // rearward lower arm
posbody=body negbody=rr_spindle pos=(-0.134,-0.083,1.060) neg=(-0.680,-0.069,1.097)

[BAR] // straight link
posbody=body negbody=rr_spindle pos=(-0.101,-0.002,1.274) neg=(-0.637,0.050,1.304)

// Rear spindle and wheel connections
[JOINT&HINGE]
posbody=rl_wheel negbody=rl_spindle pos=rl_wheel axis=(-0.757,0.0,0.0)

[JOINT&HINGE]
posbody=rr_wheel negbody=rr_spindle pos=rr_wheel axis=(0.757,0.0,0.0)